REPUBLIQUE ALGERIENNE DEMOCRATIQUE ET POPULAIRE
MINISTERE DE L'ENSEIGNEMENT SUPERIEUR ET DE LA RECHERCHE SCIENTIFIQUE
UNIVERSITE FERHAT ABBAS- SETIF-

THESE

Présentée à

LA FACULTE DE TECHNOLOGIE

Département de Génie des Procédés
Pour l'Obtention du Titre de

DOCTEUR en SCIENCES
Option: Génie des Polymères

Par

Mr. HELLATI ABDELHAK

ETUDE DES PROPRIETES RHEOLOGIQUES, MECANIQUES, THERMIQUES ET SPECTRALES DES MELANGES PET/iPP/ SEBS-g-MAH RENFORCES PAR LA MONTMORILLONITE

Soutenue le: 26 /09 / 2011

Devant le jury

Président :	**Pr. BRAHIM DJELLOULI**	**Université Ferhat ABBAS, Sétif**
Rapporteur :	**Pr. DJAFER BENACHOUR**	**Université Ferhat ABBAS, Sétif**
Examinateurs :	**Pr. NASSIRA BENHARRATS**	**Université Mohamed BOUDIAF, Oran**
	Pr. MUSTAPHA KACI	**Université Abderrahmane MIRA, Bejaia**
	Pr. HOCINE DJIDJELLI	**Université Abderrahmane MIRA, Bejaia**
	Dr. SAID BOUHELAL	**Université Ferhat ABBAS, Sétif**

ACKNOWLEDGEMENTS

ALHAMDULILLAH to ALLAH the AL-Mighty, Most Gracious and Most Merciful. It is an honour to place and record deep sense of gratitude and indebtness to all that have contributed and generously helped me in the completion of this work.

First and foremost, I wish to express my gratitude and indebtness to my supersivor, Pr. Djafer Benachour, for all his valuable guidance, critics, support and comments to complete this research work. I could not have imagined having a better advisor and mentor for my thesis study. His thoughtfulness deeply inspired me throughout in my academic and research process.

I would like to thank the committee members Pr. B. Djellouli, Pr. N. Benharrats, Pr M. Kaci, Pr. H. Djijelli and Dr. S. Bouhelal for reviewing my thesis and for their suggestions.

I gratefully thank Pr. F. J Balta Calleja, for accepting me to work with his research team and perform some characterization tests in his laboratories.

Also special thanks to Dr. E. M Caiajo, for her help in learning different polymer characterization techniques such as XRD, DSC, Microhardness and answering my technical questions regarding these equipments

I could not complete this thesis without plentiful support from my family and my friends, specially my wife for her care, love and sacrifice and also for understanding and supporting me throughout the preparation of this thesis.

Many thanks are extended to members of our department, for their help and enjoyable discussions during my research work. All my lab mates, Toufik Douibi, Abdelhakim Benmekideche, Messaoud Zerrari, at the Polymer division made it a convivial place to work.

TABLE OF CONTENTS

TABLE OF CONTENT

LIST OF TABLES

LIST OF FIGURES

LISTE OF ABREVIATIONS

PET : Polyethlene Terephtalate

iPP: Isotactic Polypropylene.

SEBS-g-MAH: Styrene-Ethylene –Butylene –Styrene grafted Maleic Anhydrid

DSC: Differential Scanning Microscopy.

TGA: Thermal Gravimetric Analysis

FTIR: Fourier Transform Infra Red.

WAXS: Wide Angle X-ray Scattering

MFI : Melt flow Index

MMT: Montmorillonite

Na-Mmt : Sodium Montmorillonite

OCDA- Mmt: Montmorillonite modified with Octadecylamine

SEM: Scanning Electron Microscopy

H: Hardness

lc: crystal thickness

INTRODUCTION

During the recent decades, interest in the recycling of polymeric materials has experienced a notable increase for both economical and environmental reasons [1,2]. However, recycled polymers are subjected to thermal and mechanical processes that give rise to structural and morphological changes, which, consequently, affect the properties of the materials. One way of improving the properties of recycled polymers is to blend them with unmodified polymers. In fact, the preparation of polymer blends is a convenient method to obtain materials with new combinations of defined properties [3-5]. These properties are closely related to the microstructure of the polymeric blend. The final properties of polymer blends to a large extend depend on the size of the minor phase and the interfacial adhesion between the two phases. The processing conditions, concentration of the dispersed phase, and the morphology of the blends play an important role in controlling the size of the dispersed phase. The role of a compatibilizer in a polymer alloy or blend is to improve interfacial adhesion between two immiscible polymers resulting in the formation of miscible blends. The compatibilizer can be a macromolecule or a block or graft copolymer conventionally.

The addition of these compatibilizers results in a decreased domain size of the dispersed phase, stabilization of the dispersed phase during melt mixing, and finally an improved interfacial adhesion in the solid state. The decreased domain size leads to increase in surface tension, which should result in coalescence but the improved interfacial interaction negates out the increased surface tension resulting in a more homogenous stable blend. A newly used compatibilization technique is the use of clay particles to compatibilize immiscible blends.

The strong adsorption of polymers on the particles provides the stabilization energy for compatibilization, and also the intercalation of the polymers inside the clay galleries along with a very high surface area per unit weight of the clay particles, further helps in compatibilization.

The addition of clay particles also results in increase in melt viscosity, which further helps in reducing the size of the dispersed phase.

We have focused our attention on blends of recycled amorphous poly (ethylene terephthalate) (PET) with isotactic polypropylene (iPP). However, as with most thermoplastics, these polymers are immiscible and need to be made compatible [6] In this study, we used as a compatibilizer a styrene–ethylene/butylene–styrene block copolymer grafted with maleic anhydride (SEBS-g-MAH). In addition, we compared PET/iPP/SEBS-g-MAH blends with their corresponding composites containing 5 wt% clay. As it is known, the addition of small amounts of layered silicates, that is clay, to the polymers greatly improves some of their properties, strength, heat resistance, impact resistance,… [7]. However, the preparation of a homogeneous dispersion of clay particles (hydrophilic) in a non polar polymer matrix is a difficult process. The clay particles tend to agglomerate, and the physical properties of the resulting material tend to be very poor. To solve this problem, as a first step, the surfaces of the clay have to be previously modified with some organophilic agent, such as, quaternary ammonium salts [8] or long-chain primary amines, like octadecylamine [9]. The resulting material is called organophilic clay or organoclay. This process lowers the surface energy of the silicate surface and improves wetting with the polymer matrix [10]. Thus, organosilicates are more compatible with most engineering plastics than is unmodified material. The second step is the preparation of the polymer–organoclay composites. This can be achieved by mixing the organoclay with the molten polymers (by a melt-mixing method, among other methods….)

Previous studies on this binary blend include the work of Bataille et al. [11] who studied tensile properties and water vapor permeability of non compatibilized PET/PP in the complete range of composition, and one composition at several compatibilizer levels.

The compatibilizer was a PP–acrylic acid copolymer (PP-g-AA).The same compatibilizer was employed by Xanthos et al. [12] who also added a transesterification catalyst. A complete characterization was carried out to evaluate compatibilization and, the heigher strength reinforcement observed was attributed to improved components dispersion, and possibly physical interactions. Successful compatibilization as evidenced by large deformation mechanical behavior and morphology was reported by Heino et al. [13]; by using a glycidyl Methacrylate modified SEBS(SEBS-g-GMA) at one ternary composition. Morye et al.[14] reported on the rheology, mechanical properties and permeability to oxygen and water vapor of PET/PP blends in a limited composition range with increased levels of PP and using ethylene–vinyl acetate (EVA) and EVA-g-MA as compatibilizers. Though compatibilization was inferred on the basis of blend melt rheology, mechanical properties did not support this conflit. As results on permeability, the conclusions were ambiguous since EVA itself may conterbalance the barrier properties of PET if the latter is present in small amounts in the blend. In a more recent paper Calcagno et al [15] studied the role of the MMT on the morphology and mechanical properties of the PP/PET blends and they have reported that the better dispersion was obtained when maleic anhydride grafted polypropylene (PP-MA) was used. The clay was preferentially situated in the PP/PET interphase and in the PET phase. They also reported that yield stress, Young modulus, and elongation at break increased when MMT and PP-MA were used without impair the impact strength.

The aim of this study was to examine the influence of a compatibilizer (SEBS-g-MAH) on the rheological, thermal, structural and micromechanical properties of PET/iPP blends with clay. For this purpose, the different blend compositions were prepared by using a direct melt blending in a brabender.

Chapter I

Polymer blends and Compatibilization strategies

I-1. Introduction to polymer blends

The realization of polymer blends is now the most suitable strategy from the point of view of prices and time for obtaining new materials since it is less expensive and faster to mix polymers than to develop monomers or new methods of polymerization. Polymer blends also offer the opportunity to obtain a wide range of characteristics and properties by just changing the composition of the combined polymers. Also, the main objectives of the materials obtained through polymer blends are to meet several requirements that may be necessary for manufacturers.

The reasons related to the preparation of a well-defined blend are:

- Development of a material which meets specific requirements,
- Improvement of a specific property,
- Adjustment of performance requirements of a consumer at a lower price,
- Recycling of industrial or municipal waste.

Furthermore, reasons related to producers are reflected mainly in:

- Improved product consistency and processability,
- Reducing the number of grades which should be stored or produced, and thus huge savings can be made on space and investment [16].

Ideally, two or more polymers can be blended to form a wide variety of morphologies, statistical or structured in order to obtain products that potentially should provide desirable combinations of characteristics. But in practice it is very difficult to have these potential combinations through simple mixtures, because of some fundamental and inherent problems and

situations at the interface which make the achievement of mixtures less profitable. Frequently, both polymers are thermodynamically immiscible, which excludes generation of homogeneous products. This is not often a problem since they generally want to have products in two phases, but for this it is imperative that synergistic nature of the products must be revealed. Thus, control of thermodynamic laws that govern these systems is the key to understanding their behavior and properties [17].

I-2: Polymer blends thermodynamic

At the equilibrium, a mixture of two amorphous polymers can exist as one phase in which the segments of the two macromolecular components are mixed, or as two separate phases, each consisting essentially of a different polymer.

These two phase states are governed by the principles of thermodynamics: a monophasic and homogeneous system is formed when the free energy of mixing ΔGm is negative:

$$\Delta G_m = \Delta H_m - T\Delta S_m \qquad \textbf{(eq. 1)}$$

ΔHm: Enthalpy of mixing

T: Absolute temperature

ΔSm: Entropy of mixing.

ΔGm must also satisfy a second condition which ensures the miscibility and prevents phase separation:

$$\left(\frac{\partial^2 \Delta G_m}{\partial \Phi_i^2}\right)_{T,P} > 0 \qquad \textbf{(eq. 2)}$$

Φi being the volume fraction of component i in the mixture and T and P are respectively the temperature and pressure.

When two polymers with high molecular weight are mixed, the entropy gained ΔSm is negligible and hence the free energy of mixing can be negative if ΔHm (enthalpy of mixing) is negative. In other words, the mixing operation must be exothermic, which requires specific interactions between

components of the mixture. These interactions can vary from very high ionic strength to weak interactions such as hydrogen bonds, and interactions of the type of ion-dipole, dipole-dipole or donor-acceptor. All these effects contribute to the achievement of a negative free energy of mixing and miscibility of the system [18,19].

I-3. Compatibilization interest of polymer blends

From a business perspective, the properties of manufactured items must be stable and reproducible. However, the change in morphology with the processing conditions and phase separation with aging are characteristics of heterogeneous systems that may deteriorate the privileged position of polymer blends on the market.

To be safe from this unpleasant situation, the manufacturer must find polymer systems that can tolerate changes in the processing conditions, transport and storage.

The first solution is to seek miscible systems with superior properties in terms of processing conditions and performance. But, practically, heterophasic systems are by far the most attractive; the dispersed phase often improves the impact resistance and always gives a strengthening effect. As a result, it is better to produce heterophasic systems which are stable and reproducible than the corresponding homopolymers. For this, the safest way is to stabilize these phases by compatibilization, which can be achieved by numerous ways which have been proved in obtaining successful polymer alloys. Stabilization of heterogeneous systems is done primarily by overcoming the interface problems.[18].

1-4. Interphase and interfacial phenomena in polymer blends

By definition, a multiphase system has two or more phases. The most frequently treated is the system composed of two phases; one is the continuous phase, or matrix, in which the other phase is dispersed. Interfaces always appear between phases regardless of the system under study (a mineral-reinforced composite material or a polymer blend), and the fact that a material has properties that necessarily reflect those of its constituents and the interface, it also appears that to

better understand the final properties of a multiphase system, it is essential to take into account the interfacial region.

It is also important to recognize that the interfacial zone can be extended to the thickness of the layer where the properties are different from bulk properties of each constituent. Therefore, in the vicinity of interfaces, an area of special structure (which is different from the two polymers in contact, but still dependent on them), is formed with a thickness Δl ranging from a few nanometers to a few hundred nanometers[16]. This area provides phase continuity condition and any kind of transfer between the continuous and dispersed phases. It is defined by the term interphase. The interphase can be considered as a third phase with its own characteristics and region of interdiffusion of the two types of macromolecules. Its stabilization results in the performance reproducibility, better processing conditions and recyclability of materials. In general, the mobility of segments in the interphase is slow and its thickness depends on the thermodynamic interactions of the macromolecular segment size, composition. Consequently, the interphase layer is not a homogeneous entity but a complex of micro and macro heterogeneities.

For all these reasons, we can conclude that in polymer technology, the concept of interface / interphase is the point of interest and its study is the key of the problems presented by heterophasic systems. Thus, discussing a product's performance means the discussion of the dispersion, morphology and adhesion between the different phases, and these are all related to the properties of the interfacial region. It was confirmed that the interphase thickness Δl varies from 2 to 60 nm [16]. The first value is typical of immiscible polymer pairs and antagonists while the second is valid for polymer alloys compatibilized through reactive ways. For these systems, it has been proved that Δl

increases with the annealing time up to a constant value. This value depends heavily on system, temperature and concentration of reactive sites. This equilibrium value ranges from 10-50 nm, whereas the thickness of the interphase is only 6-8 nm while adding a block copolymer [16].

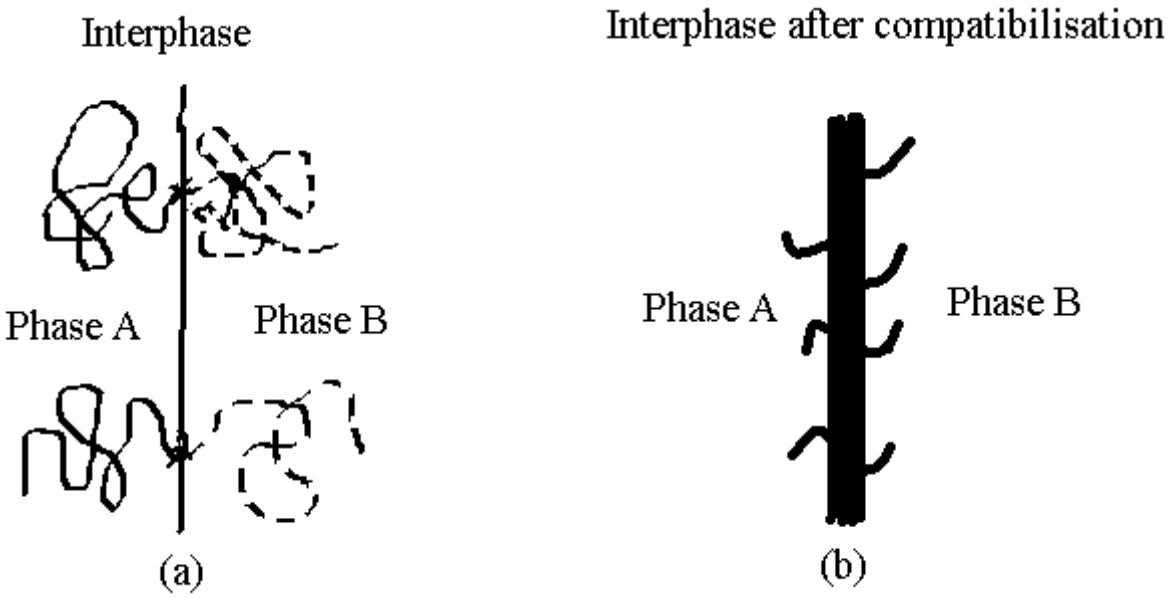

Figure I-1: (a) Configuration of a perfect block copolymer at the interface between two phases of polymers A and B. (b) promotion of an interphase between the phases A and B in the presence of a compatibilizer [19].

The interphase is characterized by two important parameters, including the coefficient of interfacial tension and adhesion area. The interfacial tension coefficient depends strongly on the structure of polymers composing the mixture and this is inversely proportional to the thickness Δl of the interphase. Also, adhesion domain is based on the size and deformability of the interphase [18]. Typical cases that can generally be encountered when carrying out any combination are a high interfacial tension, or very low interfacial adhesion between the two phases. The interfacial tension contributes to the inherent difficulty to obtain a desired degree of dispersion, and thus unstable mixtures which can subsequently lead to separations or stratification process.

Furthermore, poor adhesion leads to very poor mechanical behavior as it may also prevent certain morphologies which are highly structured [17].

Thus it is imperative to consider the interphase as the key parameter and always make a change in its thickness and structure when the components of a blend are thermodynamically immiscible and this leads to the concept of multiphase system compatibilization.

The operation of compatibilization can control the state of phase separation of a mixture in order to better respond to the problem of high interfacial tension which is manifested by the difficulty of mixing and also leads directly to poor interfacial adhesion. Thus, by replacing the clear interface by interfacial areas with blurred boundaries, which is a continuation property of the phases of the system, compatibilization helps the achievement of synergy between the characteristics of the various constituents [16].

Furthermore, the existence of physical or chemical interactions along this area controls all performance of polymer blends and composites. Strong interactions provide good adhesion and a very effective stress transfer from the continuous phase to the dispersed phase. But in the absence of these interactions or if they are weak, the use of a compatibilizer is needed [20].

I-5. Compatibilization of polymer blends

The compatibilization of immiscible polymer blends is by far the most suitable method for converting an heterophasic system to a high performance alloy, characterized by stable and reproducible properties. Also, since the performance of a material depend not only on its constituents and their concentrations but also the morphology, it is also required, in any operation, that compatibilizer must be stable and unaffected by the subsequent processing conditions [16].

I-5 - 1. Objectives of the compatibilization

The essential functions that must have a compatibilizer are generally as follows:

- The reduction of interfacial tension which is the main obstacle to obtaining an appropriate degree of dispersion, and leads to unstable systems. The compatibilizer has a role to generate a fine dispersion of the dispersed phase in the polymer matrix,
- To ensure that the morphology generated is not destroyed during the subsequent processes of transformation,
- To increase the adhesion between different phases for a very effective stress transfer between them. This helps prevent catastrophic failure initiated at the interface [16,21,22].

Thus, the refinement and stabilization of the morphology and the increase in interfacial adhesion can often promotes a material without any industrial interest, for which the beneficial properties of both components are utilized and deficiencies are effectively hidden.

Strategies for compatibilization of polymer blends are different and their choice is intimately related to the structure of mixed materials and the availability of adequate equipment to carry out the desired blend. Overall, the compatibilization of polymer system can be completed in two essential ways:

- The non-reactive compatibilization,
- The reactive compatibilization.

I-5-2. Compatibilization principles of polymer blends

The compatibilizing agents are macromolecular species that exhibit interfacial activity in heterophasic systems. These agents generally have a block copolymers structure. One of the component bloc is miscible with one of the constituents of the blend while the second block is miscible with the other component. This structure can be synthesized in an independent process and

incorporated into the polymer blend, but can also be generated in situ during the mixing process in the reactive compatibilization which, however, requires mutual reactivity of the blend components.

The role of compatibilizers in the blend is primarily to reduce the interfacial tension. When it becomes sufficiently weak and largely exceeded by the deformation tension produced by mixing, the stretching of the polymer droplets forming the dispersed phase will occur and thus contribute to its fragmentation into thinner droplets until they reach a diameter limit after which no division occurs. This dimension is strongly dependent on experimental conditions such as the viscosity of the components, interfacial properties, blend composition and operating conditions [21].

Moreover, the presence of the compatibilizer molecules on the surface can prevent the coalescence process during subsequent transformation. Indeed, focusing on the interface as emulsifiers, compatibilizers can no longer make contact between the inclusions of the dispersed phase, which effectively eliminates the flocculation and prevents coalescence. It appears that the compatibilizers generate initially a fine dispersion of one polymer in the other and contribute to the stabilization of the morphology thereafter forming a barrier against coalescence [22].

I-6-1 Reactive compatibilisation

The reactive compatibilization is the promotion of specific chemical reactions between the constituents of a mixture during processing operations where the interfacial agent is produced in situ from segments of both polymers. The reactive compatibilization is thus an integration of fine chemistry and the principles of polymer processing.

The conditions required for reactive mixing are:

- The mixing is sufficiently dispersive and distributive to ensure the renewal continuous interface,
- The reactive functions are present to react along the interphase
- The reaction rate is satisfactory to produce sufficient amount of copolymer during processing of the mixture.

The reactive compatibilization leads to the formation of grafted copolymers or block. The chemical reactions produce covalent and less frequently ionic bonds. This powerful technology allows to develop new blends as well as manage the mixtures already known with new ranges of properties [16].

I-6-2. Nonreactive compatibilization

From a historical point of view, the most traditional method for compatibilization of a mixture of polymers is the incorporation of a third component in the immiscible system. This component, in the form of a graft copolymer or block must contain segments capable of maintaining interaction with the polymer chains of the mixture such as hydrogen bonds or interactions of dipole-dipole, ion-dipole [16].

This copolymer must be synthesized in order to:

- Maximize the miscibility of the segments with the constituents of the blend,
- Minimize its molecular weight so as to have a value just sufficient to create interactions
- Incorporate a sufficient quantity for compatibilizing the system and minimize the possibility of micelles formation.

Indeed, this type of compatibilizer may change the interfacial properties and rheological but may present a major disadvantage namely the formation of micelles. The generation of compatibilizer micelles in the blend reduces its effectiveness as interfacial modifier and increases the viscosity of the system, making difficult the mixing. The amount of the compatibilizer required for saturation of the interface is a function of many variables such as time and mixing equipment, the affinity of the compatibilizing agent for the dispersed phase, the size of its particles and their orientation in the interface, and finally its ability to stabilize the dispersed phase against flocculation and coalescence.

There is evidence that during the synthesis of a copolymer, the three conditions mentioned above must be carefully taken into consideration [16].

The effectiveness of a compatibilizer is also closely linked to its architecture and its orientation in the interface. From a conformational point of view, the block copolymer is more effective than the graft copolymer [21,23].

Also, the relative length of the building blocks of a copolymer has a fundamental importance in the emulsification of a polymer blend. Indeed, the molecular weight of a block copolymer should be greater than the molecular weight of the corresponding homopolymers in order to increase the repulsion between the blocks, to facilitate their penetration into their respective phases and prevent the formation of micelles. When the blocks of the compatibilizer are very short, they can enter the different phases of the mixture and results in formation of micelles at the interface or in any phase of the system. However, copolymers with high molecular weights are not recommended because they may be responsible for an excessive increase in viscosity and a low rate of diffusion [21]. So we can say that the compatibilizers must be synthesized so that their chain segments are sufficiently long so that they can build cohesive forces also sufficient to enter deep into their homopolymer phases, without that there is no micelle formation or increased viscosity [17].

Thus it appears that the synthesis of compatibilizing agents is virtually care and very expensive because it is essential to increase their effectiveness by developing their characteristics, including molecular weight, structure and conformation so that only low concentrations are sufficient to saturate the interface and prevent the formation of micelles.

I-7. Conclusion

With the intensification of the use of polymer blends in applications where the use of a homopolymer does not provide all the required properties, it is becoming increasingly important to further accentuate the research to overcome the problem of immiscibility which is the major limitation to many applications of these materials. Compatibilization techniques are different and they all target a common goal. However, the suitability of a method to a specific industrial development depends on many factors such as price, the final performance, recyclability and the possibility of biodegradability of the mixture.

The non-reactive compatibilization requires materials designed according to stringent specifications that make their syntheses excessively costly. However, the reactive compatibilization is more attractive in terms of price and equipment. However, control of the kinetics of the reactive system must be subjected to extreme conditions to ensure a better selectivity and prevent chemical degradation reactions which can produce undesirable effects on the final properties of the mixture.

For this, science and technology of polymer blends and their compatibilization continue to grow in the future. Efforts will continue to further refine further compatibilization processes to continually improve the desired properties of these materials.

Chapter II

Clay Minerals

II-1 Introduction

Clay minerals are hydrous aluminium phyllosilicates, sometimes with variable amounts of iron, magnesium, alkali metals, alkaline earths and other cations. Clays have structures similar to the micas and therefore form flat hexagonal sheets. Clay minerals are common weathering products (including weathering of feldspath and low temperature hydrothermal alteration products. Clay minerals are very common in fine grained sedimentary rocks such as shale, mudstone and siltstone and in fine grained metamorphic slate and phyllite [24].

Clays are ultra fine grained (normally considered to be less than 2 micrometres in size on standard particle size classifications) and so require special analytical techniques. Standards include x-ray and electron diffraction methods, various spectroscopic methods such as Mossbauer spectroscopy, infrared spectroscopy, and energy dispersive spectroscopy EDS. These methods should always augment standard polarized light microscopy, a technique which is sometimes overlooked but often where fundamental occurrences or petrologic relationships are established.

The clay minerals are a part of a general but important group within the phyllosilicates that contain large percentages of water trapped between the silicate sheets. Most clays are chemically and structurally analogous to other phyllosilicates but contain varing amounts of water and allow more substitution of their cations. There are many important uses and considerations of clay minerals. They are used in manufacturing, drilling, construction and paper production [24].

Clay minerals tend to form microscopic to sub microscopic crystals. When mixed with limited amounts of water, clays become plastic and are able to be molded and formed in ways that most people are familiar with as children's clay.

Clays tend to form from weathering and secondary sedimentary processes with only a few examples of clays forming in primary igneous or metamorphic environments.

Clays are rarely found separately and are usually mixed not only with other clays but with microscopic crystals of carbonates, feldspaths, micas and quartz.

Clay minerals are divided into four major groups. These are the important clay mineral groups [24]:

II-1-1 : The Kaolinite Group

This group has three members (kaolinite, dickite and nacrite) and a formula of $Al_2Si_2O_5(OH)_4$. The different minerals are polymorphs, meaning that they have the same chemistry but different structures. The general structure of the kaolinite group is composed of silicate sheets (Si_2O_5) bonded to aluminum oxide/hydroxide layers ($Al_2(OH)_4$) called gibbsite layers. The silicate and gibbsite layers are tightly bonded together with only weak bonding existing between the s-g paired layers.

II-1-2 : The Illite (or The Clay-mica) Group

This group is basically a hydrated microscopic muscovite. The mineral illite is the only common mineral represented, however it is a significant rock forming mineral being a main component of shales and other argillaceous rocks. The general formula is $(K, H)A_{l2}(Si, Al)_4O_{10}(OH)_2 - xH_2O$, where x represents the variable amount of water that this group could contain. The structure of this group is similar to the montmorillonite group with silicate layers sandwiching a gibbsite-like layer in between, in an s-g-s stacking sequence. The variable amounts of water molecules would lie between the s-g-s sandwiches as well as the potassium ions.

II-1-3 : The Chlorite Group

This group is not always considered a part of the clays and is sometimes left alone as a separate group within the phyllosilicates

II-1-4 : The Montmorillonite/Smectite Group

This group is composed of several minerals including pyrophyllite, talc, vermiculite, sauconite, saponite, nontronite and montmorillonite. They differ mostly in chemical content.

The general formula is (Ca, Na, H)(Al, Mg, Fe, Zn)$_2$(Si, Al)$_4$O$_{10}$(OH)$_2$ - xH$_2$O, where x represents the variable amount of water that members of this group could contain. Talc's formula, for example, is $Mg_3Si_4O_{10}(OH)_2$. The gibbsite layers of the kaolinite group can be replaced in this group by a similar layer that is analogous to the oxide brucite, ($Mg_2(OH)_4$). The structure of this group is composed of silicate layers sandwiching a gibbsite (or brucite) layer in between, in an s-g-s stacking sequence. The variable amounts of water molecules would lie between the s-g-s sandwiches.

II-2 Structure

Like all phyllosilicates, clay minerals are characterised by two-dimensional sheets of corner sharing (see fig. II-1) SiO_4 and AlO_4 tetrahedra. These tetrahedral sheets have the chemical composition $(Al,Si)_3O_4$, and each tetrahedron shares three of its vertex oxygen atoms with other tetrahedra forming a hexagonal array in two-dimensions. The fourth vertex is not shared with another tetrahedron and all of the tetrahedra "point" in the same direction (i.e. all of the unshared vertices are on the same side of the sheet) (see figure II-1).

In clays the tetrahedral sheets are always bonded to octahedral sheets formed from small cations, such as aluminium or magnesium, coordinated by six oxygen atoms. The unshared vertex from the tetrahedral sheet also form part of one side of the octahedral sheet but an additional oxygen atom is located above the gap in the tetrahedral sheet at the center of the six tetrahedra. This oxygen atom is bonded to a hydrogen atom forming an OH group in the clay structure. Clays can be categorised depending on the way that tetrahedral and octahedral sheets are packaged into layers. If there is only one tetrahedral and one octahedral group in each layer the clay is known as a 1:1 clay. The alternative, known as a 2:1 clay,(Table 1) has two tetrahedral sheets with the unshared vertex of each sheet pointing towards each other and forming each side of the octahedral sheet.

Bonding between the tetrahedral and octahedral sheets requires that the tetrahedral sheet becomes corrogated or twisted, causing ditrigonal distortion to the hexagonal array, and the octahedral sheet is flattened. This minimizes the overall bond-valence distortions of the crystallite [25].

Depending on the composition of the tetrahedral and octahedral sheets, the layer will have no charge, or will have a net negative charge. If the layers are charged this charge is balanced by interlayer cations such as Na^+ or K^+. In each case the interlayer can also contain water. The crystal structure is formed from a stack of layers interspaced with the interlayers [25].

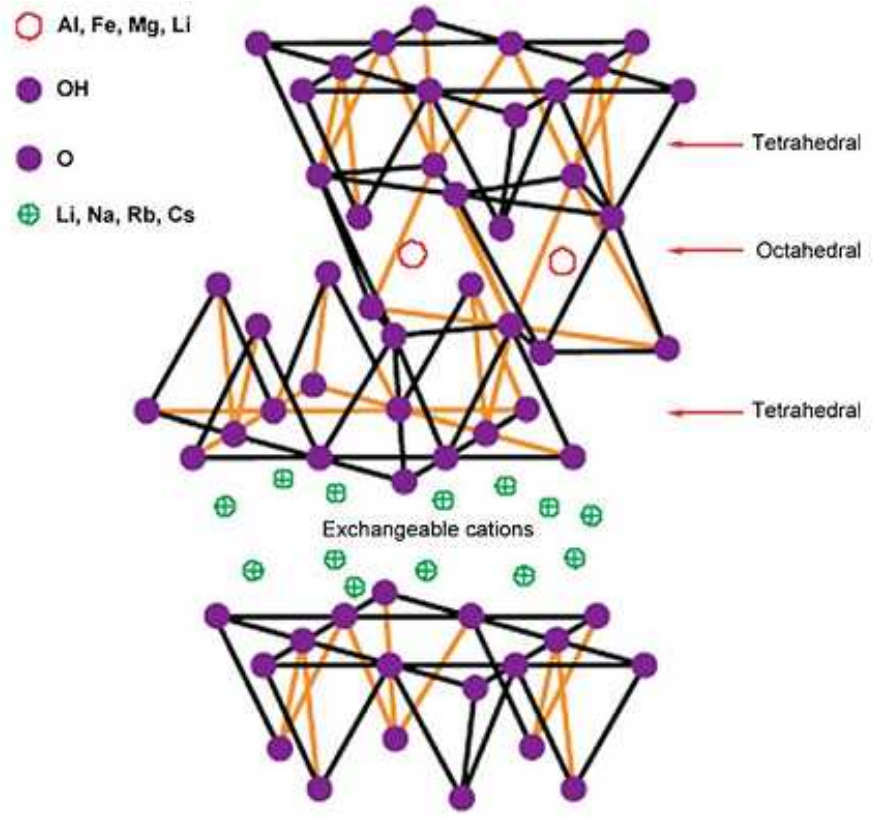

Figure II.1: Chemical structure of montmorillonite clay

Table1: Chemical structure of commonly used 2:1 phyllosilicates [26]

2:1 Phyllosilicates	General formula
Montmorillonite	$Mx(Al_4–xMgx)Si_8O_{20}(OH)_4$
Hectorite	$Mx(Mg_6–xLix)Si_8O_{20}(OH)_4$
Saponite	$MxMg_6(Si_8–xAlx)O_{20}(OH)_4$

M monovalent cation; x degree of isomorphous substitution (between 0.5 and 1.3)

II- 3 Classification of the Processing of Nanocomposites

Four different techniques for production of polymer Nano composite are available:

1. In situ polymerization
2. Melt blending
3. Solvent method
4. Sol–gel method

The in situ polymerization and the melt blending methods are the most commonly used techniques for manufacturing thermosetting and thermoplastic nanocomposites,

II-3-1: In Situ Polymerization Process

In situ polymerization was the first technique used to synthesize nano composite materials based on polyamide/nanoclay [27]. In principle, it is a very simple technique and is schematized in Fig. II.2. The organic-modified layered silicate is swollen within a liquid monomer or a monomer solution so that the monomer can penetrate into the interlayer space between lamellae [28].

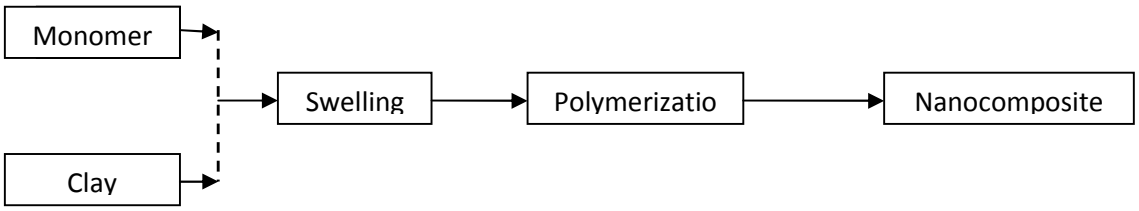

Figure II-2 Schematic diagram showing the in situ polymerization process

Then a polymerization reaction is initiated between the intercalated sheets by heat, radiation, diffusion of a proper initiator or by a catalyst fixed through cationic exchange inside the interlayer before the swelling. Polymerization produces long chain polymers within the clay galleries resulting in an intercalated Nanocomposite. Balancing intra- and extra-gallery polymerization rates, the clay layers can delaminate and the resulting material can be characterized by an exfoliated structure. This method can be used both on thermoplastic and thermosetting polymers with different nanofillers, e.g., layered silicate or metallic oxides, and can be combined with shear compounding to optimize nanofiller dispersion. Recently, this method has been applied directly to polymer extrusion, obtaining the nanocomposite in a single step by means of a highly productive industrial technique [29].

The in situ polymerization method has been used for nanocomposite manufactured with different kinds of thermoplastic polymer matrices, such as polyolefins (PP, PE, EVA) [30-33], polyethylene terephthalate (PET) [34], polymethylmethacrylate(PMMA) [35], etc. For example PET/MMT intercalated nano composite (NC) were obtained by using the in situ polymerization between the organoclay and PET monomers (ethylene glycol and terephthalic acid) [34].

II-3-2 : Solvent Method

This method is also known as intercalation of polymer or pre-polymer from solution when applied to prepare nanocomposite with layered silicates. It is based on a solvent system in which the polymer or pre-polymer is soluble and silicate layers are swellable [36]. The layered silicate is first swollen in a solvent, such as water, chloroform, toluene or other organic solvent able to swell the clay and dissolve the polymer. When the polymer and layered silicate solutions are mixed, the polymer chains intercalate and displace the solvent within the interlayer of the silicate. Upon solvent removal (done by means of solvent evaporation [37] or precipitation in non-solvent media [38], the intercalated structure remains, resulting in polymer/layered silicate Nnanocomposite as

schematically represented in Fig. II-3. This method is good for the intercalation of polymers with little or no polarity into layered structures and facilitates production of thin films with polymer-oriented clay intercalated layers.

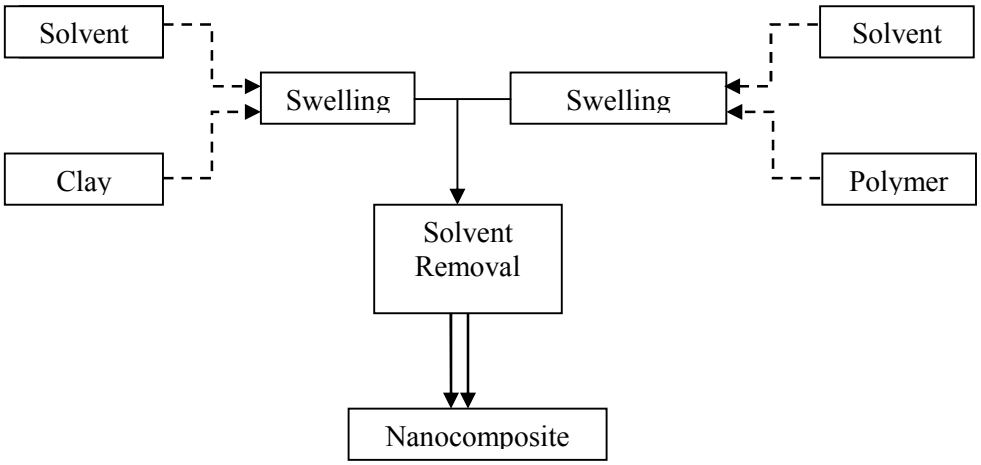

Figure. II-3: Schematic diagram showing the solvent method

II-3-3 : Sol–Gel Process

The sol–gel method is widely used in the preparation processes for inorganic/organic nanocomposite [39]. The advantages of the sol–gel method are first the synthesis process is done at room temperature and second organic polymers can be introduced at the initial stage, in which the nanoparticle of sol can remain homogeneously dispersed at a nanometric scale. The sol–gel method consists of hydrolysis of the constituent molecular precursors and subsequent polycondensation to glass-like form. It allows incorporation of organic and inorganic additives during the process of formation of the glassy network at room temperature. This method has been used traditionally to fabricate glasses and ceramics[39]..

II-3-4: Melt Blending.

Extrusion melt compounding of dispersive nanofillers with polymeric materials is considered the most effective way for producing nanocomposites. From the practical point of view, if technologically possible, this process is more economical and more profitable than in situ polymerization, solvent casting techniques and sol–gel methods. This procedure allows NC to be formulated using ordinary compounding devices: extruders or special mixers, without the necessity of using advanced polymer technology. The melt blending technology does not represent any limitation, provided that the best mixing condition and formulation are defined for each polymer. Indeed mixing parameters strongly affect the polymeric nanocomposite morphology [40].

NC preparation has been reported by using new mixing devices imparting elongational flow rather than shear flow. Utracki carried out melt compounding using an extensional flow mixer (EFM) attached to a single screw extruder or a twin screw extruder [41]. The preparation of PA6 (Nylon-6) and PP composites was accomplished by using the above extruders with or without EFM. By comparing the NC final features, the most effective method turned out to be the one based on a single screw extruder with EFM. More recently it was demonstrated that the elongational deformation, which the material undergoes during an injection molding process, might favor the clay dispersion in the polymer matrix [42]. However, no matter how well these process considerations are optimized, it is clear that complete dispersion of nanoparticles, or nearly so, cannot be achieved unless there is a good thermodynamic affinity between the nanofiller surfaces and the polymer matrix.A. More recently [43] the nanostructure and micromechanical properties of reversibly crosslinkined isotactic polypropylene/clay composites was followed by melt compounding.

II-4: Modification of Na^+MMT Clays:

The MMT (Na^+MMT) clays are hydrophilic in nature and most polymers are hydrophobic or water susceptible in nature. As a result, they are not compatible with each other. However, The MMT clays have a unique structure and high intercalation capabilities which allow them to be chemically modified by organic molecules that are compatible with polymers which make them attractive in clay based polymer nanocomposite. Na^+MMT clays have unique structure with a thickness about 1 nm and an aspect ratio of 100-1500. They also have low layer charges which lead to weak forces between the adjacent layers. This makes interlayer cations exchangeable. These interlayer cations can be replaced by inorganic and organic cations by facile methods, which is an important aspect of their use in polymer nanocomposites fabrication [44-46].

In clay modification, mostly interlayer cations (Na^+, Ca^{2+}) are replaced by organic bulky ammonium or phosphonium cations [46,47]. This leads to an increase in interlayer spacing and a decrease in clay layer-layer attraction. The quaternary ammonium ions are normally chosen to make clays compatible with polymer resin (Fig. II.4).

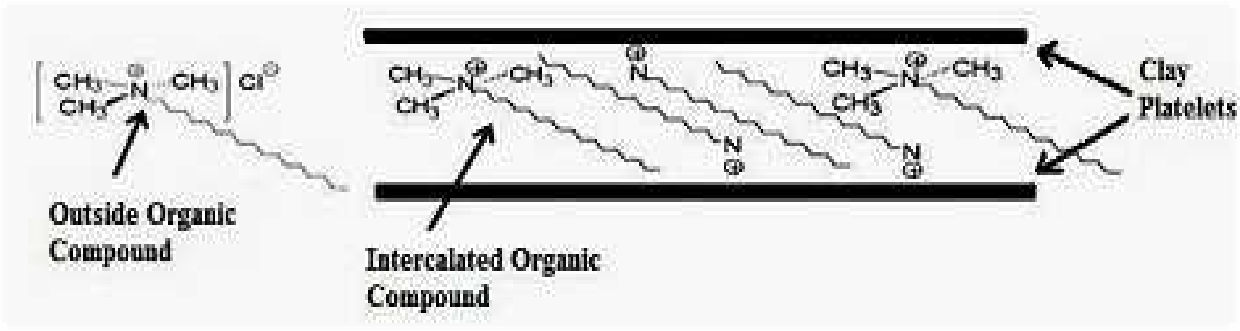

Figure II.4: Modification of clay by long chain bulky ammonium ion [47]

The molecular structure of ions, such as alkyl chain length, number of alkyl chains and insaturations, is an important factor determining compatibility and thermal stability of polymer/MMT nanocomposites [47]. These modifying agents are getting significant success in preparation of polymer nanocomposite; however, their main shortcoming for PET nanocomposites is their poor thermal stability.

II-5: Advantages of Polymer/Clay Nanocomposite [48]:

- Mechanical properties: Increased strength and stiffness, high elongation of the matrix. Decreased permeability to gases and water: Increased permeation resistance helps to increase shelf-life of nanocomposite packaged materials
- Transparency: Low loadings and good filler dispersion maintain inherent polymer transparency
- Recyclability: Thermally stable nanofillers are not affected or degraded during processing, physical properties of polymer composites are not seriously affected by recycling
- Flame resistance: Good dispersed nanofillers increase thermal stability, excellent flame resistance
- Transport properties: Density of nanocomposites do not increase too much as percolation at very low loadings in high aspect ratio systems

Depending on the nature of compounding and processing conditions, two types of structure can be formed when clay platelets are dispersed into a polymer (Fig.II-5). Sometimes polymer can not intercalate into the galleries of clay platelets, which leads to formation of conventional composites. Properties of such composites are similar to those of polymer composites reinforced by micro particles.

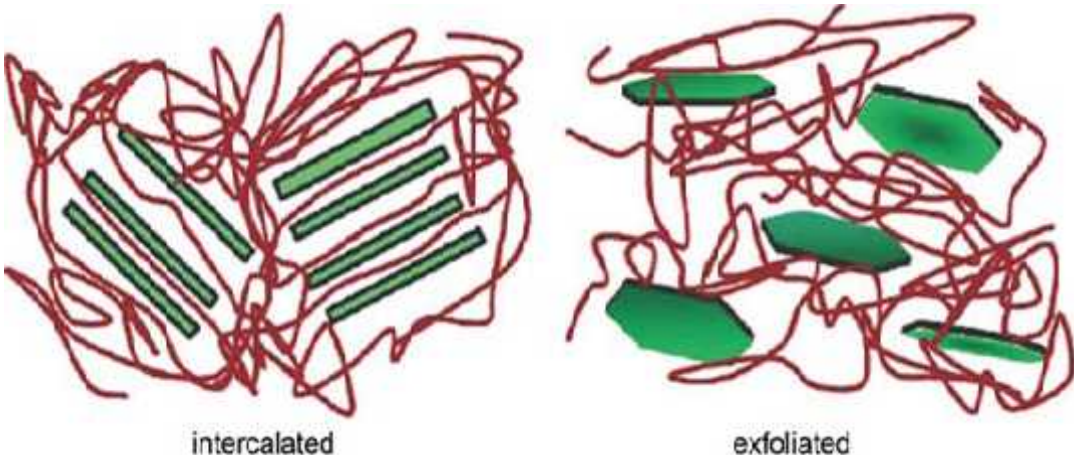

Figure II.5: Schematic illustration of two different types of achievable polymer/layered silicate, intercalated and exfoliated [49, 50]

When extended polymer chains are inserted into interlayer spaces of clay platelets, they increase the interlayer gallery space between clay platelets, however most of the time they do not separate clay platelets completely and result in a well ordered multilayer stacking alternately polymer layers and clay platelets, this leads to intercalated nanocomposites. The other type is the exfoliated nanocomposites, in which the clay platelets are completely and uniformly dispersed in a continuous polymer matrix. Completely exfoliated nanocomposites have shown excellent increase in barrier and mechanical properties of polymers. There are different theoretical models that have been suggested to explain these increases in barrier and mechanical properties.

II.6 Need for Polymer Nanocomposites:

Polymer nanocomposites are the materials in which nano-sized inorganic particles, typically nano-scale in at least one dimension, are dispersed in organic polymer matrices in order to dramatically improve the performance properties of the polymer. They are a new class of polymer composites that contain relatively small amounts (<10%) of nanometer-sized clay particles. The particles, due to their extremely high aspect ratios (about 100-1500), and high surface area (750-800 m^2/g) promise to improve structural, mechanical, thermal and barrier properties without substantially increasing the density or reducing the optical properties of the polymer [51, 52].

Polymer nanocomposites can be prepared from a variety of nanoparticles, including disk-like nanoparticles (clay platelets), spherical and polyhedral nanocomposite (colloidal silica) and nanofibers (nanotubes, whiskers) [**53, 54**]. We are focusing on clay based polymer nanocomposites because they are to date the most attractive and promising polymer nanocomposites. The layered clays, which can be used to prepare polymer nanocomposites, may be divided into natural clays (montmorillonite, hectorite and saponite) and synthesized clays (fluorohectorite, laponite, and hydrotalcite). Among them, montmorillonite (MMT) is the most commonly used one for the preparation of polymer nanocomposite [**52**]. Polymer nanocomposites show many dramatically improved properties together with some novel properties not exhibited by the individual components or their macro and micro counterparts.

II-7. Conclusion.

The academic and industrial aspects of the preparation, characterization, materials properties, crystallization behavior, melt rheology, and processing of polymer/layered silicate nanocomposites. is becoming nowadays more and more investigated. These materials are attracting considerable interest in polymer science research. Montmorillonite is among the most commonly used smectite-type layered silicates for the preparation of nanocomposites. Smectites are a valuable mineral class for industrial applications because of their high cation exchange capacities, surface area, surface reactivity. In their pristine form they are hydrophilic in nature, and this property makes them very difficult to disperse into a polymer matrix. The most common way to remove this difficulty is to replace interlayer cations with quarternized ammonium or phosphonium cations, preferably with long alkyl chains.

In general, polymer/layered silicate nanocomposites are of three different types, namely (1) intercalated nanocomposites, for which insertion of polymer chains into a layered silicate structure occurs in a crystallographically regular fashion, with a repeat distance of few nanometers, regardless of polymer to clay ratio, (2) flocculated nanocomposites, for which intercalated and stacked silicate layers flocculated to some extent due to the hydroxylated edge–edge interactions of the silicate layers, and (3) exfoliated nanocomposites, for which the individual silicate layers are separated in the polymer matrix by average distances that depend only on the clay loading. This new family of composite materials frequently exhibits remarkable improvements of material properties when compared with the matrix polymers alone or conventional micro- and macro-composite materials.

Chapter III

Plastics recycling

III-1 Introduction

For more than 100 years, plastic products have revolutionized the way we live. Polyethylene terephthalate, or PET ,is a particularly notable example. Global consumption of PET for packaging is valued at $17 billion this year, and is forecast to reach $24 billion by 2011. Asia Pacific, central and eastern Europe, and parts of Latin America showed the strongest growth between 2001and 2006. The United State is the largest user of PET packaging, followed by China and Mexico [55].

Polyethylene terephthalate is a thermoplastic polymer resin of the polyester family that is produced by the chemical industry and is used in synthetic fibers; beverage, food and other liquid containers; thermoforming applications; and engineering resins often in combination with glass fiber. It is one of the most important raw materials used in man-made fibers. It also used for microwave food trays and food packageing films. This is due in part to its inherent properties that are well suited for light weight, large-capacity and shatter-resistant containers. because it provides an excellent barrier against oxygen and carbon dioxide and due to consumer trend favoring healthier beverage options, the carbonated soft drink sector has been growing more rapidly than other applications in the past five years.

Because of these wide spread applications the PET waste disposal poses a serious problem to maintain a clean environment. However, the most important cause for recycle and reprocess the waste PET has arisen from the awareness and concern for environmental pollution. PET recycling represents one of the most successful and widespread examples of polymer recycling. The main driving force responsible for this increased recycling of post-consumer PET is its wide spread use, particularly in the beverage industry. A very important feature of PET, decisive in the choice of its wide application in the manufacture of packaging for the food industries is that it does not have any side effects on the human beings. It should be pointed out, that PET does not create direct hazard to the environment, but due to its substantial fraction by volume in the waste stream and its high resistance to the atmospheric and biological agents, it is seen as anxious material. Therefore, the

recycling of PET does not only serve as a partial solution to the solid waste problem but also contributes to the conservation of raw petrochemical products and energy. Products made from recycled plastics can result in50–60% energy saving as compared to making the same product from virgin resin.

III-2 Classification of Polymer Recycle

The recycling of waste polymers including PET can be carried out in many ways. Four main classes have been proposed: primary, secondary, tertiary and quaternary recycling.

III-2-1: Primary recycling (pre-consumer industrial scrap)

It is the recycling of clean, uncontaminated single-type waste which remains the most popular, as it ensures simplicity and low cost, especially when done‘‘in-plant’’ and feeding with scrap of controlled history [56]. The recycled scraps or wastes are either mixed with virgin material to assure product quality or used as a second-grade material [57]. Primary recycling of industrial scraps produced during the manufacture of food-contact articles is not expected to pose a hazard to the consumer.

III-2-2:- Mechanical recycling (secondary recycling)

In this approach, the polymer is separated from its associated contaminants and it can be readily reprocessed into granules by conventional melt extrusion. Mechanical recycling includes the sorting and separation of the wastes, size reduction; melt filtration and reforming of the plastic material. The basic polymer is not altered during the process. The main disadvantage of this type of recycling is the deterioration of product properties in every cycle. This occurs since the molecular weight of the recycled resin is reduced due to chain-scission reactions caused by the presence of water and trace of acidic impurities. A secondary recycling process presents some problems that may cause it to be inappropriate for the production of food-contact articles, particularly if the recycler had little or no control over the waste stream entering the recycling facility [58–60].

III-2-3: Chemical recycling (tertiary recycling)

Unlike physical recycling, chemical recycling involves transformation of polymer chain. The polymer backbone under the recycling process is degraded into monomer units (i.e. depolymerisation) or randomly ruptured into larger chain fragments (i.e. random chain scission) with associated formation of gaseous products. The chemical recycling is carried out either by solvolysis or by pyrolysis; the former through degradation by solvents including water, and the latter through degradation by heat in absence of oxygen or air, or vacuum. Chemical recycling yields monomers, petroleum liquid sand gases. Monomers are purified by distillation and drying, and used for manufacture of polymers.

III-2-4: Energy recovery (quaternary recycling)

The energy content of plastics wastes can be recovered by incineration. When the collection, sorting and separation of plastics wastes are difficult or economically not viable, or the waste is toxic and hazardous to handle, the best waste management option is incineration to recover the chemical energy stored in plastics wastes in the form of thermal energy. This is carried out in special type of reactors called incinerators, to burn wastes in the presence of air in a controlled manner to convert hydrocarbons of the plastic into carbon dioxide and water. The heat produced by burning plastics in the waste in the form of superheated steam can be utilized for generating electricity through turbine generators, and the residual heat from the waste stream is used for heating residential and industrial buildings. The melt residue from the incinerator is free from toxicity hazards and may be disposed off by landfill.

Although polymers are actually high yielding energy sources, this method has been widely accused of being ecologically unacceptable owing to the health risk from airborne toxic substances such as dioxins (in the case of chlorine containing polymers). It should be admited that it is not possible to have zero-emission in the incineration of waste plastic. Apart from the aforementioned

methods,direct reuse of a plastic material (i.e., PET) could be considered absorb contaminants that could be released back into food when the bottle is refilled. Moreover, refilling of a PET bottle with a drink with high alcohol content may lead to degradation of the macromolecular chains with unexpected

results. Worldwide, the main end-use of post-consumed PET is for the production of fibers (almost70%), with only 4 % of PET recycled with chemical methods. Among the above recycling techniques, the only one acceptable according to the principles of sustainable development (development that meets the needs of the present generation with out compromising the ability of Future generations to meet their needs) is chemical recycling, since it leads to the formation of the raw materials (monomers) from which the polymer is made [57]. It his way the environment is not surcharged and there is no need for extra resources (monomers) for the production of PET.

III-3: Uses of plastic (PET)

Plastics are used in a wide range of applications and some plastics items, such as food packaging, become waste only a short time after purchase. Other plastic items lend themselves to be reused many times over [61].

Plastic is preferable to recycling as it uses less energy and fewer resources. Long life, multi-trip plastics packaging has become more widespread in recent years, replacing less durable and single-trip alternatives, so reducing waste. According to Environment Agency report, 80% of post-consumer plastics wastes is sent to landfill, 8% is incinerated and only 7% is recycled. In addition to reducing the amount of plastics waste requiring disposal, recycling plastic can have several other advantages [62]:

- Conservation of non-renewable fossil fuels - Plastic production uses 8% of the world's oil production, 4% as feedstock and 4% during manufacture.

- Reduced consumption of energy.
- Reduced amounts of solid waste going to landfill.
- Reduced emissions of carbon-dioxide (CO_2), nitrogen-oxide (NO) and sulphur-dioxide (SO_2).

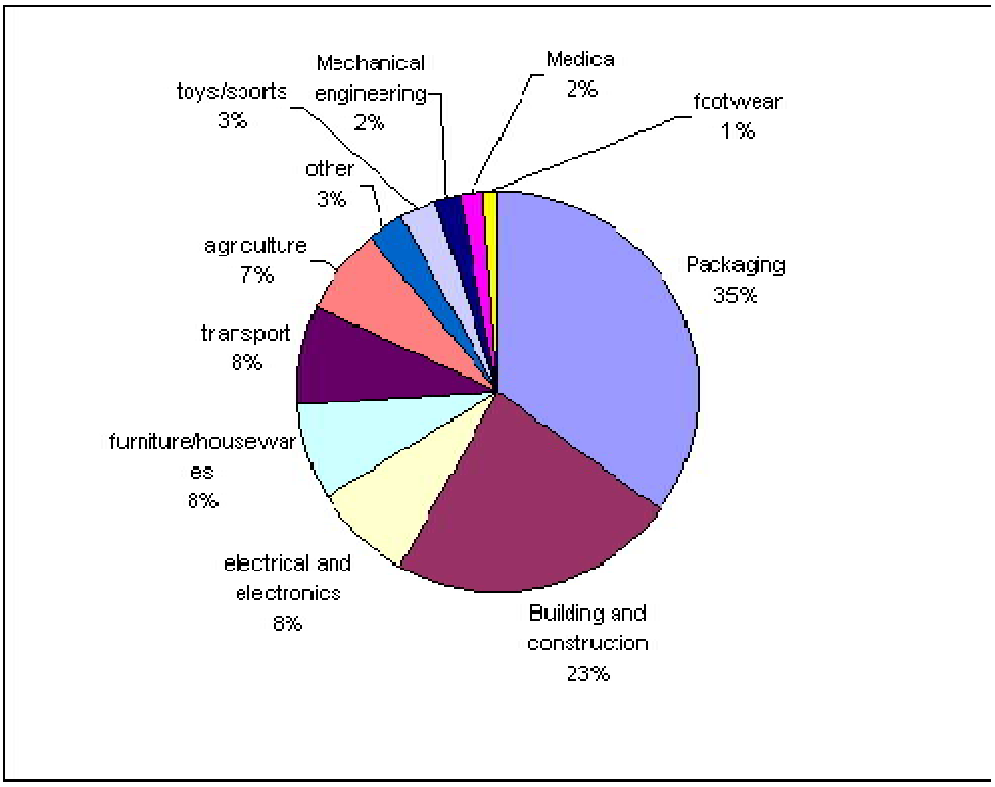

Figure III-1: % use of Plastics consumption 2002[61].

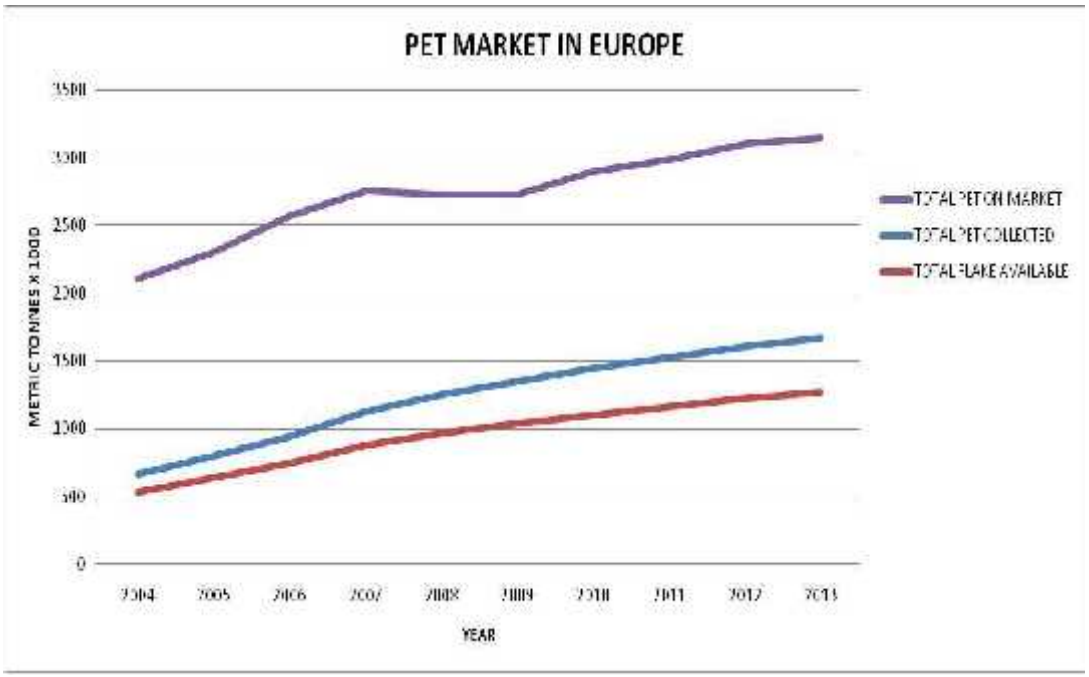

Figure III-2: Total PET market in Europe [63]

Tables 2 and 3 are providing a complete summary about PET resin production and bottle PET recycling accross the World. The triumphal procession of the PET bottle started during the 90th of the last century and we have not yet reached the stage of saturation. Table 2 is showing the expected market development of the bottle resin between 2004 and 2010 [63].

Table 2: Bottle PET resin production 2004 – 2010

PET Resin Capacity [kt/a]	2004	2005	2006	2007	2008	2009	2010
North America	3 686	3 745	3 923	4 595	4 595	4 595	5 000
South America	513	500	500	725	950	950	1 200
Europe	2 411	2 895	3 515	3 766	4 005	4 005	4 205
Africa, Middle East	308	338	499	604	843	843	843
Asia (ex China)	4 107	4 411	4 636	4 636	4 636	4 636	4 636
China	1 469	2 490	3 217	3 255	3 255	3 255	3 255
Total WORLD	12 493	14 378	16 290	17 585	18 284	18 284	19 139

The huge potential of PET bottle recycling is becoming obvious by comparing data of resin and flake production in Tables 2 and 3. If the production amount estimated at 5 Mi tons in 2010 is realistic, the amount of world wide recycling achieved is a little more than 25% [63]..

Table 3: Bottle PET recycling market development estimation

R-PET Capacity all in [kt/a]	1999	2002	2003	2004	2006	2010
North America	470	480	500	550	600	800
Europe	211	350	430	680	944	1200
ME, Asia, South America, Others	218	370	470	680	1700	3000
World R-PET Bottle Flakes	899	1 200	1 400	1 900	3 100	5 000
World PET-resin	7 100	9 900	11 800	12 500	16 300	19 200
Recycling potential	6 201	8 700	10 400	10 600	13 200	14 200

III-4. Conclusion.

Extensive use of polymeric materials, lead to the waste disposal management difficulties. Incineration helps produce energy but has problem of emission of toxic fumes and gases due to the decomposition of polymer chain molecules and particular additives present. Land filling of plastics is not preferred because of space constraints and land pollution. On the other hand recycled polymers are also not a permanent solution either since recycling led to the poor quality product.

Since PET is light in weight, its feedstock are readily available and cheap, and the energy requirement for PET processing and fabrication for consumer articles is the lowest of those for the other materials. This has resulted in the single use of PET products for mass consumption, and consequently a large volume of such products are being thrown into the garbage. It is true that disposal of PET waste, if done in the same way as followed for other materials, may create environmental problems. That PET is made durable according to the market demand, is the reason for their persistence in the environment causing litter problem and pollution. Thus PET become a red herring to the environmentalists.

Chapter IV

Microhardness

IV-1 Introduction :

Microindentation with a point indenter involving a deformation on a very small scale is one of the simplest methods of determining the microhardness of a material. The method uses a diamond pyramid indenter which penetrates the surface of a specimen upon application of a given load at a constant rate. A convenient measure of the hardness may be obtained by dividing the peak contact load P by the projected area of impression A, H= P/A. Microhardness has been used for a very long time to characterize metals and ceramics, when it has been shown to be sensitive to chemical composition and microscopic structure of the materials [64,65]. The application techniques to polymers are a new approach with a great potential for the characterization of solid molecular materials. During the last two decades, investigations of the microhardness properties of polymers have evolved from topics applied significance [66] to fundamental studies aiming at acquiring an understanding about the morphology-property relationship of these materials [67,68].

IV-2: Geometry of indentation:

Figure IV-1 shows the contact geometry for a pyramid indenter (with a semi angle α of 74°). This is the most common geometry in indentation tests because of the geometrical similarity of the residual impressions. The contact pressure is then independent of indent size, and thus affords a convenient measure of the hardness [64]. According to Marsh [69], the material under the indenter consists of a zone of plastic deformation (a few times the penetration distance h) surrounded by a larger outer zone of elastic deformation. The strain boundaries below the indenter for plastic deformation have been shown to depend on the morphology of the polymer material. Typical loads of 50 mN, using a square based diamond (Vickers) of ~200 µm in height, when applied onto the surface of a conventional polymer PET, produce penetration depth, h, of about 3-4 µm. Thus with this technique we can displace and plastically deform stacks of a few hundreds of crystals. In other words, we probe the surface of the polymer sample “quasi” non destructively within a small volume

element. During an indentation cycle the following effects must be distinguished [67]:

a) An elastic deformation upon removal of the load leading to a recovery of the indentation.

b) A permanent plastic deformation (measure of hardness).

c) A time dependant contribution during loading (creep).

d) A long delay recovery of indentation after load removal (viscoelastic relaxation).

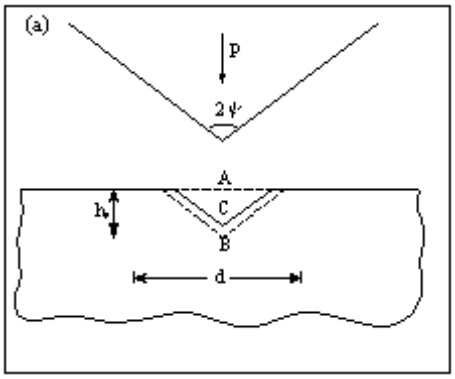

Figure IV-1: Contact geometry for pyramid indenter with a semi angle of 74°, A) zero load; B) maximum load and C) complete unload

IV-3: Hardness of semicrystalline polymers.

The unoriented semicrystalline polymer can be considered as a two phase composite of amorphous compliant regions sandwiched between hard crystalline lamellae (figure IV-2- top). Crystal lamellae are normally 10-25 nm thick (l_c) and have transverse dimensions of 0.1-1 µm while the amorphous layer thickness l_a has dimensions of 5-10 nm. Melt crystallized polymers generally exhibit a spherulitic morphology in which ribbon-like lamellae are arranged radially in polycrystalline aggregates [70]. Since the indentation process involves plastic yielding under the stress field of the indenter, microhardness is correlated to the modes of deformation of the semicrystalline polymer. These involve, at small strains, shearing motions of lamellae and lamellar separation. Beyond the yield point, irreversible deformation processes take place, including lamellar fracture, microfibrillation.

In dealing with the hardness of semicrystalline polymers it has long been recognized that the following general empirical relationship holds [67]:

$$\mathbf{H = \alpha H_c + (1-\alpha) H_a} \qquad \textbf{(eq. 3)}$$

Where H_c and H_a are the intrinsic hardness values of crystalline and amorphous phases and α is the volume fraction of crystalline material. In the simple case of flexible polymers like polyethylene (PE) or polyethylene oxide (above Tg) with rubbery amorphous layers [67] (when indentation is done at Tg <T<Tm), H_a «H_c and we are led to

$$\mathbf{H \sim \alpha H_c} \qquad \textbf{(eq. 4)}$$

This equation assumes that the semicrystalline polymer is a two-phase system and that hardness is due to plastic deformation taking place only in the crystalline regions. However for polymers like Poly(ethylene terephtalate) PET or Poly(ether-ether-ketone) PEEK, when Tg >T >Tm; Ha ≠0 [68].

IV-4: Models to predict hardness of lamellar crystals

From equation 4 it is clear that α controls the microhardness value of a polymer. However, the structure of the semicrystalline polymer, as pointed out above, is characterized by stacks of crystalline lamellae. It was soon recognized the direct influence of crystal thickness l_c upon microhardness in case of chain extended polyethylene samples [67]. Popli and Mandelkern [71] and Crist et al [72] provided later independent evidence for the strong dependence of yield stress σ_y upon l_c . The above authors found that spherulite size does not have direct influence upon yield in PE. On the basis of heterogeneous deformation model involving the heat dissipated by plastically deformed, Balta Calleja and Killian [73] developed an approach to calculate the dependence of hardness on the average crystal thickness Figure IV-2 (bottom) shows the model of lamellar deformation under an indenter involving the generation of a number of shear planes.

The hardness of the crystals can then be described by :

$$H_c = \frac{H_c^{\infty}}{1 + b/l_c} \qquad \text{eq. 5}$$

Where H^{∞}_c is the hardness of an infinitely thick crystal (maximum possible value of dissipated energy through plastic deformation) and b is a parameter related to the surface free energy σ_e of a crystal and to the energy Δh required for plastic deformation of the crystals through formation of a great number of shearing planes. The parameter is equal to:

$$b = 2\,\sigma_e/\Delta h \qquad \text{(eq. 6)}$$

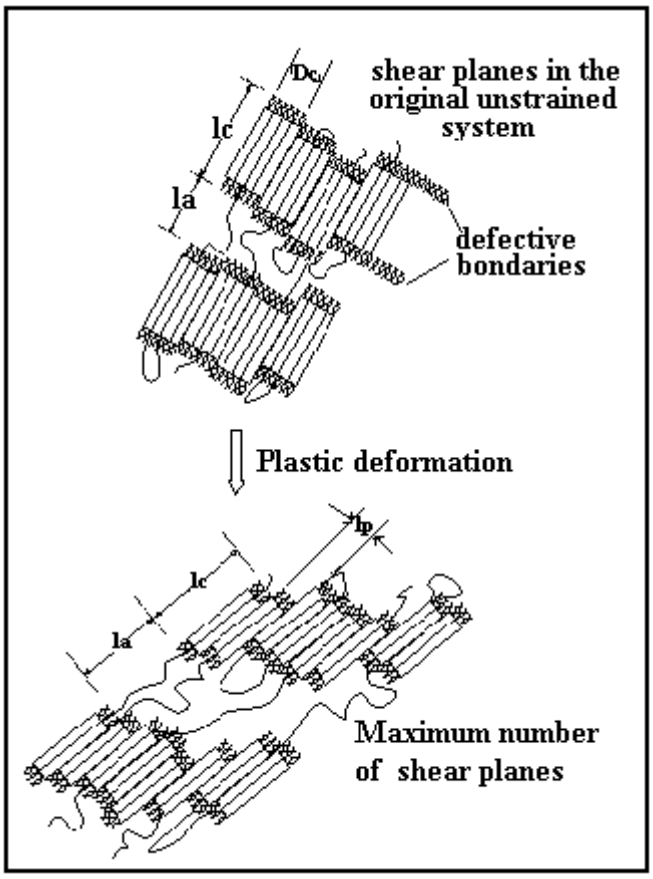

Figure IV-2 : Model of lamellae deformation under the stress field of the indenter [73]

IV-5: Polymer Blends

Other results show that hardness is a promising technique for the microstructural investigation of polyblends of known composition and can provide information on the level of structural segregation. The case of blends of low density and high density polyethylene is an example where the microhardness can be very well described in terms of an additive system of two independent components, H_1, (LD) and H_2 (HD) [74]

$$H_{blend} = H_1\Phi + H_2(1-\Phi) \qquad \textbf{(eq.7)}$$

Where Φ is the weigh fraction of the HDPE component. Equation 7 emphasizes the existence of distinct H values for the two phases owing to a molecular segregation at a crystal level.

In other systems like PE/PP/PA blends [75] a conspicuous deviation from the additivity law given by equation 7 is detected, in this case equation 7 can be written as:

$$H = \left[H_c^{PE}\alpha^{PE} + H_a^{PE}(1-\alpha^{PE})\right]\Phi^{PE} + \left[H_c^{PP}\alpha^{PP} + H_a^{PP}(1-\alpha^{PP})\right]\Phi^{PP} + \left[H_c^{PA}\alpha + H_a^{PA}(1-\alpha^{PA})\right]\Phi^{PA} \qquad \textbf{(eq. 8)}$$

Which describe the microhardness of the blend in terms of H values of the independent crystalline and amorphous components. It has been shown that the deviation from the additivity law is due to a decrease of the hardness values of the crystalline phase of PE and PP

IV-6. Conclusion.

Microhardness can be seen as a bridging parameter between microstructure and macroscopic mechanical properties. In semicrystalline polymers H can be described on the basis of a composite consisting of hard lamellae intercalated by compliant disordered layers. On can expect that the microhardness technique can lead to future developments in the understanding and characterization of physical aging phenomena in glassy polymers.

Also microhardness offers, in addition future posssibilies for the mechanical characterization of specific parts in a micron scale of processed polymers (prepared by extrusion injection molding etc), and therefore investigate the elastic and plastic flow properties of the near-surface region of polymer materials.

Chapter V

PREVIOUS RESEARCH WORK

V-1: Relation ship between surface and bulk morphologies For immiscible polymer blends

G.Verfaillie, J. Devaux, R. Legras [76]

The aim of their work was to investigate the relation existing between the surface and the bulk morphology in heterogeneous polymer materials after compression moulding. and also, to examine the influence of blend composition and processing conditions, keeping the moulding surface constant.

The surface morphology of compression-moulded PP/PET blends is investigated and compared to the bulk morphology. Before compression moulding the blends are prepared by melt mixing in a Brabender plastograph. Model experiments are developed to analyse the influence of the processing conditions and of the nature of the moulding surface on the surface and bulk morphologies. Films are prepared under different shear conditions with Poly Imide as the moulding surface.

Tey found that when a very low shear is applied the bulk and surface morphologies are very similar. However, the difference of polarity between the moulding surface, the dispersed phase and the matrix phase induces a difference indispersed phase size between the surface and bulk. The dispersed phase size at the surface is different than in the bulk. The difference can be attributed to the polarities of the moulding surface, the dispersed phase and the matrix. It is also shown that the concentration at the surface is equal to the bulk concentration when PET is the dispersed phase.

This is not the case when PP is the dispersed phase; this has to be attributed to the experimental setup (loss of nodules). Finally for processing times shorter than 8 min no change of the dispersed phase size and of concentration at the surface is observed.

When the shear on the blend is high, the surface morphology is strongly influenced by the interplay between flow and the affinity of the dispersed phase for the contact surface while the bulk morphology remains undeformed. In the case where the dispersed phase (PET) has a higher affinity for the moulding surface than the matrix, the surface is enriched in dispersed phase and when there

is no affinity for the moulding surface the dispersed phase (PP) shows a tendency to enter into the bulk.

V-2: Comparison of compatibilizer effectiveness for pet/pp blends: their mechanical, thermal and morphology characterization

C.P. Papadopoulou, N.K. Kalfoglou [77]

The authors have examined the compatibilizing efficiency for PET/PP blends using tensile testing, dynamic mechanical analysis (DMA), differential scanning calorimetry (DSC) and scanning electron microscopy of crycrofractured surfaces before and after etching. Compatibilizers used were maleic anhydride modified, PP (PP-*g*-MA), LLDPE (LLDPE-*g*-MA) and hydrogenated SBS block copolymer (SEBS-*g*-MA). Large deformation behavior of aged blends indicated that SEBS-*g*-MA performed best by far. However, addition of a thermoplastic polyolefin alloy (TPO), PP/ethylene–propylene copolymer, increased the compatibilizing efficiency of PP-*g*-MA to a level comparable to that of SEBS-*g*-MA. Improved efficiency of SEBS-*g*-MA and PP-*g*-MA 1 TPO compared to PP-*g*-MA or LLDPE-*g*-MA is attributed to better emulsification of the former at the interface, reduced migration of PP-*g*-MA into the PP phase and retardation of PET crystallization in the presence of the elastomeric additive. In addition, the elastomeric compatibilizers absorb more efficiently, the stresses developed at the PET/PP interface

V-3: Effect of incorporation of PET fibres on properties of PP/ elastomer blends

Lopez-Manchado and M. Arroyo[78]

The main goal of their study is to analyze the effect of the incorporation of short poly(ethyleneterephtalate) (PET) fibres on mechanical behaviour and morphology of thermoplastic elastomers based on Ethylene-Octene copolymer (PP/EOC) blends. The authors aimed to obtain composites with balanced properties, and analyze their behaviour /morphology relationship. The mechanical properties showed a strong dependence on matrix composition. So, as

the rubber content in the thermoplastic was increased, the material became more elastomeric, giving rise to a marked decrease in the modulus and material strength. On the other hand, incorporation of the PET fibres generated a more rigid and stable material, with better mechanical properties. These results strongly support the assumption that the PET fibres behave as a reinforcing agent for PP/octhene blends. It is important to note that this reinforcing effect is more significant with higher elastomer content in the thermoplastic.

These results are in concordance with those obtained by dynamic mechanical analysis, where an increment in the storage modulus was observed in the presence of PET tibres. The modulus gradually increased with increased fibre percentage in the composite. Microscopy conlfirrned the results of the composite behaviour, where good adhesion at the fibre-matrix interface was observed, which was correlated with improved composite properties.

V-4: Mechanical properties of polypropylene reinforced with recycled-PET fibres

Palova Santos, Sergio Henrique Pezzin [79]

The presence of rrecycled PET Fibers in a PP matrix can be an efficient way to recycle PET, increasing significantly the impact properties of the PP. Despite of the low amount of r-PETF (7%,w/w) incorporated to the PP, the results are interesting, even considering the lack of affinity of the PP (London dispersion forces) with the PET fibres (dipole–dipole interactions). Aiming to improve the affinity matrix–reinforcement and increase the content of r-PETF in the composite, it is suggested the addition of compatibilizers, as maleic anhydride, and the use of a twin screw extruder with feeding of fibre in the polymer melt to obtain a better homogenization of the fibre distribution in the matrix.

V-5: Microfibrillar reinforced composites from PET/PP blends: processing, morphology and mechanical properties

K. Friedrich et al [80]

The aim of there is to the manufacturing of a microfibrillar reinforced composites MFC structured blends from recycled PET and PP under industrially relevant conditions; and then study of the structure–property relationships of these materials after the different processing steps. The peculiarity of MFC offers the opportunity to use this approach for recycling purposes. The SEM observations show a high level of orientation, a high aspect ratio and a small diameter of the fibrils (300 nm–1 μm) as well as the effect of the compatibilizer upon the distribution and the size of the dispersed PET phase. The MFC blends with compatibilizer have shorter fibrils, because the compatibilizer forms a thin shell around the PET spheres and does not allow their coalescence. The MFC-structure could be preserved after the injection molded processing, although the orientation of the fibrils was random.

The flexural strength and modulus of the blends are superior by 60–70% to Those of the neat PP and blends without MFC structure; this fact demonstrates the reinforcing effect of the PET fibrils. Compression molded blend without compatibilizer represents an isotropic trans crystalline structures. The PP crystallites in the trans crystalline layers are reoriented at approximately 40° with respect to the direction of the fibrils. The presence of Ethylene-glycidyl Methacrylate (E-GMA as a compatibilizer in the blend hinders the nucleation effect of the PET fibril for the PP matrix during cooling from the melt.

The compression molded samples possess better mechanical indices (than the IM specimens) and even than those of the PP+GF, because of the uniaxial orientation of the PET fibrils (when being oriented in the samples length direction).

The impact energy of the injection molded unmodified PET/PP blend is lower than that of the neat PP because of the incompatibility between PET and PP samples but it increase with increasing amount of the compatibilizer. The impact energy of the compression-molded specimens with a Micro Fiber Composite structure is slightly higher than that of the PP+GF, and 3–4 times higher than that of the neat PP.

V-6: Microfibril reinforced polymer–polymer composites: Application of Tsai-Hill equation to PP/PET composites

C. Fuchs, D. Bhattacharyya, S. Fakirov [81]

The main goal of their work was to check the extent of Tsai-Hill equation's applicability to polymer–polymer microfibril reinforced composites MFC for characterizing their mechanical behaviour, especially in comparison to the common composites. In the MFC, the reinforcing elements represent microfibrils with diameters around 1–3 μm and aspect ratios of approximately 100. For this purpose, compression moulded plates from highly drawn bristles of a PP/PET (70/30 by wt%) blend has been prepared and its structure has been characterised by wide angle X-ray scattering and scanning electron microscope analysis. The WAXS and SEM characterization of the starting, intermediate and final material lead to the conclusion that : (i) the compression moulded PP/PET plates consist of a quasi-isotropic matrix (PP), reinforced with microfibrils (PET), (ii) the microfibrils in the plates are placed as uniaxially oriented morphological elements with almost no dispersion of the orientation angle, (iii) the plates represent a polymer–polymer composite with an MFC structure, and (iv) samples with such a structure provide a good scope for verifying the application of Tsai-Hill equation to polymer–polymer composites.

The measured values on test specimens cut out at various angles are shown to be slightly higher than the calculated values and this finding is explained by the higher aspect ratio, more homogenous fibril distribution and the better matrix/reinforcement adhesion. The fracture mechanism, as

concluded from the SEM observations, is also discussed and a definite change is foundin the failure mechanism (brittle to ductile) as the specimen angle (with respect to fibril axis) increases.

V-7: Effect of composition on transcrystallization with reorientation of polypropylene in drawn PET/PP blend

A. A Postolov, et al [82]

Studied the crystallization behavior of three blend compositions of poly (ethyleneterephthalate)/polypro pylene (PET/PP), namely 30/70, 50/50 and 70/30 wt.%. The samples were heated up to temperature between the melting temperatures of the blend components and then cooled to 30°C. The application of synchrotron radiation for WAXS studies offers the opportunity to observe the very first stages of crystallization and to reveal the chain orientation of the crystallized fractions

X-ray pictures were taken at every stage and it was shown that a recrystallization with reorientation of the PP crystallites took place during the non isothermal recrystallization. The PP crystallites in the PET/PP blend reorient with molecular axis tilted at approximately 49° against the fibber axis during the recrystallization. The amount of PP in the blend does not directly affect the process of trancrystallization with reorientation but has only a masking effect. Such reorientation was observed for all three blends. No reorientation occurs if the PET crystallites have been melted before the recrystallization, i.e., when oriented they induce the reorientation of the PP crystallites.

V-8: The role of the MMT on the morphology and mechanical properties of the PP/PET blends

C. I. W. Calcagno et al [83]

Polypropylene/poly(ethyleneterephthalate) blends containing montmorillonite (MMT) were prepared using a twin screw extruder followed by injection molding. The MMT dispersion was

evaluated byX-ray diffraction and transmission electron microscopy. The results showed a better dispersion of the MMT when maleic anhydride grafted polypropylene (PP-MA) was used. The clay was preferentially situated in the PP/PET interphase and in the PET phase. Scanning electron microscopy revealed the presence of elongated PET domains and fibers, besides the spherical shapes. The mechanical properties were studied through tensile and impact tests. The yield stress, Young modulus, and elongation at break increased when MMT and PP-MA were used without impair the impact strength. The dynamic mechanical properties were also evaluated. Higher E' values were observed for PP/PET/PP-MA/MMT.

It was demonstrated that the simultaneous incorporation of MMT and PP-MA into PP/PET blends has increased the mechanical properties relative to neat blend. Intercalated morphology was observed when MMT was used in the PP/PET blends. When PP-MA was used, the clay particles were smaller, and for all nanocomposites the clay was preferentially situated in the interphase and in the PET domains. PP/PET blends showed two phases in which PET appears as a dispersed phase with spherical shapes, elongated domains, and fibers. The PET domains in the compatibilized systems are smaller than in uncompatibilized. The elongated domains and fibers were originated in the extrusion. In the injection molding, besides the orientation of these domains with flow direction, a decrease of their diameter also occurs, probably due to elongation of the PET domains during the injection process. The PET domains were less susceptible to deformation in the PP/PET/PP-MA/MMT during the injection molding than in the PP/PET/PP-MA. When the clay was used, the uncompatibilized blend showed a decrease in mechanical properties due to the poor interfacial adhesion between the phases. In the PP/PET blends thee xclusive use of the clay was not enough to compatibilize the polymer phases. The optimum result was observed when simultaneously PP-MA and MMT were used. The dynamic mechanical behavior studies in the PP/PET blends had demonstrated that the incorporation of PET into PP matrix leads to an increase of the storage and loss modulus, and this increase was more significantly at temperatures higher than the Tg of the PP.

The shoulder in the E" temperature curve for the compatibilized nano composite in intermediate Tg's of the pristine polymers is an indicative of the formation of an interphase due to the interaction of the PP and PET. It is believed that when MMT are presented, it could constitute an interphase with PP, PET and PP-MA, promoting a better adhesion between PP and PET, and consequently improving the stress transfer between these phases.

V-9: Non-isothermal crystallization and melting behavior of compatibilized polypropylene/recycled poly(ethylene terephthalate) blends

Youji Taoa and Kancheng Mai , [84]

Binary blends of polypropylene (PP)/recycled poly(ethylene terephthalate) (r-PET), r-PET/ maleic anhydride grafted PP (PP-g-MA), r-PET/glycidyl methacrylate grafted PP (PP-g-GMA), and ternary blends of PP/r-PET (80/20 w/w) compatibilized with various amounts (2–10 wt%) of PP-g-MA or PP-g-GMA were prepared on a twin-screw extruder. The nonisothermal crystallization and melting behavior, and the crystallization morphology were investigated by DSC and POM. The chemical reactions of r-PET with PP-g-MA and PP-g-GMA were characterized by FT-IR. DSC results show that the crystallization peak temperatures of r-PET and PP increased when blending them together, due to the heterogeneous nucleation effect on each other. The of r-PET increased with increasing the content of PP-g-MA while slightly influenced by the content of PP-g-GMA in the binary blends of r-PET with grafted PP, implying different reactivity of r-PET with PP-g-MA and PP-g-GMA. The of PP in the ternary blends retained or slightly decreased, dependent on the compatibilizers and their contents. The melting peak temperature of r-PET in PP/r-PET blends compatibilized by PP-g-MA was lower than that of compatibilized by PP-g-GMA, indicating that PP-g-MA had stronger reactivity towards r-PET compared to PP-g-GMA. The crystallization and melting behavior of

blends was influenced by the pre-melting temperature, especially the melting behavior of r-PET in the blends. The crystallization behavior of PP in the blends was also evaluated by Mo's method. POM confirmed the heterogeneous nucleation effect of r-PET on PP.

Chapter VI

MATERIALS AND RESEARCH METHODOLOGY

VI-1: Materials

The materials used in this study were:

PET issued from bottles recycled material (melting range of 242–250° C); Bangkok

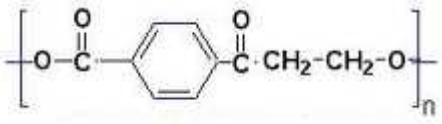

Polyester Public Co., Bangkok (Thailand)

The iPP is a commercial grade iPP EMB 13014C, Montell, Milan (Italy);

and SEBS-MAH compatibilizer is KRATON FG-1901X, Shell, The Hague (Netherlands).

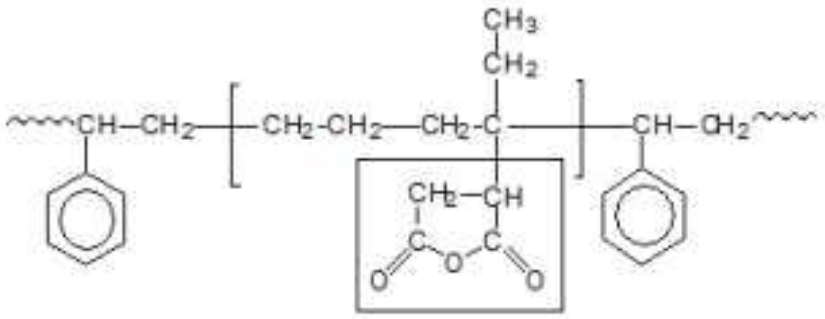

The KRATON thermoplastic rubber FG-1901X is a copolymer with three blocks of S-EB-S type which is grafted with about 2% by weight of maleic anhydride, the percentage of the polystyrene phase in the polymer is about 29% by weight It has a density of 0.919 g/cm^3 and a melting flow index (MFI) of 3.2 g/10 min at 230 ° C

The organophilic clay has been prepared in our laboratory by using bentonite (a montmorillonite-type silicate) supplied by Bental, Maghnia (Algeria); the preparation method is described next.

VI-1-1: Preparation of organophilic clay

All experiments in this work were carried out on the same lot of bentonite. The main characteristics of the bentonite are listed in Table 4 **[85,86].**

TableI 4: Chemical analysis of the natural bentonite used (wt%)

	SiO_2	Al_2O_3	Fe_2O_3	MgO	CaO	Na_2O	K_2O	TiO_2	As	LOI
%	69.4	14.7	1.2	1.1	0.3	0.5	0.8	0.2	0.05	11

LOI: Lost on ignition at 900 °

The treatment of natural bentonite by homo-sodium ion is to remove all impurities and crystalline phases contained in the clay (quartz, feldspath, calcite, organic materials) to replace all exchangeable cations by cations of sodium and collect all the same size fraction less than 2 nm. This is done in several stages wich are:

- Grinding of bentonite
- Purification of the bentonite ,
- Cation exchange,
- Washing, rinsing, drying, grinding, packaging.

The raw bentonite was first crushed and then filtered to eliminate impurities. Then,30 g was dispersed in 1L of a sodium chloride (NaCl) solution (1N), and the mixture was stirred for 24h; this operation was repeated four times. The suspension obtained was washed with distilled water several times until chloride ions completely disappeared, and then, the suspension was left for 48 h to be decanted .After sedimentation, the suspension was centrifuged, dried, and finally crushed. The obtained powder (5g) was spread in a hot solution (80°C) containing 2.3 g of octadecylamine ($C_{18}H_{39}N$), and the mixture was stirred for 3h [**86**].

To eliminate the organic cations, the suspension obtained was washed several times with a water/ethanol (50/50) mixture at 60°C. The organophilic montmorillonite thus obtained was dried for 36 h before it was crushed and stored. This powder was analysed with Wide angle X-ray diffraction (see figure VI-1 and figure VI-2).

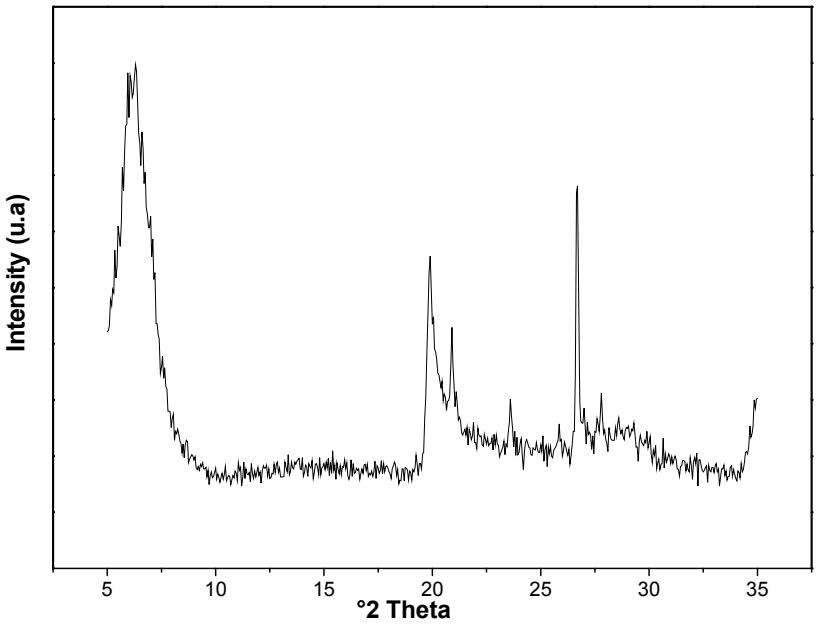

Figure VI-1: X-ray difractogram of the raw clay

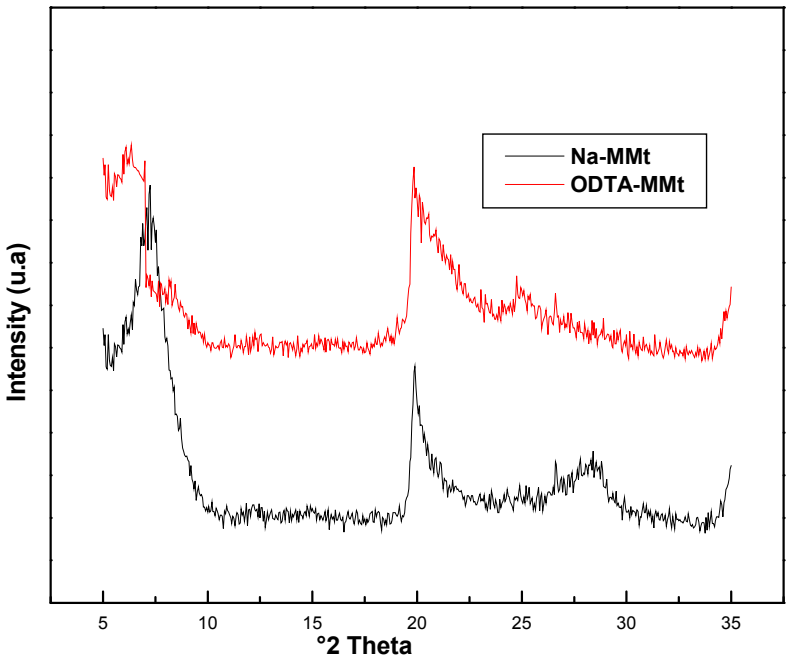

Figure VI-2: X-ray difractogram of the Na-Montmorillonite and organoclay (Octadecyl amine)

VI-2: Blend preparation

Before blending, the PET pellets were dried in vacuum at 105°C for 24 h. The dried PET pellets were dry-mixed with iPP and SEBS-MAH pellets in the following weight ratios (Table 5):

Table 5: Blends compositions of PET/iPP

PET (%)	100	80	60	50	40	20	0
iPP (%)	0	20	40	50	60	80	100

The amounts of the compatibilizer added are 7, 10, 15 % by weight whereas the amount of the clay is 5 % by weight

The blends were prepared in a Brabender Haake Rheocord (Cergy-Pontoise,France), at 270° C and 32 rpm in two steps; first, the PET was fed into the chamber, and once the PET melted, the iPP , the compatibilizer, and the organoclay were added.

From the preceding blends, films were prepared by compression molding in a Zwick machine (Ulm,Germany), mode l7102, working at a pressure of 150 kg/cm^2). The compression was performed at 275°C during 6 min (4 min for preheating and 2 min for compression).

Flowchart of the blend preparation steps :

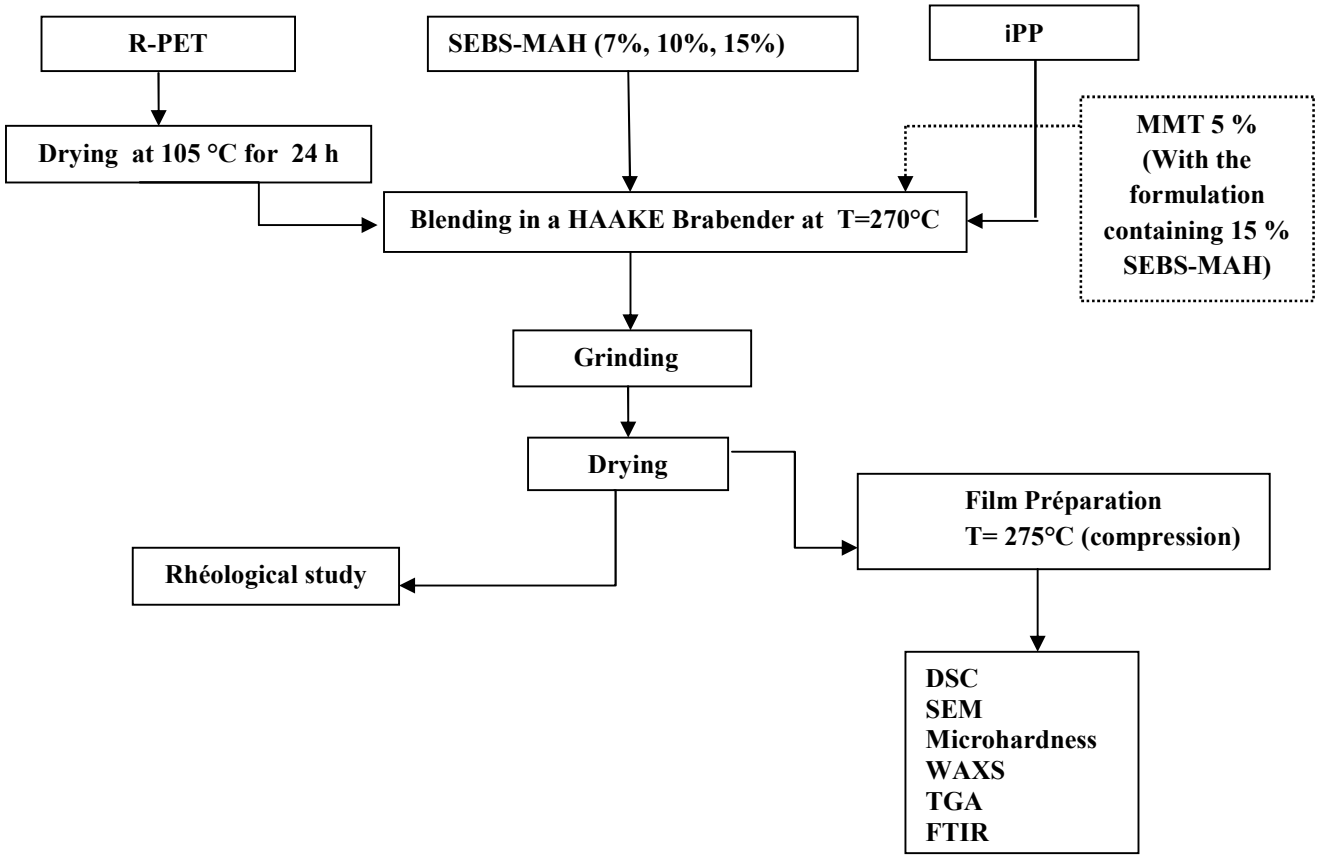

VI-3: Differential Scanning Calorimetry (DSC):

Differential scanning calorimeter is a very valuable tool in polymer science and engineering. The differential scanning calorimeter or DSC for short determines critical information, such as: the glass transition state, the melt transition state, the crystallization transition state, and heat capacity and percent crystallinity. These characteristics are critical pieces of information used in polymer processing and research. This makes the differential scanning calorimeter a very important instrument in the polymer industry. The setup of the DSC instrument is fairly simple. In the instrument, there are two pans placed in to a chamber. One of the pans contains a polymer sample of a known weight. The other pan is identical to the first one; however, it contains no sample. This is the reference pan. These pans are heated up, simultaneously, with the instruments heating element. Precisely, similar conditions for each pan are essential. Also nitrogen gas is used to create nitrogen gas atmosphere around both pans [87].

This eliminates the possibility of any moisture or oxygen contamination with the pans. Both pans in the chamber are heated at a desired rate. Computer software makes sure that both pans get heated at absolutely the same heating rates. Since the sample pan contains a polymer sample, it takes more energy to heat it in comparison to the reference pan. The difference in energy is measured by the DSC. The difference in the energy is shown as a graph on computer screen called as a thermograph [87].

The thermal study was performed with help of a Perkin Elmer (Norwalk, Connecticut, USA) DSC-7Differential scanning calorimetry (DSC) instrument in an

inert N_2 atmosphere. Sample weights were 5–10 mg. The temperature range studied was 50–300°C. The heating rate was 10°C/min.

The crystallinity measured by DSC (α_{DSC}) was derived from the melting enthalpy obtained by DSC with the following expression:

$$\alpha_{DSC} = \Delta H_m / \Delta H_m^{\infty} \qquad \text{eq. 10}$$

where ΔHm and ΔHm^{∞} are the experimental melting enthalpy and the melting enthalpy for an infinitely thick crystal, respectively.

VI-4: Thermal Gravimetric Analysis (TGA) Measurements:

Thermal gravimetric Analyzis is a simple technique that measures the weight loss of material over wide range of temperature. It requires high degree of precision in weight, temperature and temperature change measurements. As materials are heated, they can loose weight by water loss, by drying, decomposition by chemical reactions such as oxidation and result in liberating gases. Since the weight loss is a disruptive process for a sample material, knowledge of the magnitude and temperature range of those reactions are necessary in order to design adequate thermal ramps and holds during those critical reaction periods [**88**].

Thermal Gravimetric Analysis (TGA) was conducted on a SETARAM LABSYS TMA 1400/1600 instrument under nitrogen atmosphere. The samples with weight between 5-10 mg were heated from room temperature to 800°C at a rate of 20°C/min. Each sample was placed into a platinum pan attached to a sensitive microbalance assembly. The sample holder portion of the TGA balance assembly is then placed into a high temperature furnace. The balance assembly measures the initial sample weight at room temperature and then continuously monitors changes in sample weight as heating rate increases. Weight loss profiles are analyzed for the amount or percent of weight loss at any given temperature, the amount or percent of non-combusted residue at some final temperature, and the temperatures of various sample degradation processes.

VI-5: Wide Angle X-ray Diffraction:

Wide angle diffraction of monochromatic X-rays is often used to study clay dispersion in polymer nanocomposites. X-ray powder diffraction (XRD) is a rapid, non-destructive analytical technique used for phase identification of a crystalline material and can provide information on unit cell dimensions and clay dispersion. As the wavelength of x-rays is in the range of the size of atoms, because of this, they are useful for investigating the structural arrangement of atoms and molecules in different materials. The x-rays penetrate into the materials and provide information about the morphological structure (Fig. VI-3) [89].

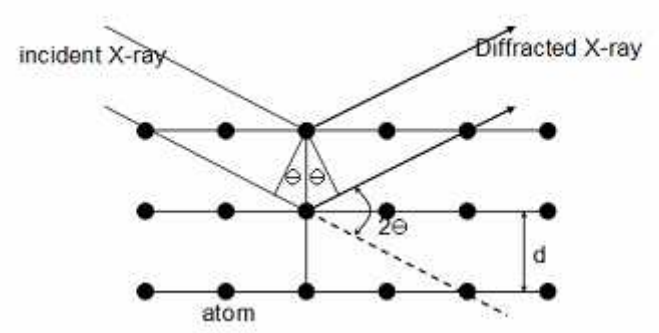

Figure VI-3: Schematic representation of X-ray diffraction

The general relationship between the wavelength of the incident x-rays, angle of incidence and spacing between the crystal lattice planes of atoms is known as Bragg's law,

$$n\lambda = 2d\sin\Theta \qquad \textbf{(eq.11)}$$

Where, n (an integer) is the "order" of reflection,

λ is the wavelength of the incident X-rays,

d is the interplanar spacing of the crystal

Θ is the angle of incidence.

When clay platelets are completely exfoliated in a polymer matrix, it can be observed from the disappearance of any coherent XRD, whereas the finite layer expansion observed in intercalated nanocomposite is associated with the appearance of new diffraction peaks corresponding to larger gallery height [89]

The wide-angleX-ray scattering (WAXS) study was carried out with a Seifert (Ahrensburg, Germany) diffractometer working in the reflection mode. The experimental conditions were the following: Ni-filtered Cu Ka radiation with a wavelength of 0.15418 nm, 40 kV and 35 mA, angular range (2θ) = 5-35° and scan rate = 0.02°/s. The WAXS-determined crystallinity (α_{WAXS}) of every sample was calculated as the ratio of the area corresponding to the crystal-line peaks to the total area of the diffractogram.

VI-6: Microhardness Measurements

H was determined at room temperature with a Leitz (Wetzlar, Germany) microindentation tester with a square-based diamond indenter. The H value was derived from the residual projected area of indentation according to the following expression:

$$H = kP/d^2 \qquad \textbf{(eq.12)}$$

where d is the length of the impression diagonal (m), P is the contact load applied (N), and k is a geometrical factor equal to 1.854. Loads of 0.5 and 1N were applied. The loading cycle was 0.1 min. Eight to ten indentations were performed on the surface of each sample, and the results were averaged.

VI-7: Optical Microscope

In order to highlight the effect of the compatibilizer SEBS-MAH and its concentration on the blend PET / PP, we performed microscopic observations through an optical microscope of the type: OPTIKA (B-353A) and Camera: SONY. This digital microscope is a microscope equipped with a digital camera allowing observation of a sample via a computer. It can also be partly or wholly

computer-controlled with various levels of automation. It can allows greater analysis of the image**VI-8: Scanning Electron Microscopy (SEM):**

To investigate polymer nanocomposite structure thoroughly, it is necessary to perform SEM analysis. It has been observed that XRD does not give clear idea about polymer morphology and it is used to estimate intercalation and exfoliation. The scanning electron microscope (SEM) would help further investigate morphology of polymer nanocomposites. Scanning Electron Microscopy is the microscopy technique which operates on the same principles as the light microscope but uses electrons instead of light to form an image. A beam of electrons is produced at the top of the microscope by heating of a metallic filament. The electron beam follows a vertical path through the column of the microscope. It makes its way through electromagnetic lenses which focus and direct the beam down towards the sample. Once it hits the sample, other electrons (backscattered or secondary) are ejected from the sample. Detectors collect the secondary or backscattered electrons, and convert them to a signal that is sent to a viewing screen similiar to the one in an ordinary television, producing an image [90].

By using SEM to analyze polymer nanocomposites, it is possible to obtain information within the range 1 to 100 nm with varying degree of difficulty. This is beyond the range of light microscopy. Another main advantage of the SEM is that it can be easily adjusted and thus facilitating the investigation of crystal structure, orientation and enabling particular morphological analysis. The formed image is made visible on a fluorescent screen or it is documented on photographic material. Photos taken with electron microscopes are always black and white [91]. To do the morphological analysis, we used a Quanta 200 Scanning Electron Microscope.

VI-9: Infra-red spectroscopy:

Infrared spectroscopy has become one of the most important working tools for characterizing the chemical and physical nature of polymers. It allows the identification of qualitative and quantitative information concerning the detailed structural polymers, for example: The chemical nature of the groups. The apparatus used is of type: FTIR-84005 (SHMADZU), number of scans 40, resolution 2.

VI-10: Rheological study:

The rheological study was performed on a capillary rheometer COMTROLAB for only one temperature 285 ° C. and the die used has a ratio L / D (length / diameter) greater than 25.

By measuring the values of the pressure change Δp as a function of piston speed Vp. The results obtained are used to calculate the shear stress (τ), the apparent shear rate (γ_a) and apparent viscosity (μ_a). Then the Rabinowitch correction is performed to correct shear rate and viscosity:

$$\tau = (R.\ \Delta P)\ /2.L \qquad \textbf{(eq. 13)}$$

where :

τ **:** Shear stress (Pa).

ΔP : Pressure drop (K_g/cm^2).

$$\gamma_a = 4.V_f/R \qquad \textbf{(eq. 14)}$$

with

$$\gamma_a = 8\ D_p^2.V_P/D_C^3 \qquad \textbf{(eq. 15)}$$

where :

γ_a : apparent shear rate (sec^{-1}).

V_f : velocity (mm/min).

V_P: Piston falling speed (mm/min).

D_P : Piston diameter (mm), D_p=20mm

$$\mu_a = \tau / \gamma_a \qquad \textbf{(eq. 16)}$$

where :

μ_a : apparent viscosity (Pa .s)

$$\gamma_c = (3n+1).\ \gamma_a /4n \qquad \textbf{(eq. 17)}$$

where :

γ_c **:** corrected shear rate (sec^{-1}).

n: flow index

$$n = d\ (Log\ \tau) /d\ (Log\ \gamma) \qquad \textbf{(eq. 18)}$$

Chapter VII

RESULTS AND DISCUSSION

VII-1 : Differential Scanning Calorimetry

The DSC plots of all samples included in this study show the melting peaks of each compound clearly distinguished indicating the immiscibility of the different mixtures investigated. The constant position of these peaks around T_m = 163-164 ºC for the iPP and T_m = 246-247 ºC for the PET (Figure VII-1), according to the composition, suggests that the crystal thickness **lc** of these two compounds is nearly constant. Figure VII-2. illustrates the DSC thermograms for all mixtures of the series of PET/PP without compatibilizer .

The DSC spectra in Figure VII-3 corresponding to the compatibilized blends show no fundamental differences between neat iPP, PET and the compatibilized blends. Crystallization temperatures and melting temperature (Tm) of polymers samples remained almost unaffected.

This was for most compositions, together with the iPP melting peak, both, the crystallization and melting peaks of the PET component appear in the thermograms. For the α_{DSC} calculation, we have taken the following values: ΔH_m^{∞} = 140.1 J/g [92] for the PET and H_m^{∞} = 207.33 J/g [92] for the iPP. Nevertheless, in the corresponding thermograms, the enthalpic balance for the PET component, i.e., the difference between the melting enthalpy and the crystallization enthalpy is always positive

The crystals thickness **lc** of the components, derived from the Thomson-Gibbs equation:

$$T_m = T_m^0 [1 - (2\sigma_e / \Delta H_m^{\infty} l_c)] \qquad \textbf{(eq. 19)}$$

is not affected by the blending process. In the preceding equation, ΔH_m^{∞}, as mentioned above, is the melting enthalpy for an infinitely thick crystal; σ_e is the surface free energy and T_m^0 is the equilibrium melting point of each component. For iPP, we have taken T_m^0 = 460.7 K [61] and σ_e = 100 erg/cm^2 [93]; for the PET component, we have used T_m^0 = 553º K [61], and σ_e = 151-161 erg/cm^2 [94]. The crystal thickness values obtained from equation (2) for both components are: 26 nm for the PET and 19 nm for the iPP. On the other hand, the crystallization temperature

T_c measured for the PET component shifts to a lower values (minimum, 115ºC) compared to the neat PET, i.e., 125ºC.

The DSC analysis shows that, the compatibilizer does not induce any change in the thermograms. for almost all the blends containing SEBS-g-MAH, whereas three major effects are noticeable: first, only the crystallization and melting peaks of PET appear in the blend containing PET/iPP/SEBS-g-MAH (80/20/7). Secondly, only the melting peak of PP appears in the blend containing PET/iPP/SEBS-g-MAH (20/80/7). Thirdly we observe appearance of the iPP and PET melting peaks but not of the PET crystallization peak for the blends PET/iPP/SEBS-g-MAH (20/80/15). The disappearance of the crystallization peak at high temperature is related to the change of morphology that is caused by the addition of SEBS-g-MAH. During blending in the brabender of PET/iPP/SEBS-g-MAH blends, the compatibilizer locates at the interface. The partial miscibility is therefore reflected in the decrease in crystallization, this has been already noted [**95,96**]

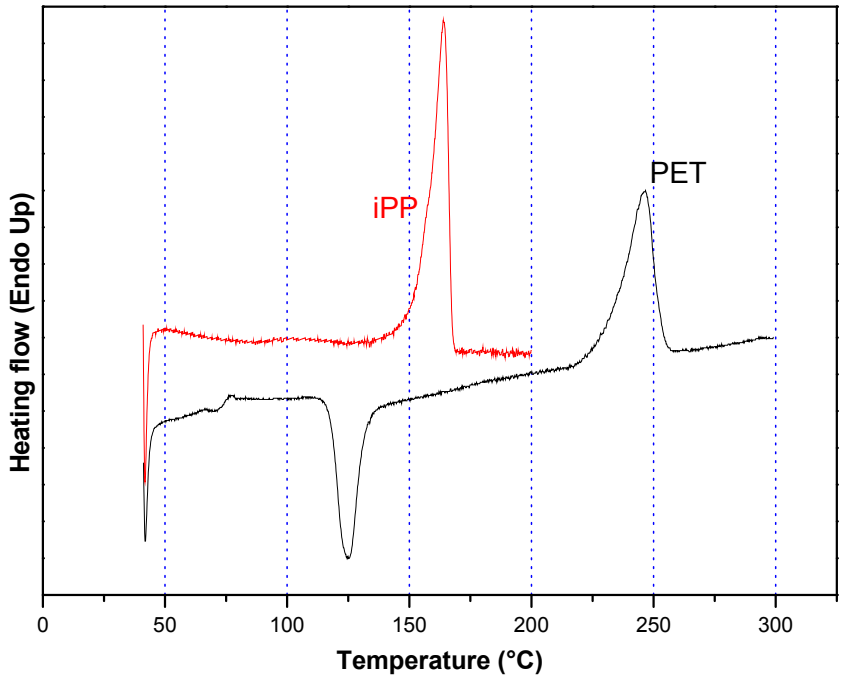

Figure VII-1 : DSC thermographs of the neat PET and iPP

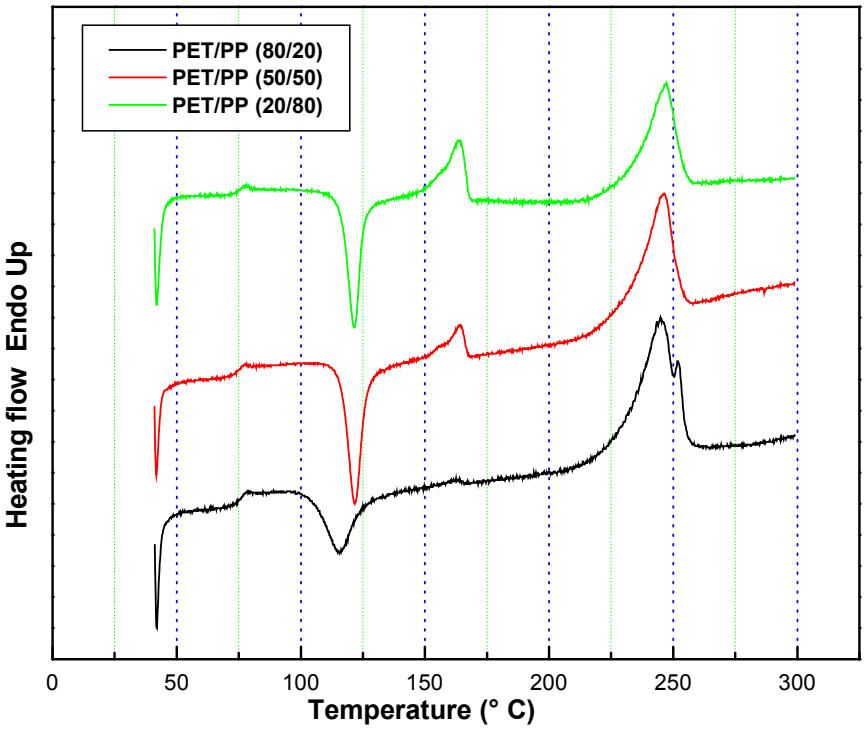

Figure VII-2 : DSC thermographs of the blends PET/iPP (20/80), (50/50) and (80/20) without compatibilizer

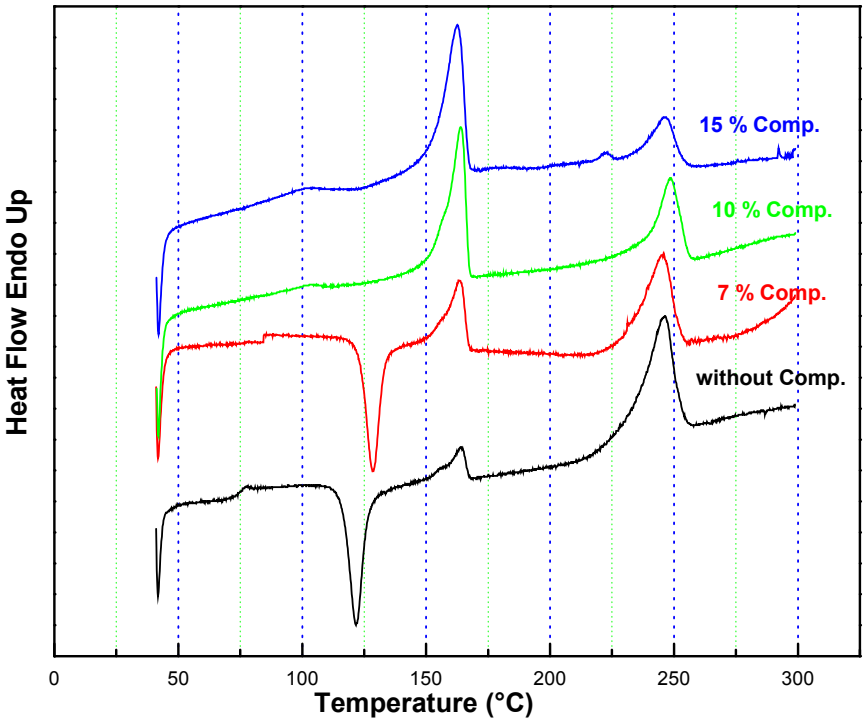

Figure VII-3 : DSC thermographs of the blends PET/iPP (50/50) with 0; 7; 10 and 15 % compatibilizer

The effect of clay on the blends is illustrates in Figure VII-4 Thus, it is clear that the presence of the clay had a nucleating effect over the crystallizability of the iPP component. On the other hand, as it happened in the blends with and without compatibilizer, the enthalpic balance for the PET component was positive for all of the compositions.

The same behavior is observed in the blends with and without compatibilizer, in the blends with compatibilizer and clay , the Tm values of both components remained constant for all compositions and were practically equal to the values found for the pure components. This means that the **lc** values also remained constant and equal to 26 and 19 nm for the PET and iPP, respectively

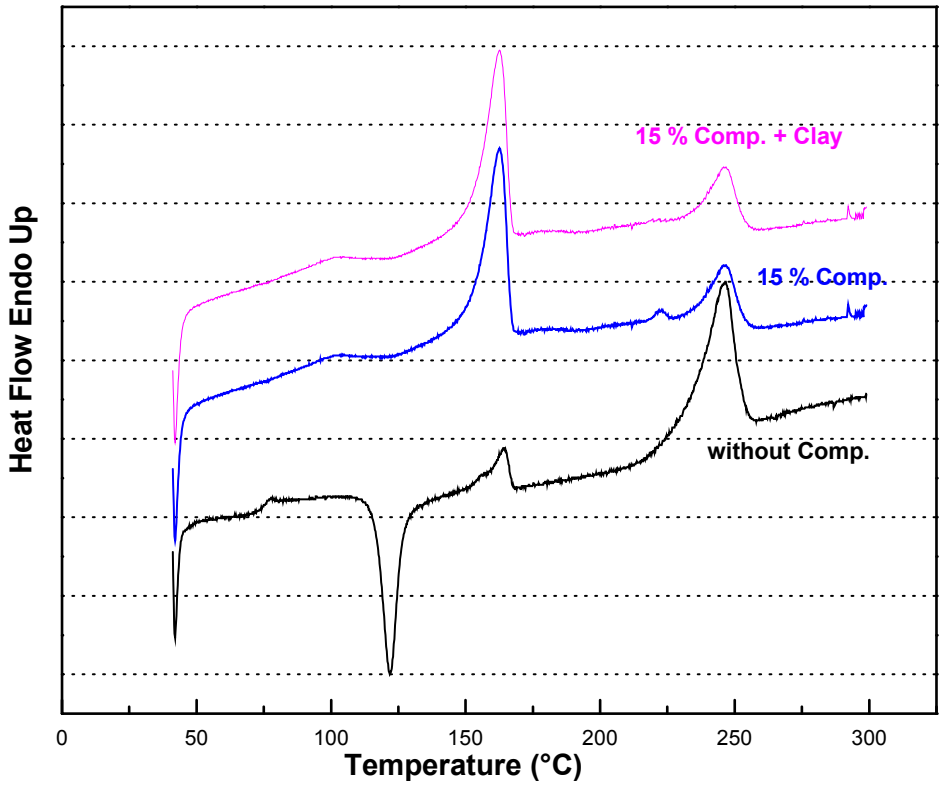

Figure VII-4 : DSC thermographs of the blends PET/iPP (50/50) blends with 15% compatibilizer (pure and with 5% clay).

VII-2 : Thermogravimetric analysis

Another highly interesting property exhibited by polymer modified montmorillonite nanocomposites concerns their thermal stability. The thermal degradation of a material is usually determined by a thermogravimetric analysis. The important parameter is the onset temperature of the degradation, which is measured as the point at which 10% of the sample is lost [97]

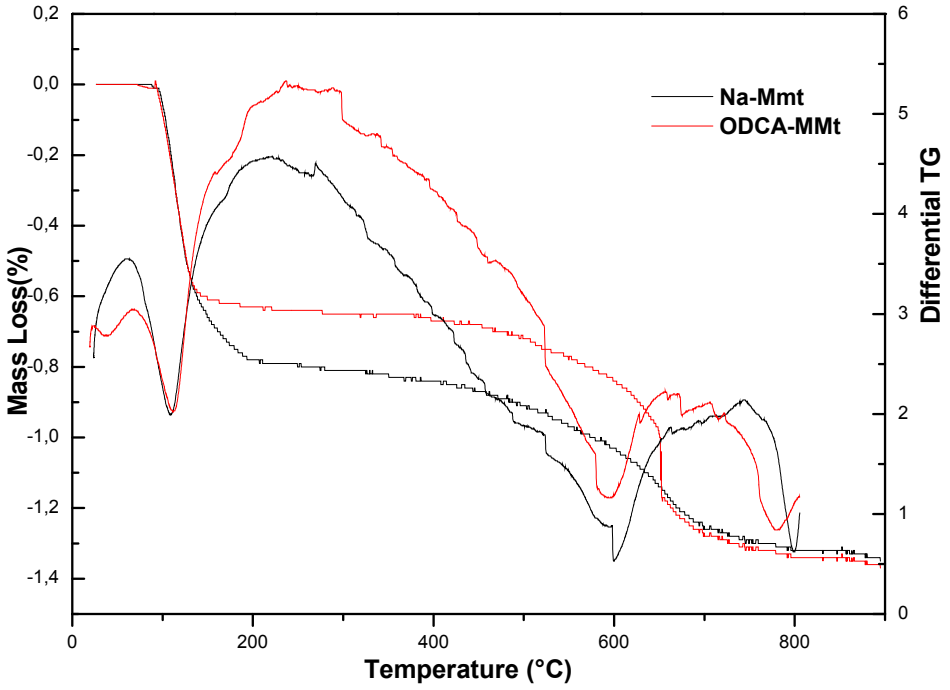

Figure VII-5 TG and DTG plots of Na- Mmt and OCDA-Mmt

FigureVII-5 displays the TG and DTG results for the montmorillonite with and without intercalation of the Octadecyl amine. It is apparent from this study that the initial degradation temperatures are similar fort both samples. It is noted that the TG's of the unmodified and modified montmorillonite have two mass loss steps the first one between ambient and 150°C, (at about 135.5°C) and the second one about 630 °C.

These mass loss steps are attributed to desorption of water from the clay, and the dehydroxylation of the montmorillonite respectively[**97**].

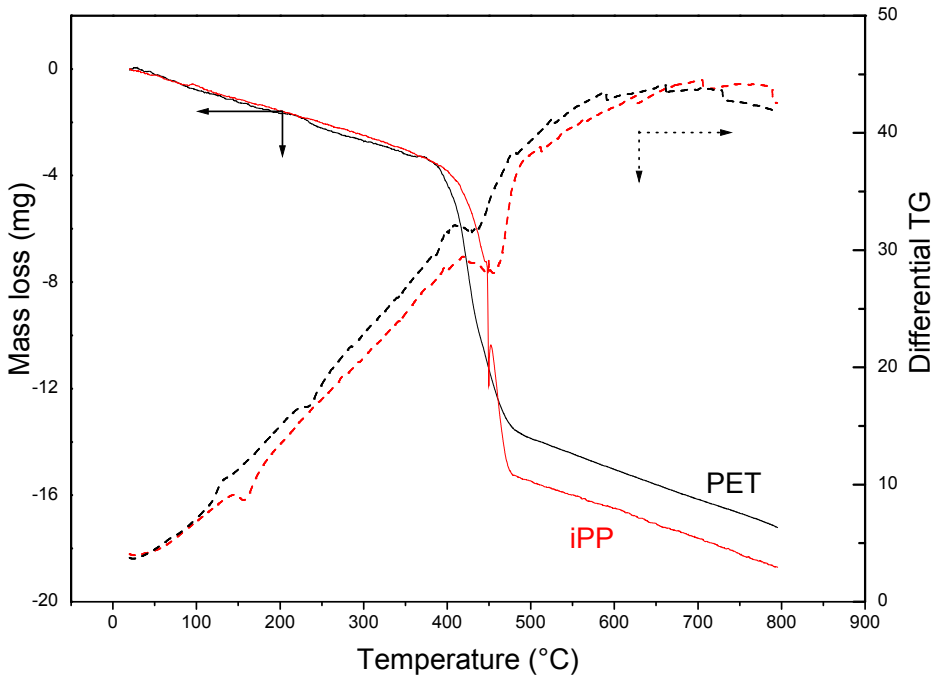

Figure: VII-6 Thermal decomposition plots of pur PET and iPP

The thermal degradation of PET and iPP, tested by TG in nitrogen atmosphere are shown in Fig. VII-6 were we can note that the decomposition temperatures for both polymers are slightly different, the onset decomposition temperature of the neat PET is around 410 °C whereas the one of the iPP is about 475 °C.

From the plots shown in Figure VII-7 obtained for the blends PET/iPP with the compatibilizer it is observed that there are not much difference between thermal degradation onset temperature of the compatibilized blends. From these results, it can be concluded that the neat compounds, i.e. PET

and iPP, and their compounds compatibilized with SEBS-g-MAH have nearly the same thermal stability and therefore the compatibilizer has no effect on the thermal stability of the blends.

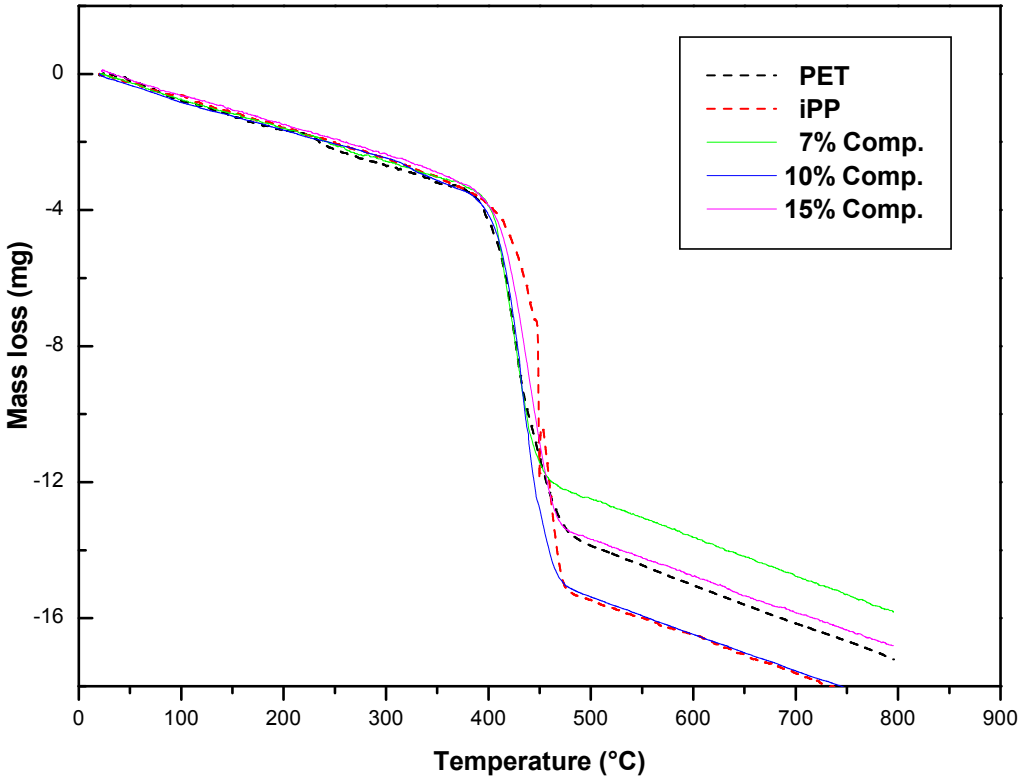

Figure VII- 7: TG plots of the blends of PET/iPP (50/50) with 0,7,10 and 15 % SEBS-g-MAH

The role of clay in the nanocomposite structure may be the main reason for the difference in TG results of these systems when compared to neat polymers. The clay acts as a heat barrier and assists in the formation of char after thermal decomposition [97]. Many studies have concluded that the dispersion of clay nanoparticles into the polymer matrix can improve the thermal stability of the composite [98- 100]. The presence of organoclay enhances the formation of char and hinders diffusion of volatile decomposition products. However, in our case and with OCDA clay addition

nanocomposites, this trend was not observed. As well, there was not much difference in the onset temperatures observed for the whole range of compositions. However we have to bear in mind that it has been indicated that at low clay loading (1–5 wt%), exfoliation dominates but the amount of exfoliated nanoclay is not enough to enhance the thermal stability through char formation. The situation changes with larger clay concentration (≥ 7 wt%), where more exfoliated clay is formed, and char forms more easily, this will effectively and consequently promotes the thermal stability of the nanocomposites [**101**].

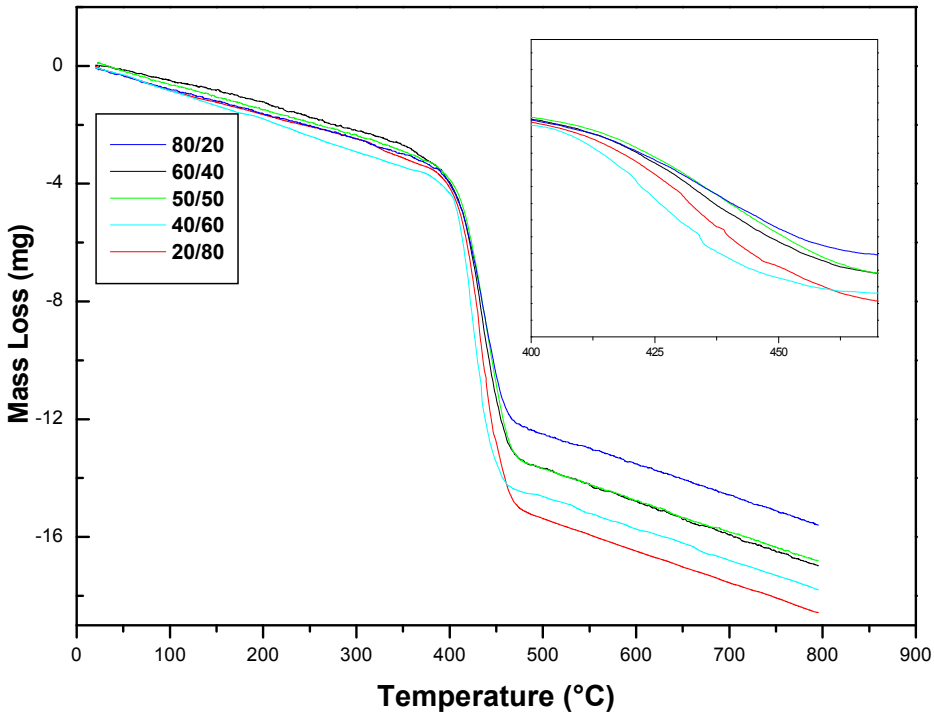

Figure VII-8: TG plots of PET/iPP with 15 % SEBS-g-MAH and 5% Clay

VII-3 : Wide Angle X-ray diffraction.

The structure of all the blends is determined by using the WAXS results. The figure VII-9 and Figure VII-10 represents the pattern of the pure iPP and PET respectively. A Gaus-Lorentz functions are applied to describe the amourphous background.and an iterative peak –fit procedure was used to fit the crystalline reflections of WAXS profiles. As expected from the WAXRD pattern for the neat iPP which exhibits four intence α-form crystal diffraction peaks at 14.1°,16.9°, 18.5° and 21.8° corresponding to (110), (040), (130) and (111), (131) doublet respectively [**102**] whereas the diagram obtained for PET it shows a broad halo form indicating that the PET is almost amourphous.

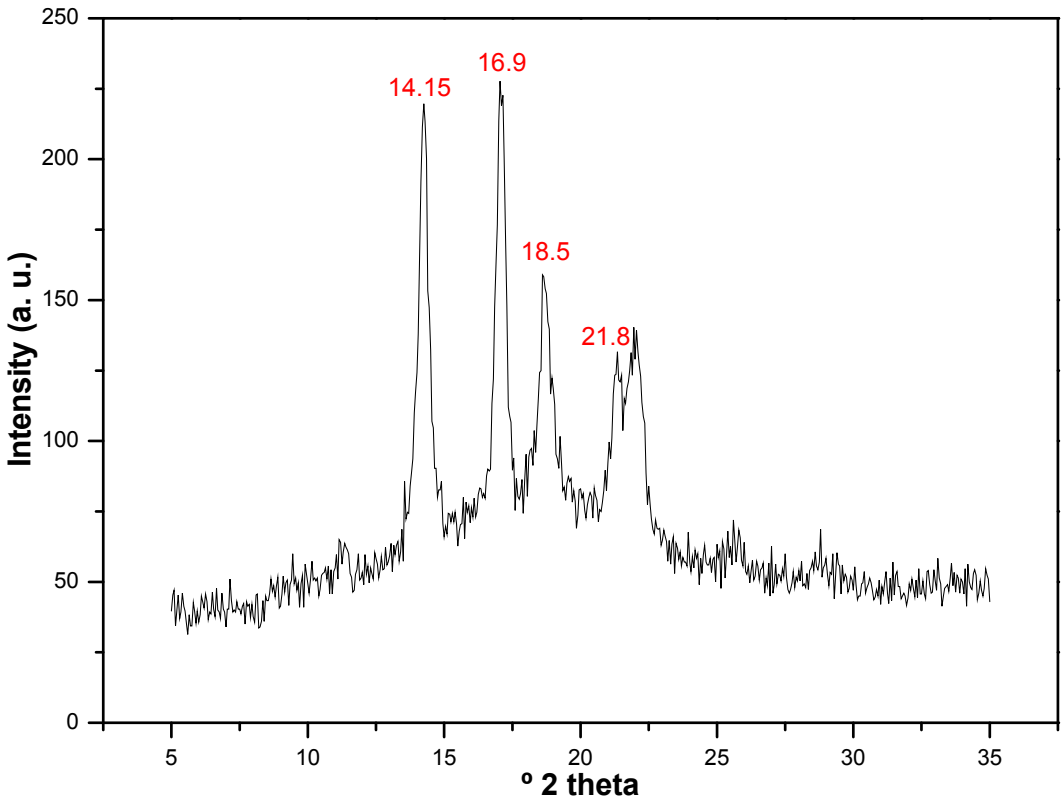

Figure VII-9: X-ray difractogram of neat iPP

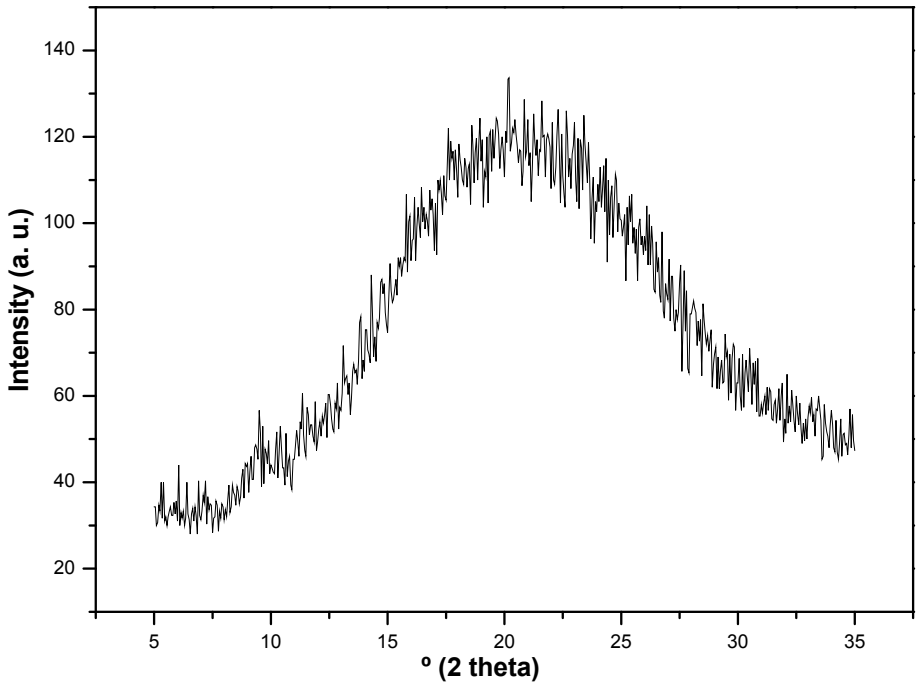

Figure VII-10: X-ray difractogram of neat PET

The majority of the WAXS diagrams obtained for the different blends showed broad halos and narrow peaks corresponding to the iPP α form see Figure VII-11. The diffractogram of the PET/iPP 80/20 blend without compatibilizer only exhibited the main crystalline reflection of iPP at about 14.2° (2θ), superposed to a broad halo from PET. Whereas the diffractograms of the blends with the same composition plus 7 , 10 or 15 % compatibilizer showed totally amorphous halos. In addition, only some compatibilized blends with a 50/50 % composition exhibited, together with those of iPP, other peaks that were attributed to a certain content of crystallized PET. As indicated above, in most of the WAXS diagrams of the blends only the crystalline reflections of the iPP component appear. Thus, it seems that the blending process gives rise to the crystallization of a certain amount of the initially amorphous PET component, even if the crystalline PET peaks are not detected in the diffractograms. For this reason, the total crystallinity (calculated for both components iPP and PET, derived from the thermograms is slightly higher than that calculated for the iPP alone.

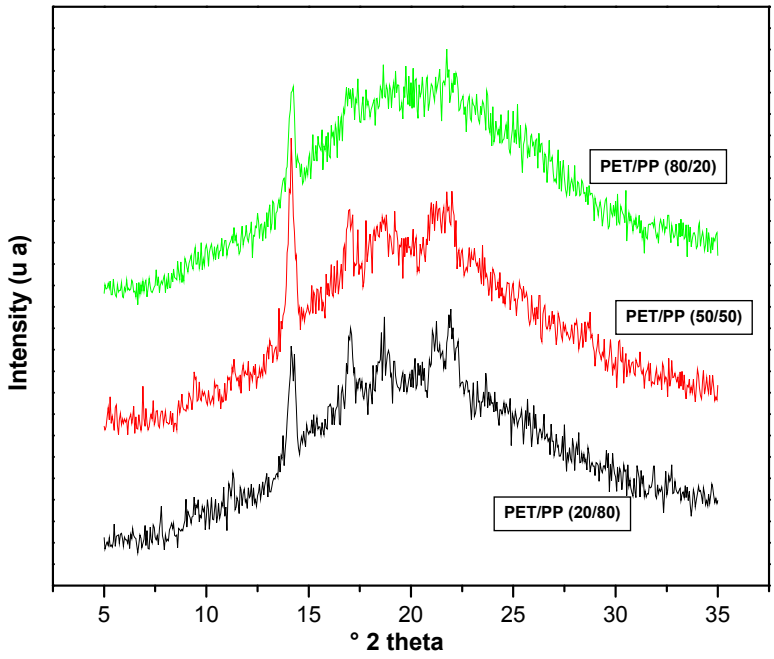

Figure VII-11: X-ray difractograms of the blends PET/iPP (20/80), (50/50) and (80/20)

From the curve figureVI-2 seen in chapter VI, the Na- MMT shows a characteristic diffraction peak at 6.50°. The Organo-modified MMT shows a diffraction peak at 6.00°, indicating increased d-spacing of OCDA-MMt which confirms the presence of the salt molecule intercalation between montmorillonite layers.

In an attempt to evaluate whether, the nanocomposite structure was formed or not. The XRD profiles of the nanocomposites blends containing 15 % compatibilizer and 5 wt% clay are shown in Figure VII-13. XRD patterns of PET/iPP/SEBS-g-MAH/OCDA- MMT samples indicate that the d-spacing of the clay in the composite has disappeared. This can indicate the formation of a nanocomposite structure, thus indicating that almost complete exfoliation of the silicate layers took place.

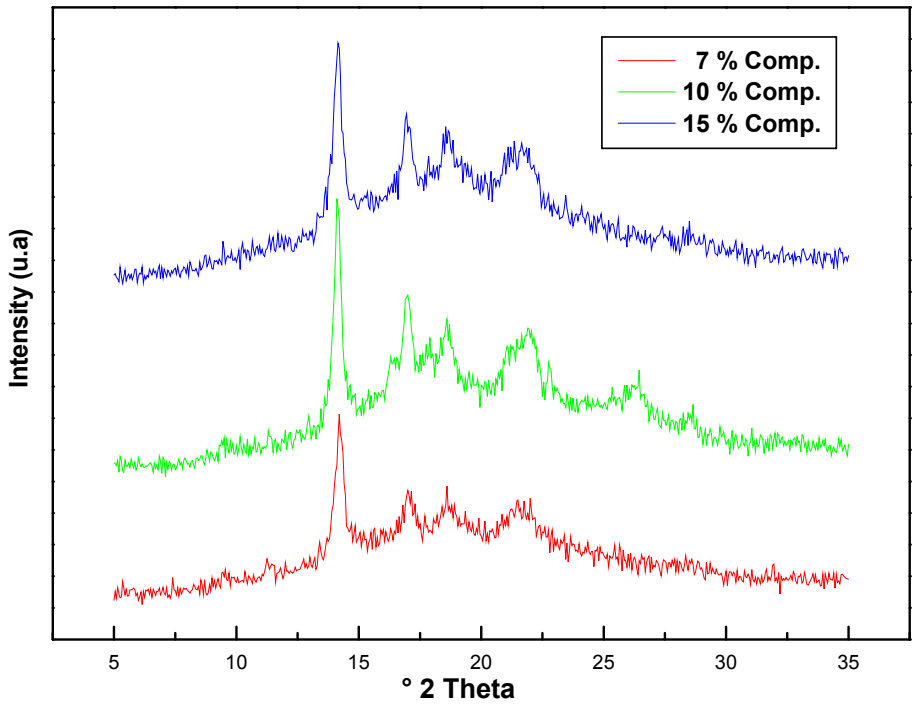

Figure VII-12: X-ray difractogram of the blends PET/iPP (50/50) compatibilized with 7, 10 and 15 % SEBS-g-MAH

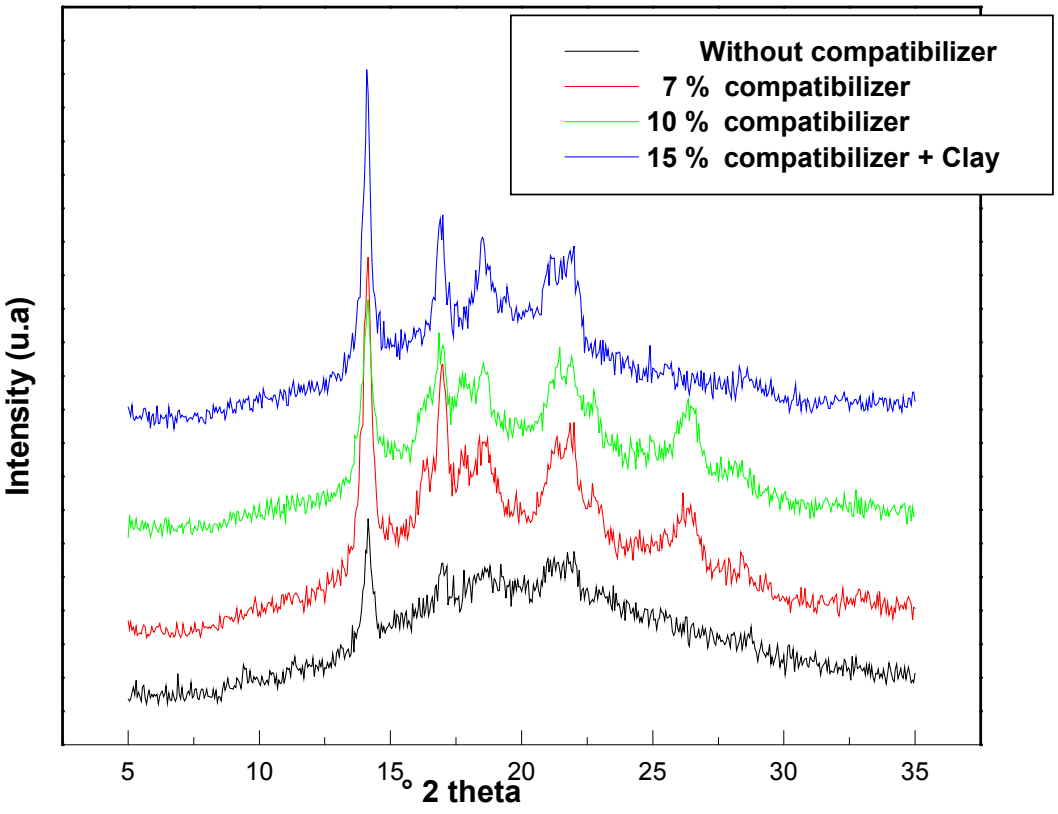

Figure VII-13: X-ray difractogram of the blends PET/iPP (50/50) compatibilized with 7, 10 and 15 % SEBS-g-MAH and 5% Clay

Crystallinity study:

As it can be seen in Table 6 and Figure VII-14, the presence of the amorphous PET induces a decrease in the crystallinity of the pure iPP/PET blends, from 50 % for pure iPP down to less than 5 % for the 20/80 composition (α_{WAXS}), or from 40 % down to less than 1 % (α_{DSC}). It is noteworthy that, in all cases, the α_{DSC} values included in Tables 2 and 3 have been calculated only for the iPP component. The α_{WAXS} values are slightly higher than those obtained by DSC (see Table II for comparison). By adding the SEBS-MAH compatibilizer, the crystallinity level of the blends increases again. In fact, the crystallinity α_{WAXS} values obtained for blends with 15 % of compatibilizer practically follow the additivity law (dashed line in Figure VII-14) as a function of composition. Blends with 7 and 10 % of SEBS-MAH, however, show α_{WAXS} values that are smaller than the predicted by this law (see Figure VII-14 and Table 6).

The crystallinity of the compatibilized blends is higher than that of pure PET. This is attributed to heterogeneous nucleation due to the presence of iPP crystals in the quenched blends [**96**]. The decrease of PP crystallinity as the PET/iPP ratio increases is due to the concomitant increase of the SEBS-MAH/PET reaction, the reaction product hindering PP crystallization. This can also be limited by the hindrance of cold crystallized PET above 100°C whereas the PET crystallinity is increasing slightly [**103**].

The figure VII-15 represents the α_{waxs} of the 50/50 PET/iPP bends with the clay and 15% compatibilizer were it is noticed that the crystallinity of iPP decreases for both the blends as the content of the PET increases in the blends. From the results shown in FigureVII-14, figure VII-15 and Table 7, we deduced that the presence of 5 wt% clay in the blends with 15% compatibilizer increased α_{WAXS} by, approximately, 5–10 % (see Tables 6 and 7). As happened in their counter parts without clay, the α_{WAXS} values obtained for these blends obeyed the additivity law as a function of composition [see Figure VII-15].

Table 6: DSC and WAXS cristallinities of the blends with SEBS-MAH as a compatibilizer

Composition	Total crystallinity (WAXS)	iPP crystallinity (DSC)
100/0 PET/PP	0.00	0.00
80/20 PET/PP	0.040	0.003
50/50 PET/PP	0.12	0.04
20/80 PET/PP	0.09	0.07
0/100 PET/PP	0.50	0.40
100/0 PET/PP - 7% compatibilizer	0.00	0.00
80/20 PET/PP - 7% compatibilizer	0.00	0.00
60/40 PET/PP - 7% compatibilizer	0.04	0.07
50/50 PET/PP - 7% compatibilizer	0.19	0.15
40/60 PET/PP - 7% compatibilizer	0.18	0.19
20/80 PET/PP - 7% compatibilizer	0.41	0.31
0/100 PET/PP - 7% compatibilizer	0.51	0.40
100/0 PET/PP - 10% compatibilizer	0.00	0.00
80/20 PET/PP - 10% compatibilizer	0.00	0.04
50/50 PET/PP - 10% compatibilizer	0.40	
40/60 PET/PP - 10% compatibilizer	0.15	0.25
20/80 PET/PP - 10% compatibilizer	0.46	0.25
100/0 PET/PP - 15% compatibilizer	0.00	0.00
80/20 PET/PP - 15% compatibilizer	0.08	0.05
60/40 PET/PP - 15% compatibilizer	0.18	0.15
50/50 PET/PP - 15% compatibilizer	0.22	0.19
40/60 PET/PP - 15% compatibilizer	0.21	0.17
20/80 PET/PP - 15% compatibilizer	0.41	0.28
0/100 PET/PP - 15% compatibilizer	0.43	0.32

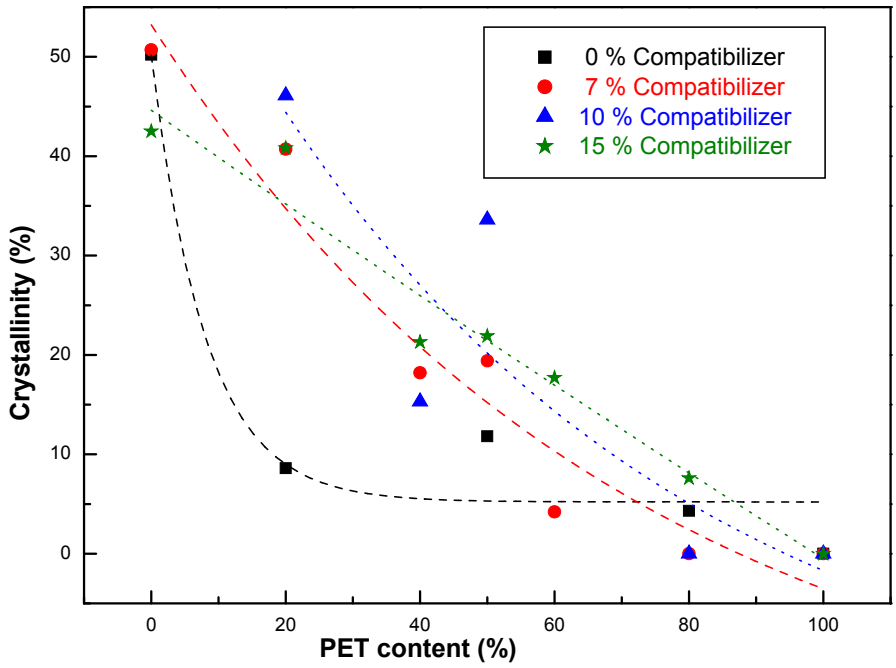

FigureVII-14: Plot of α_{WAXS} as a function of the PET content: PET/iPP (50/50)blends (pure and with different amounts of the compatibilizer)

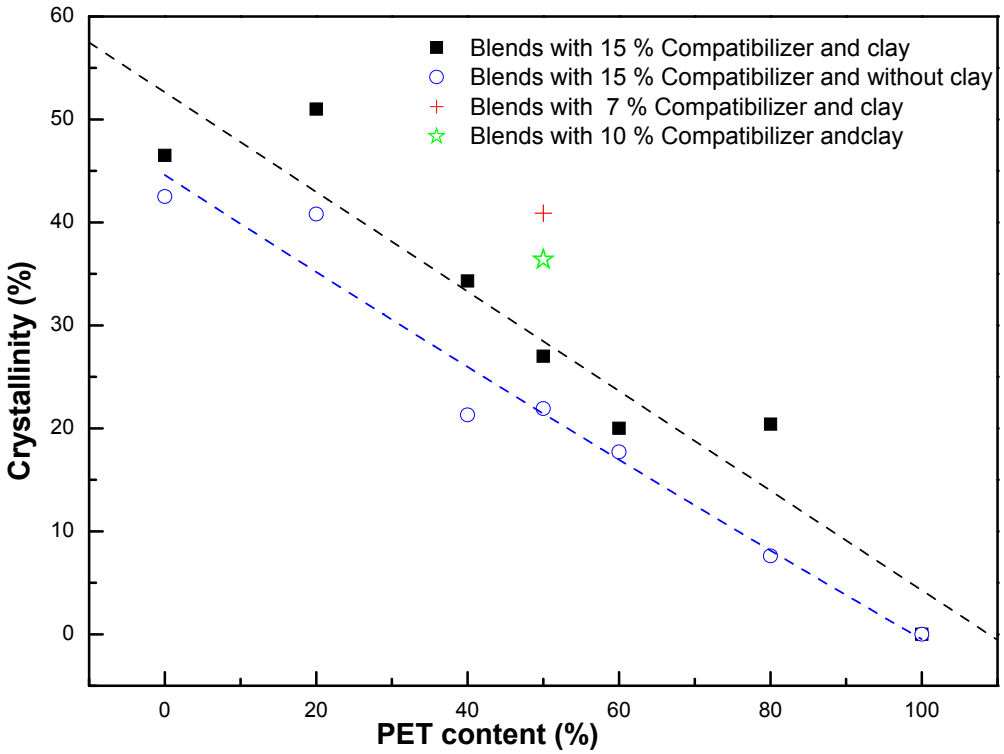

Figure VII-15: Plot of α_{WAXS} as a function of PET content of PET/iPP (50/50) blends with 15% compatibilizer (pure and with 5% clay).

Table 7: PET/iPP/SEBS-g-MAH blends with 5 % Clay as a compatibilizer

Composition	Total crystallinity (WAXS)	iPP crystallinity (DSC)
100/0 PET/PP - 15% compatibilizer- clay	0.00	0.00
80/20 PET/PP - 15% compatibilizer - clay	0.20	0.07
60/40PET/PP - 15% compatibilizer - clay	0.20	0.11
50/50PET/PP - 15% compatibilizer - clay	0.27	0.11
40/60PET/PP - 15% compatibilizer - clay	0.34	0.17
20/80PET/PP - 15% compatibilizer - clay	0.51	0.20
0/100PET/PP - 15% compatibilizer - clay	0.47	0.40
50/50PET/PP - 7% compatibilizer - clay	0.45	0.18
50/50PET/PP - 10% compatibilizer – clay	0.41	0.10

VII-4: Microhardness study.

H of the blends without compatibilizer showed a linear behavior. **H** rose with increasing PET content [see Figure VII-16] according to the additivity law of a binary blend as a function of composition:

$$H = H_1\Phi_1 + H_2(1 - \Phi_1) \qquad \textbf{(eq20)}$$

where H_1, H_2, Φ_1,and $(1 - \Phi_1)$ are the hardness values of the blend components and their molar fractions, respectively. However, the results obtained for the blends with compatibilizer showed a decrease in hardness with increasing PET content up to the equivolumic composition (50/50), and for larger PET content values, **H** increased again. Also, the hardness of the blends decreased with increasing amounts of compatibilizer. On the other hand, according to the two-phase model, **H** of a semicrystalline polymer can be described by the following expression [104].

:

$$H = H_c\alpha + H_a(1 - \alpha) \qquad \textbf{(eq. 21)}$$

where $\mathbf{H_c}$ and $\mathbf{H_a}$ are the intrinsic hardness values of the crystalline and amorphous phases, respectively, and α is the volume fraction of the crystalline material. By combining eqs. (20) and (21), we obtain the following [**104**]:

$$H = H^{PET}\Phi_1 + \left[H_c^{PP}\alpha^{PP} + H_a^{PP}(1-\alpha)\right](1-\Phi_1) \qquad \textbf{(eq 22)}$$

$\boldsymbol{\alpha^{PP}}$ is the degree of crystallinity of iPP; $\mathbf{H_c^{PP}}$ and $\mathbf{H_a^{PP}}$ are the intrinsic hardness values of the crystalline and amorphous phases of iPP, respectively; and $\mathbf{H^{PET}}$ is the microindentation hardness of PET. This expression takes into account **Hc** and **Ha** of every component, their α values, and the compositions of the blends. Here, again, the blends with compatibilizer showed **H** values that were notably lower than the ones derived from the additivity law according to (eq. 22).

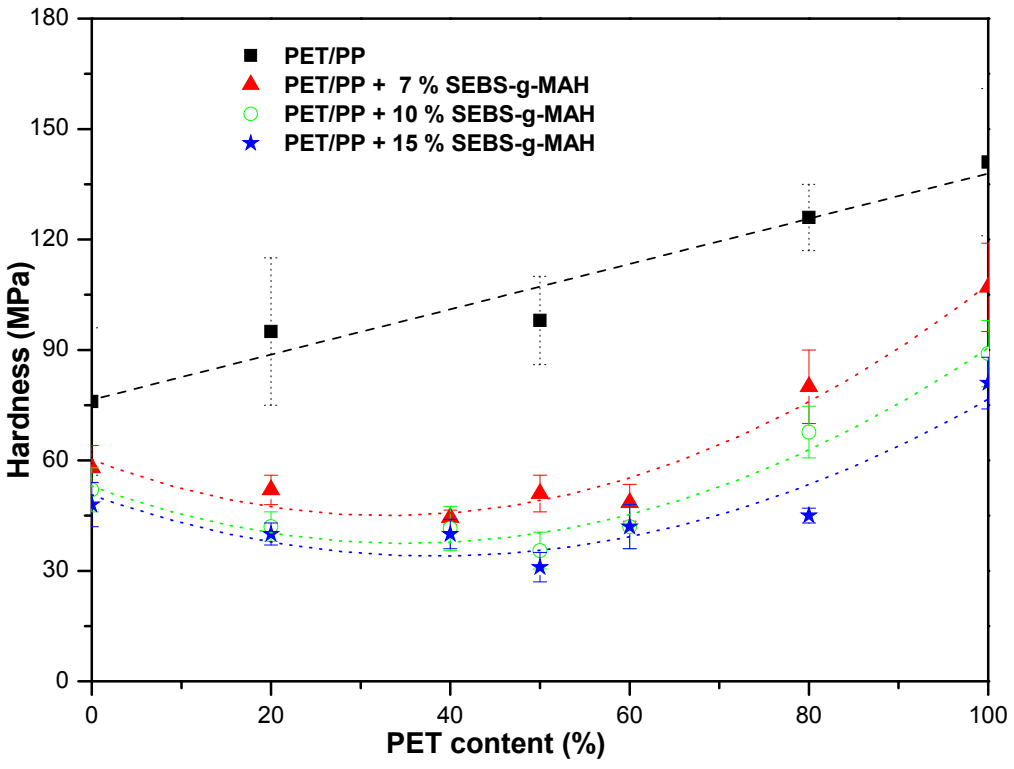

Figure VII-16: Dependence of the hardness on the PET content of PET/iPP blends (pure and with different amounts of the compatibilizer

From the foregoing, it is clear that the two main effects to be considered when the compatibilizer was added to these blends were the increase in the crystallinity and the simultaneous decrease in their hardness. Both effects could be associated with the presence of the SEBS-g-MAH compatibilizer. On one hand, one may think that the compatibilizer contributed to an increase of the iPP chain flexibility so that they could crystallize more easily. On the other hand, the hardness diminution in the compatibilized samples could have been explained by the decrease in $\mathbf{H_c^{iPP}}$.

The relationship between **Hc** and **lc** is [104].

$$H_c = \frac{H_c^{\infty}}{1 + b/l_c} \qquad \text{eq. 5}$$

where H_c^{∞} is the hardness for an infinitely thick crystal and parameter b is defined as $\mathbf{b = 2\sigma_e/\Delta h}$. In this expression, Δh is the energy required to plastically deform the crystalline lamellar stacks.

As **lc** for both components remained practically constant in all compositions, the diminution in the $\mathbf{H_c}$ value for the iPP component could be explained by an increase in parameter b (eq. 5) through $\mathbf{\sigma_e}$, which is known to be related with the degree of order at the crystal surface. [105]. Thus, the b increase might have originated from the blending process of the samples; by the disorder created in the crystals surface due to the presence of amorphous chains of elastomeric character, originating from the compatibilizer; [106] or by a combination of both effects. Equations (5,21-22) suggest that the microhardness of a polymer material is an additive property of the hardness of the crystalline and amourphous phases. All of these equations were initially proposed to explain certain experimental observations and represent nowadays well-established correlations with sound experimental evidence [107-112]

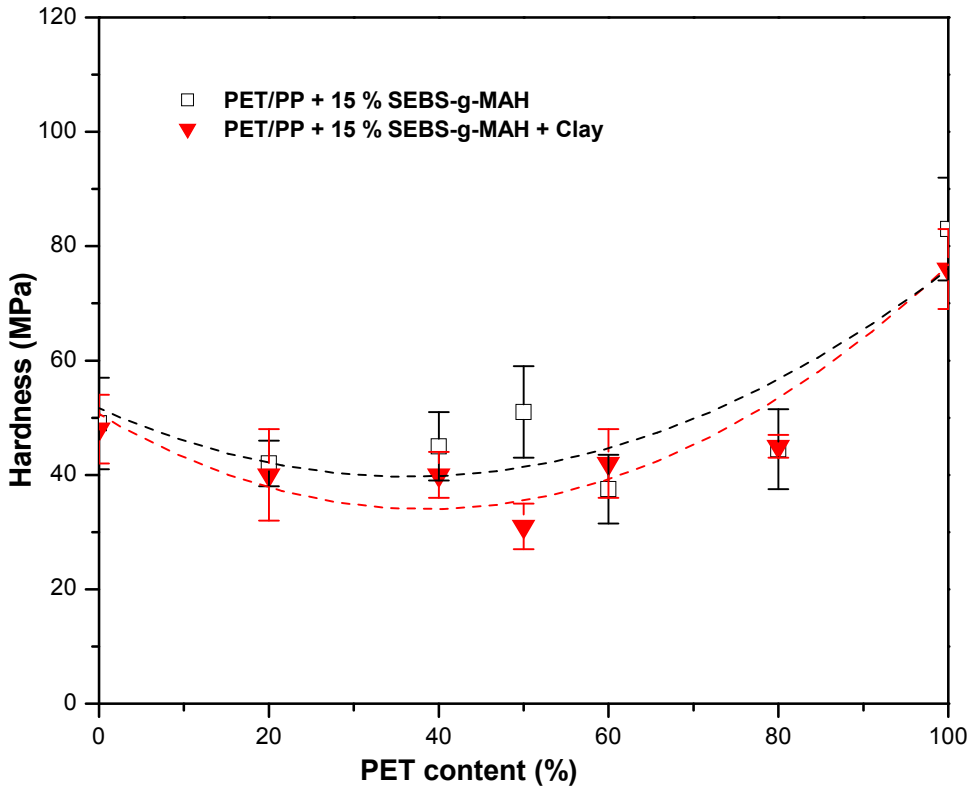

Figure VII-17: Dependence of the hardness on the PET content of PET/iPP blends with 15% Compatibilizer (pure and with 5%clay).

The **H** values of the blends containing clay were higher than their counterparts without clay. However, the hardness dependence with the PET content was similar in both sets of blends [see Figure VII-17]. In the blends with clay , the theoretical hardness values calculated by (eq.22) were close to the experimental ones (for compositions up to 50/50). The same as in the blends with and without compatibilizer, in the blends with compatibilizer and clay , the Tm values of both components remained constant for all compositions and were practically equal to the values found for the pure components (see previous discussion). This means that the **lc** values also remained constant and equal to 26 and 19 nm for the PET and iPP, respectively. Therefore, the decrease in the measured **H** in the blends with compatibilizer plus clay could be explained again as due to the decrease in **Hc** of the iPP component. As observed in the blends with and without compatibilizer,

this probably originated by the increase in the **b** parameter (eq.5) through σ_e in the iPP crystals, which finally was related to the blending process of the samples and to the presence of anamorphous compatibilizer [75]. However, this effect was smaller in the blends with clay (see Figure VII-17).

VII-5: Optical Microscope.

From the photograph (a) presented in the figure VII-18 we can observe that there is an uneven dispersion of the size and shape of the PET phase that corresponds to the minor phase in the formulation of PET /iPP (20/80), we also note that the domains are covered by a continuous phase (dominant), which corresponds to the iPP phase in the blends, which is (80%). The photograph (b) illustrates the dispersion of PET domains in the mixture of iPP in the blend of PET / iPP (80/20), where we observe the same phenomenon as in the previous case.

These two results confirm the incompatibility of the microscopic components that cause the formation of a biphasic structure consisting of large particles or rather small areas with poor interfacial adhesion.

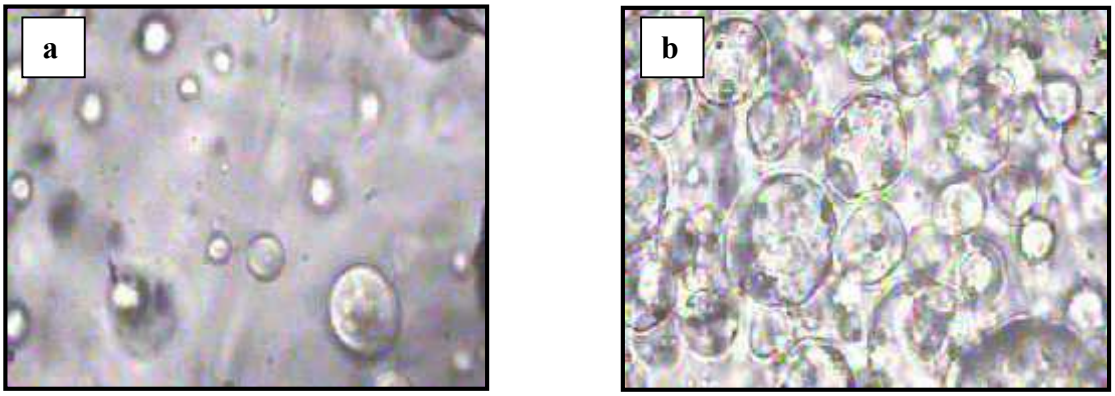

Figure VII-18: Optical microscope photos of blends PET/iPP [a] 80/20; [b] 20/80

It is widely accepted that the two main roles of a compatibilizer on morphology control are the prevention of coalescence and interfacial tension reduction [113].

In Figure VII-19, the optical micrograph (a) shows two different phases the most dominant is polyethylene terephthalate (PET), the other is polypropylene (iPP) which forms the minor phase following its percentage in the blend PET / iPP (80/20). These observations confirmed the separation and incompatibility of the two polymers and by comparison of the image (a) with images (b) and (c) we see clearly the disappearance of PET domain in partially image (b) and almost completely in (c). Tis effect shows clearly that the addition of SEBS-g-MAH in the blends forms a very homogeneous phase between the two blend components , therefore, strong interactions are created and good adhesion is achieved with these materials.

This result can be interpreted by the role played by the SEBS-g-MAH by acting on the interaction forces between polypropylene (iPP) and polyethylene terephthalate (PET) and improving therefore their interfacial adhesion. However it is accepted that the addition of SEBS-g-MAH reduces the domain size of the dispersed phase (PET) and, at the same time, decreases the interfacial tension [114].

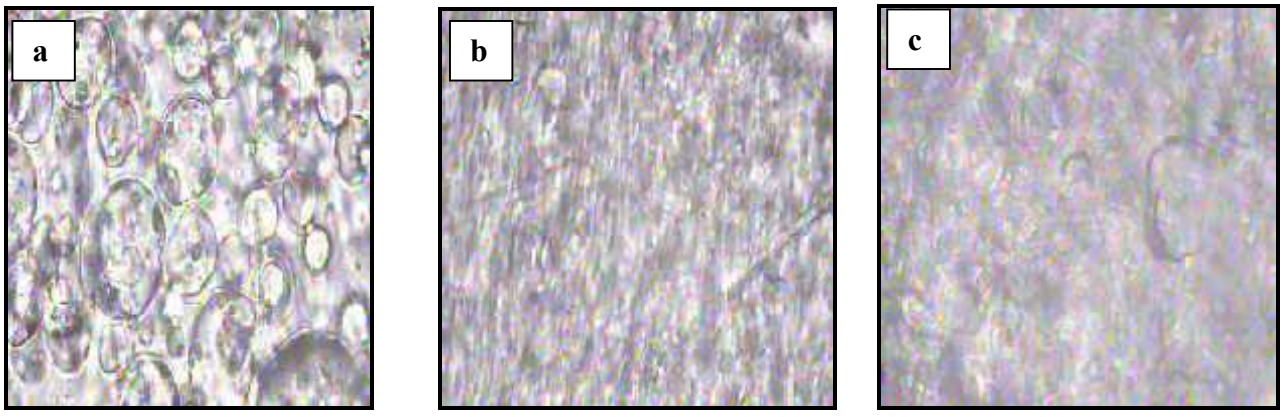

Figure VII-19: Optical microscope photos of blends (a) PET/iPP (80/20), (b) PET/PP/SEBS-g-MAH (80/20/7), (c) PET/PP/SEBS-g-MAH (80/20/15)

In the case of the addition of the clay, optical microscope observation (see figure VII-20) of surfaces reveals a dispersed structure, it is noticed a complex structure showing both a fine micro-voids which are probably attributed to the PET or iPP phase depending on whether the PET is the major phase or the iPP . Whereas the clay particles are in the form of sticks located vertically and horizontally within the matrix.

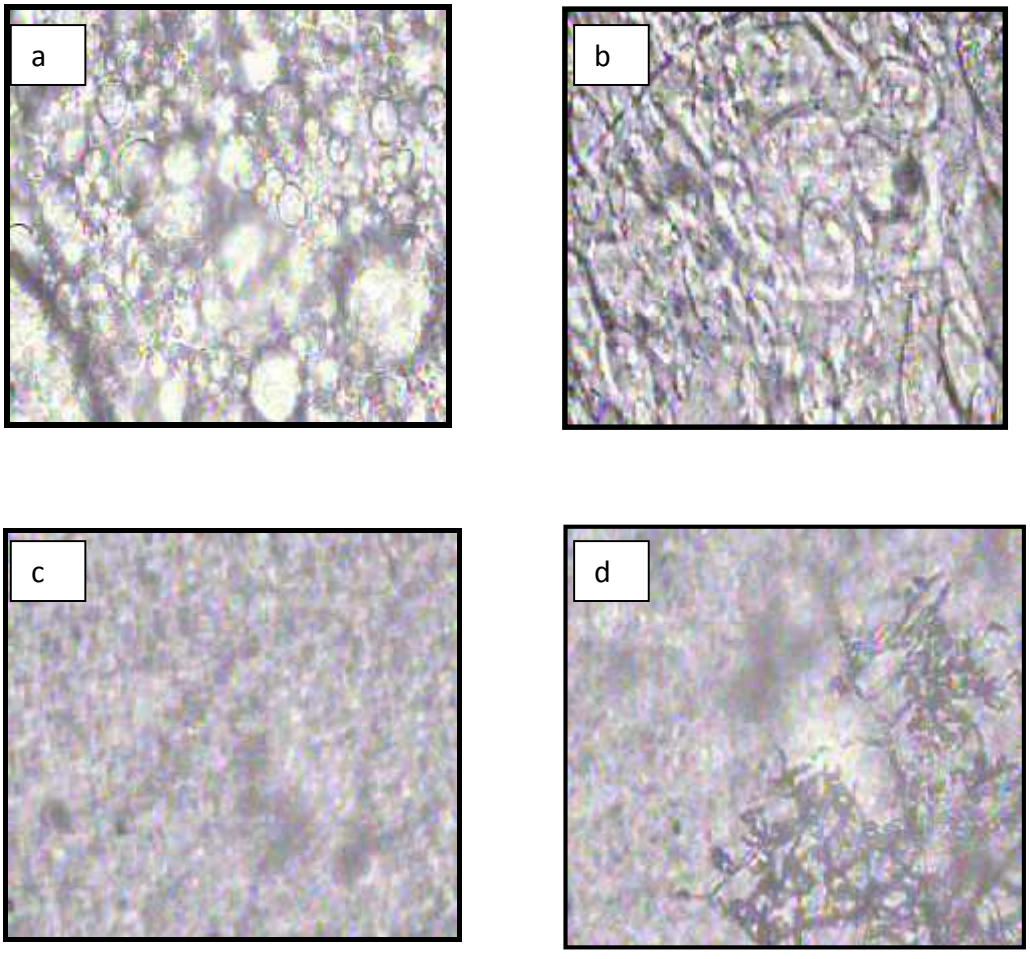

FigureVII-20 : Optical microscope photos of the blends PET/iPP avec (PET/PP/SEBS-g-MAH) and clay (a) :(50/50/Without Com), (b) :(50/50/7), (c) :(50/50/10), (d) :(50/50/15)

.

VII-6: SEM Study.

The morphologies of the iPP/PET blends with different compositions are presented in FigVII-21 . The electron microscope observation (a) serie of the surface for the blend (PET / iPP 80/20) clearly shows two distinct phases, a continuous phase (the matrix and is represented by the PET), and a dispersed phase in a more less uniform distribution in the form of voids (iPP). It is also important to note that the continuous phase also occurs in the form of long areas of smaller droplet size containing very fine dispersed phase Whereas the 50/50 PET/iPP blend represented in (b) shows two wide phases [**115**] . The addition of compatibilizers produced regular shaped and relative uniformly sized matrix domains. The series of images (a) and (b) (see figure VII-22) shows the effect of adding SEBS-g-MAH as a compatibilizer on the blend morphology of the compatibilized blends ; however, the cocontinuous morphology is retained. In fact, The addition of the compatibilizer SEBS-g-MAH in the blend PET / iPP resulted in a significant change in the morphology, we note that the dispersion of the minor phase is finer, the system is more homogenous than its counterpart without compatibilizer, where very fine and well dispersed particles in the continuous phase are attributed to the compatibilizer. It is also observed that the addition of 7 % compatibilzer did not have a substantial effect on the blend morphology compared to the blend with higher compatibilizer contents However the interaction that takes place between the SEBS-g-MAH, PET and iPP resulting in the stabilization of the interface by reducing the coalescence and the lowering the interfacial tension.

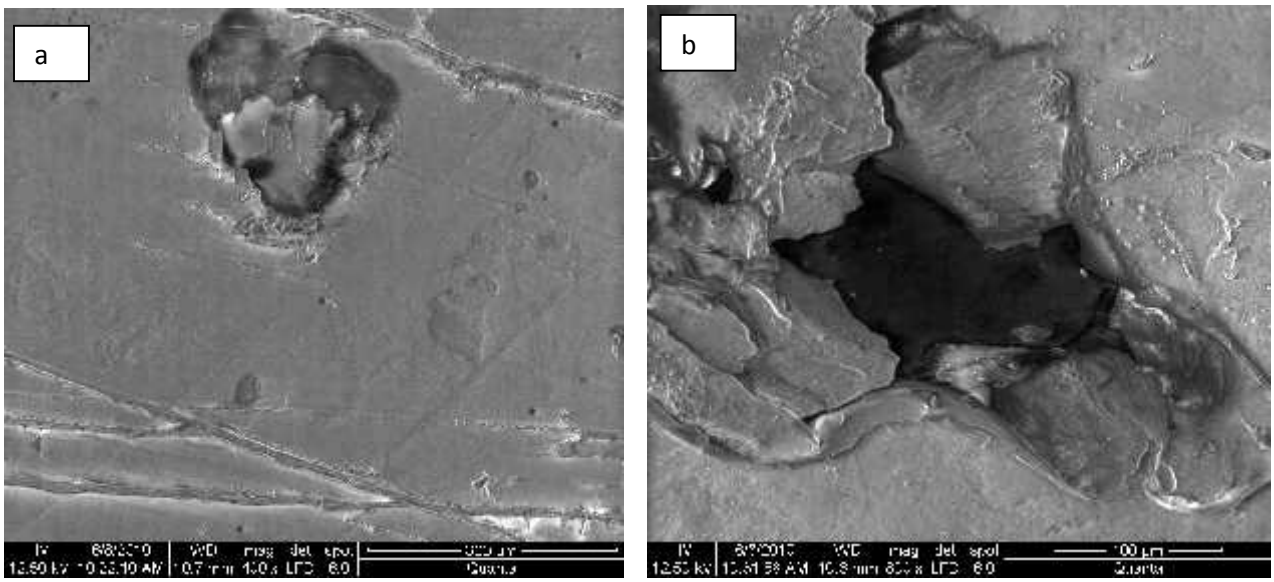

PET/PP 80/20 PET/PP 50/50

Figure VII-21: SEM micrographs of the blends of PET/iPP (a) 80/20, (b) 50/50

Considering the images of the PET/iPP / SEBS-g-MAH blends with clay (see Figure VII-22 (c) and (d) it is evident that the microscopic dispersion of these samples is poor, These composites are very heterogeneous, containing large, undispersed organoclay agglomerates separated by extensive areas of virtually pure Polymers. Except for the micrographs taken for the blend 50/50 PET/iPP with 15 % compatibilizer were the presence of the clay leads to a passage from a dispersed structure to another co-continuous, it can be clearly seen that a very fine dispersion of the clay are in the form of small white particles[**116**].

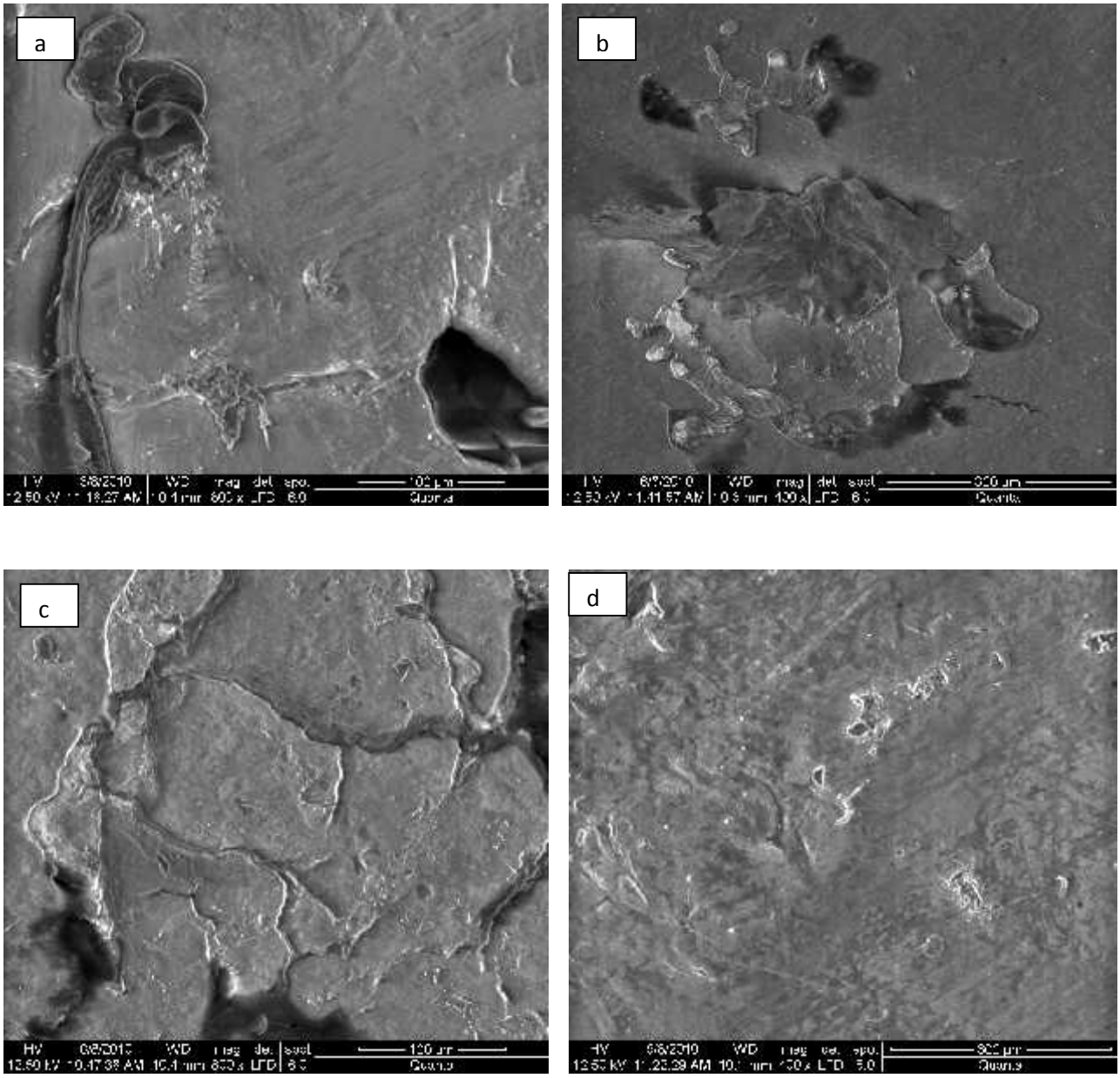

Figure VII-22: SEM micrographs of the blends of PET/iPP/SEBS-g-MAH, (c) 80/20/10, (d) 50/50/15 and with clay (e) 50/50/10, (f) 50/50/15

VII-7: FTIR study:

The Characterization by IR spectroscopy is important, it can confirm the different phenomena that occured.

The study itself is to analyze the characteristic peaks of both polymers and blends.

From the spectrum of neat polypropylene (iPP) shown in Figure (Fig.VII-23) it is observed:

- ✓ The development of a broad peak in the region 2500 - 3000 cm^{-1}, this peak indicates the presence of (CH) bond.
- ✓ The appearance of a characteristic peak of methyl groups (CH_3) in the region of 1500-1000 cm^{-1}.

✓ The appearance of a peak characteristic of the (C-C) bond in the 1200-700 cm^{-1}

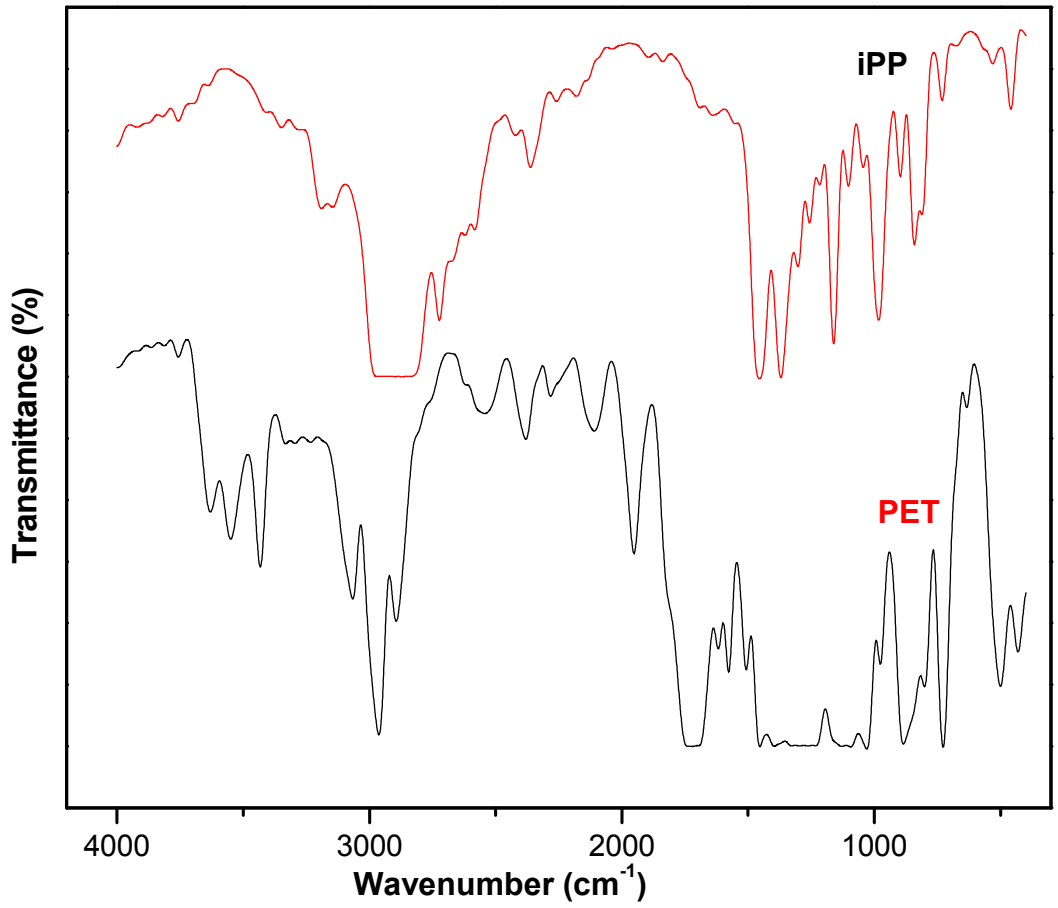

Figure VII-23: FT-IR spectra of the neat PET and neat iPP

Whereas in the same figure, the second spectrum shows the spectroscopic characteristics of PET:

- ✓ 3600 - 3300 cm^{-1}: Stretching vibration of hydroxyl group.
- ✓ 3050 cm^{-1}: Stretching vibration bands (CH) aromatic.
- ✓ 2950 cm^{-1}: Stretching vibration bands (CH) aliphatic.
- ✓ 1750 -1700 cm^{-1}: Stretching vibration groups (C = O).
- ✓ 1600 - 1400 cm^{-1}: Stretching vibration bands (C = C) in the plan ring.
- ✓ 1300 - 1000 cm^{-1}: Stretching vibration of the band (CO) polyester.
- ✓ 900 - 700 cm^{-1} : Deformation out of the of plane aromatic bands (C-H).

All the results obtained by infrared spectroscopy are shown in Figures VII 24-25). Which represent a spectroscopic comparison between different formulations of blends (PET / PP) with SEBS-g-MAH as a compatibilizer:

In these figures the same observation can be made, regarding the appearance of new bands. Indeed, we only observed the bands characteristic of the three compounds (PET / iPP / SEBS-g-MAH) without any new band. In this case we can predict that there is a physical adhesion between the dispersed phases. From these results, one can also say that, we have no chemical reaction between the three blend components.

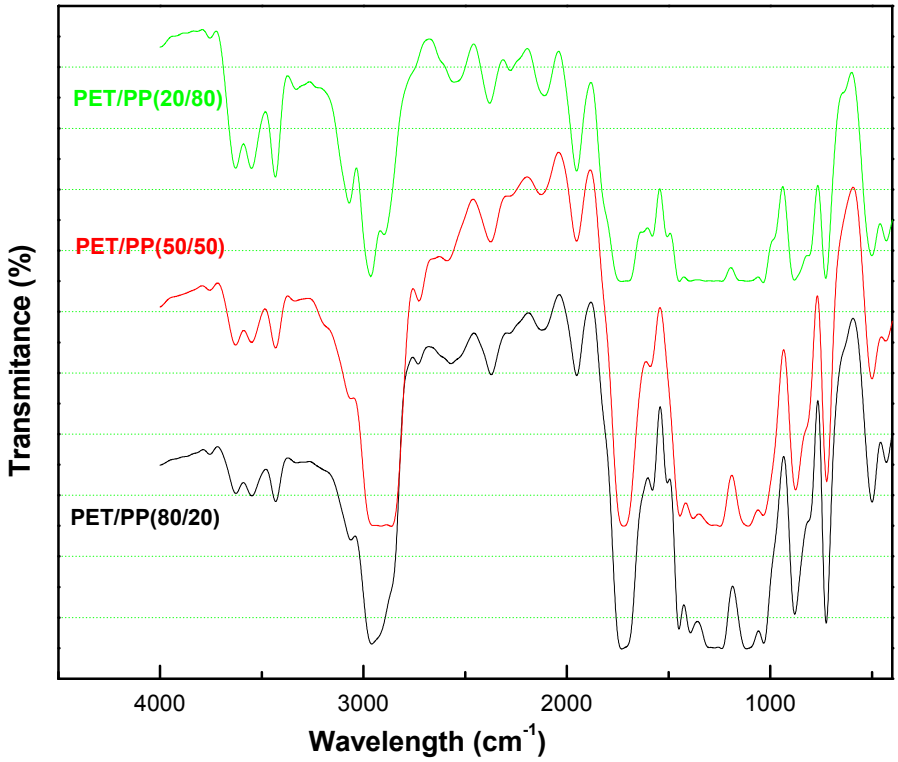

Figure VII-24: FT-IR spectra of the PET/iPP blends

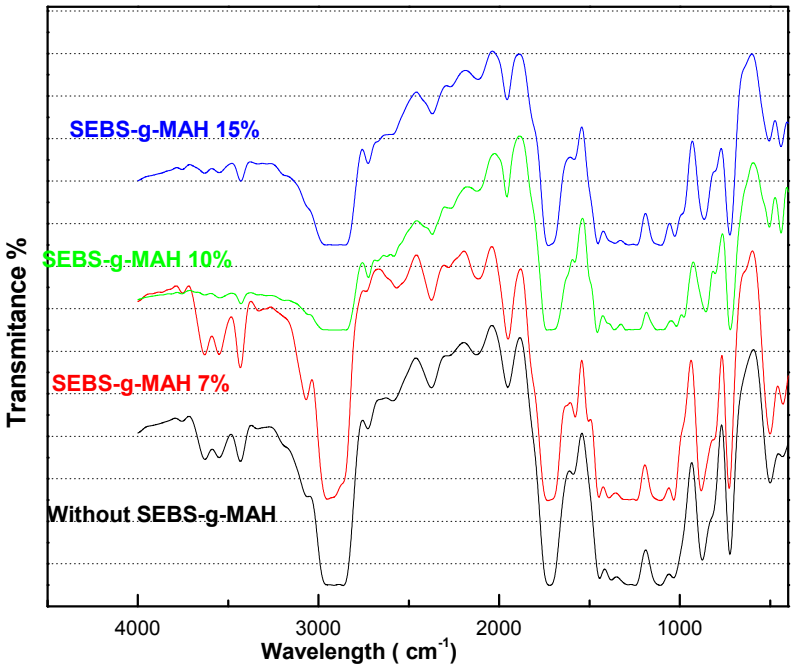

Figure VII-25: FT-IR spectra of the PET/iPP (50/50) blends compatibilized with SEBS-g-MAH

In FigureVII-26 we give the FT-IR spectra of the raw clay , the sodium modified clay Na-Mmt and the octadecylamonuim modified montmorillonite .The examination of these tree spectra shows absorption bands that are assigned as follows:

The band that stretches between 1600 and 1700 cm^{-1} is attributed to stretching vibrations of OH group of water content. The interlayer water appears at 1640 cm^{-1} and inter particle water rises around 3440 cm^{-1}.

IR spectra of montmorilonites located near 1040 cm^{-1} belongs to the Si−O stretching vibrations. The next intensive bands at 523 cm^{-1} and 467 cm^{-1} are due to the bending vibrations of Al−O−Si and Si−O−Si bonds, respectively. OH stretching modes of structural hydroxyl groups and water molecules lie in the spectral region of 3000-3800 cm-1.

The stretching vibrations of the C−H bonds occuring in the 2800 – 2950 cm^{-1} region reflect C_{18} chains of alkyl ammonium compounds. The transmission band at 2925 cm^{-1} and 2850 cm^{-1} corresponding to antisymmetric and symmetric stretching CH_2

The bending vibrations of C−H fragments appear at 1474 cm^{-1}. It is evident that OCDA alkylammonium cations are present in the modified montmorillonites.

The FTIR spectra of the compatibilized blends and with the addition of the clay (see figure VII-27) reveal the peaks associated with pure PET, iPP and the principal clay peaks. The strong peak at 3420 cm^{-1}, 2470 cm^{-1}, and 1630 cm^{-1} are characteristic peaks of MMT clay. The spectra also show the characteristic PET and iPP peaks. There is not much difference for the compatibilized PET/iPP blends spectra compared to PET/iPP/SEBS-g-MAH/clay spectra.

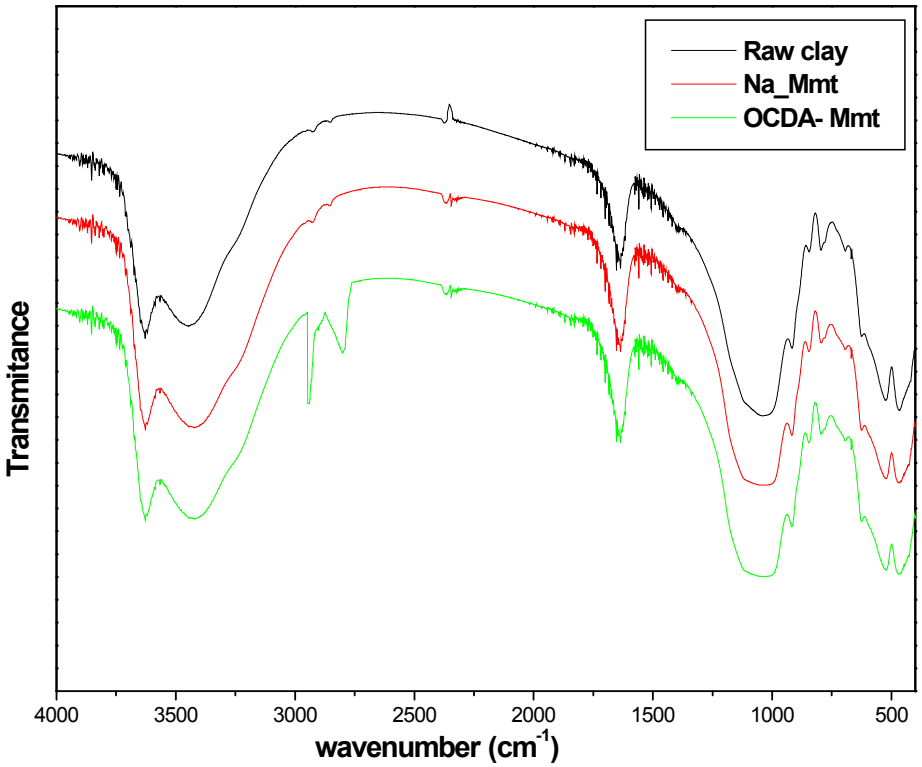

Figure VII-26: FT-IR spectra of the unmodified and modified clay

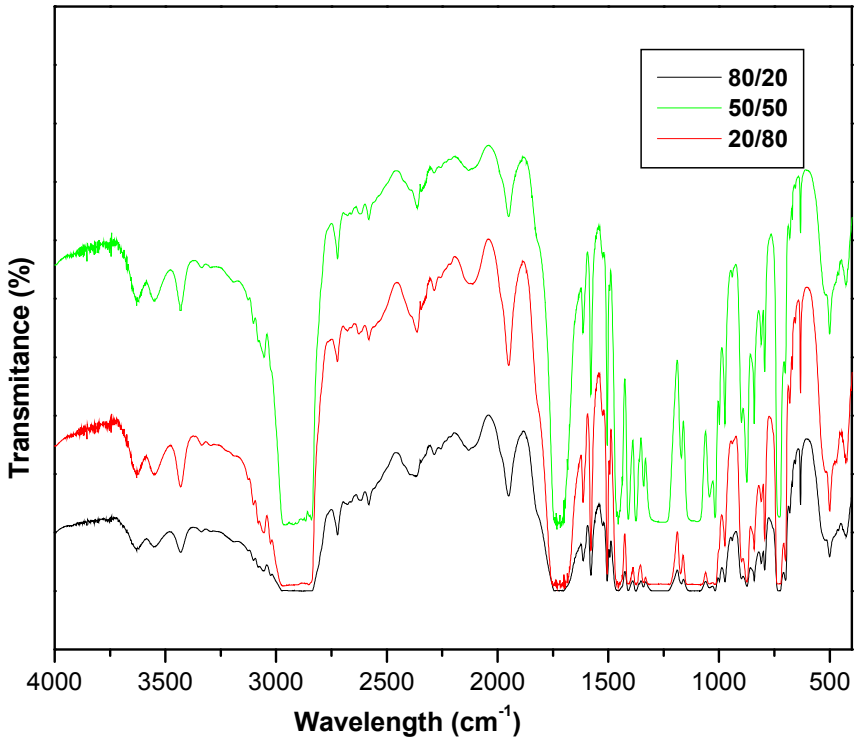

Figure VII-27: FT-IR spectra of the blends PET/iPP/SEBS-g-MAH with 15 % compatibilizer and 5% Clay

VII-7: Rheological characterization:

The results of the shear rate and shear stress characterization are shown in Figures VII-28 -32, the flow index (n) for each mixture was determined. We found that our blends have a pseudoplastic behavior ($0 < n < 1$), we also found that the shear stress increases with shear rate for all blends, due to the increased in friction between macromolecular chains and the inner walls of the capillary.

For blends (PET / iPP) without compatibilizer, results are shown in Figure VII-28, it was observed that the shear stress increases with the increase of iPP content in the blend, this is probably due to the nature of the iPP which has a higher viscosity than PET.

For blends with the compatibilizer SEBS-g-MAH, we observe (Figures VII-29-31) that the shear stress increases with increasing the amount of iPP in the blends. This increase can be explained by the fact, that addition of compatibilizer (SEBS-g-MAH) in mixtures causes physical interactions between the two phases (PET / iPP). However the same effect was noticed (see figure VII-32) with the addition of the clay to the blends with 15 % compatibilizer, that is, the shear stress increases with the increase of the shear rate for all the range of composition. Also the values are higher when the iPP content is above the equivolumic composition.

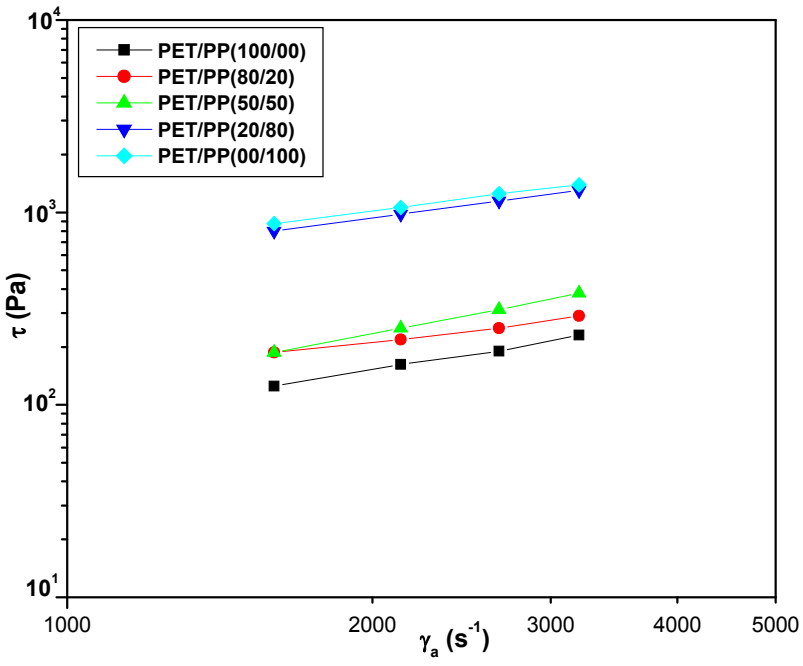

FigureVII-28: Effect of Shear stress on the corrected Shear rate of the incompatibilized blends

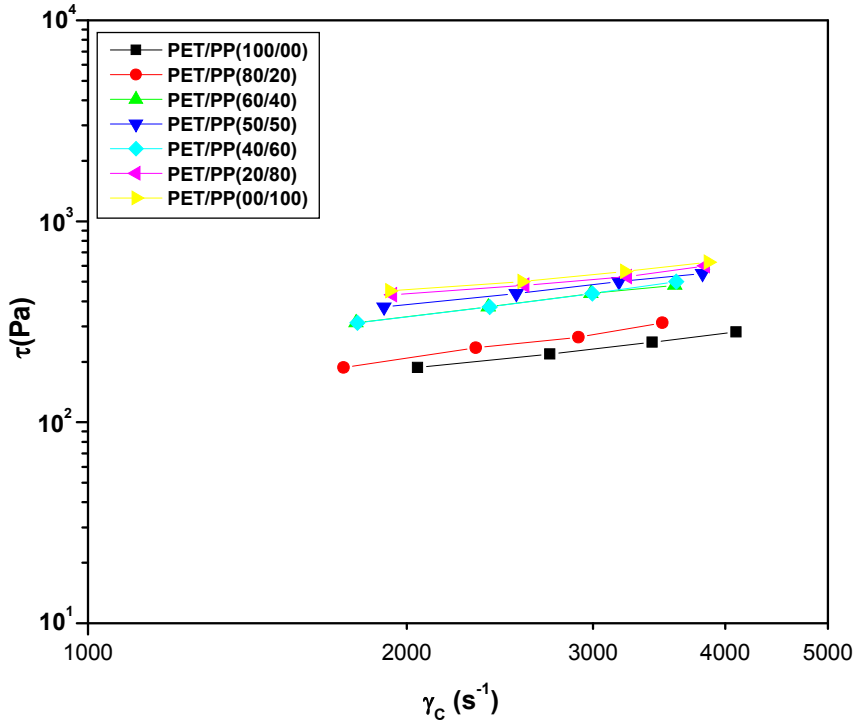

Figure VII-29: Effect of shear stress on shear rate of the blends PET/iPP compatibilized with 7 % SEBS-g-MAH

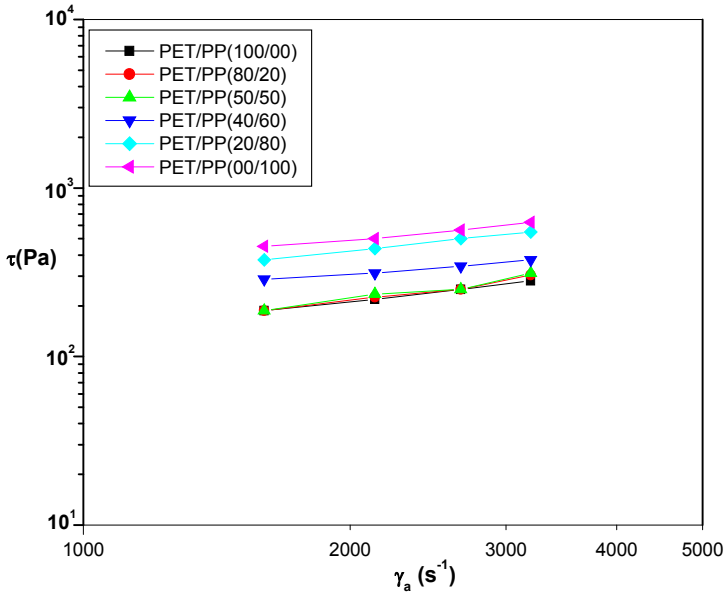

Figure VII-30: Effect of shear stress on shear rate of the blends PET/iPP compatibilized with 10 % SEBS-g-MAH

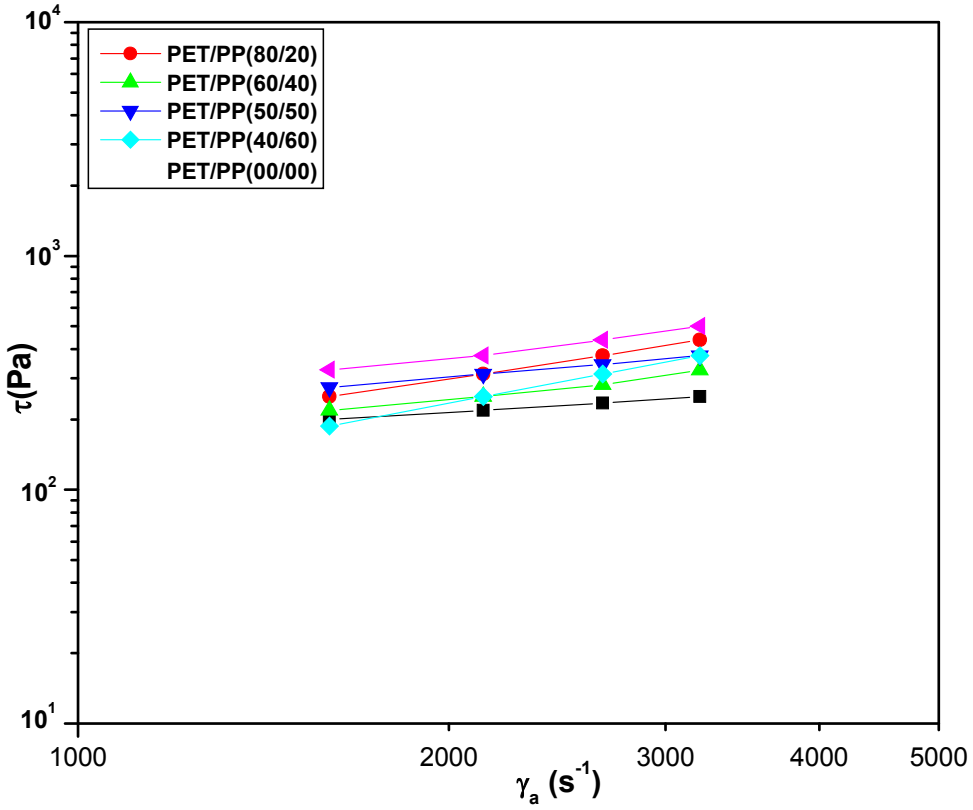

Figure VII-31: Effect of shear stress on shear rate of the blends PET/iPP compatibilized with 15% SEBS-g-MAH

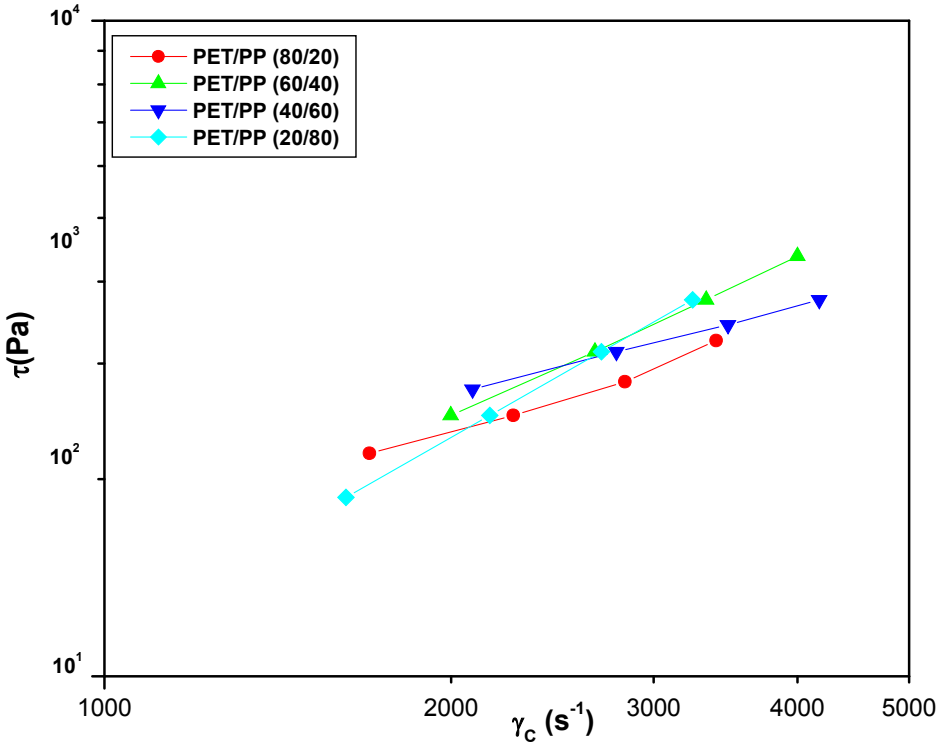

Figure VII-32: Eeffect of shear stress on shear rate of the blends PET/iPP compatibilized with 15 % SEBS-g-MAH and with 5% clay

Effect of viscosity:

According to figures VII-33-34) showing the variation of the corrected viscosity with the corrected shear rate for blends PET / iPP with and without compatibilizer, we find that the corrected viscosity decreases with increasing shear rate for all compositions, due to increased interaction forces and friction between the macromolecular chains resulting in increased system temperature, and consequently a decrease in viscosity.

For the blends without compatibilizer: according to the figure (Fig.VII-33) which shows that the viscosity of the system increases with the increase of iPP. This result may be explained by the increase of the phase of iPP, the latter is more viscous and contributes to increased repulsive forces between the two phases, so we observe that blends (PET / iPP) without compatibilizer show an heterogeneous behavior.

For the blends with compatibilizer: from Figures VII-34-36 we observe that blends exhibit homogeneous behavior and laminar flow.

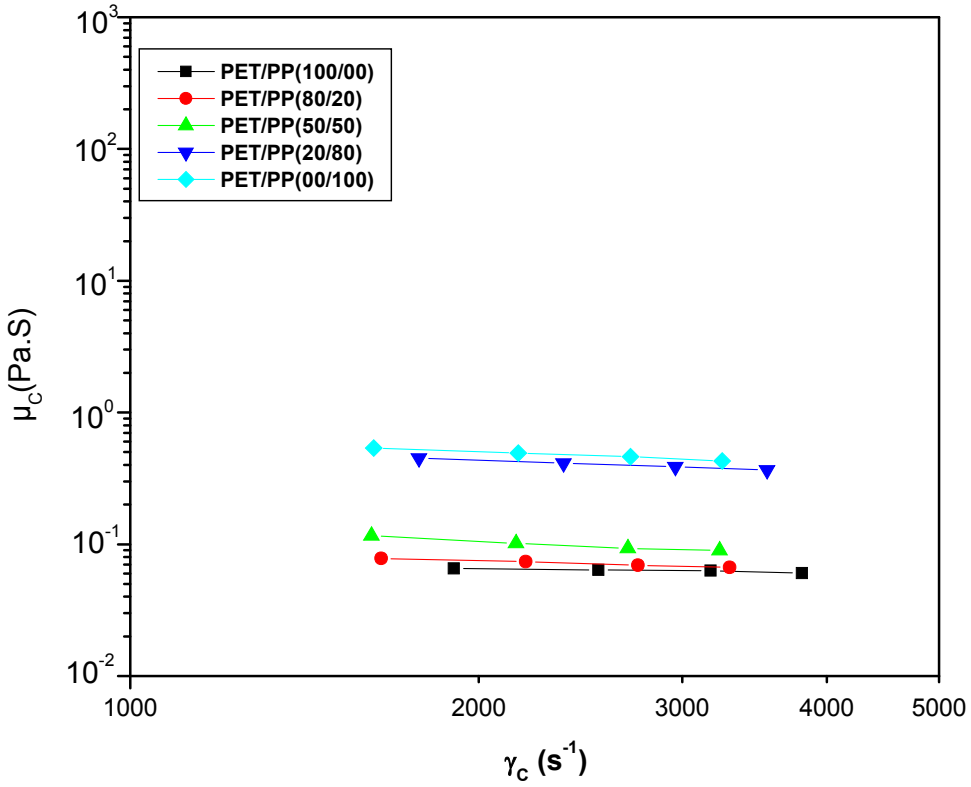

Figure VII-33: Variation of the viscosity with shear rate of the blends PET/iPP without compatibilizer

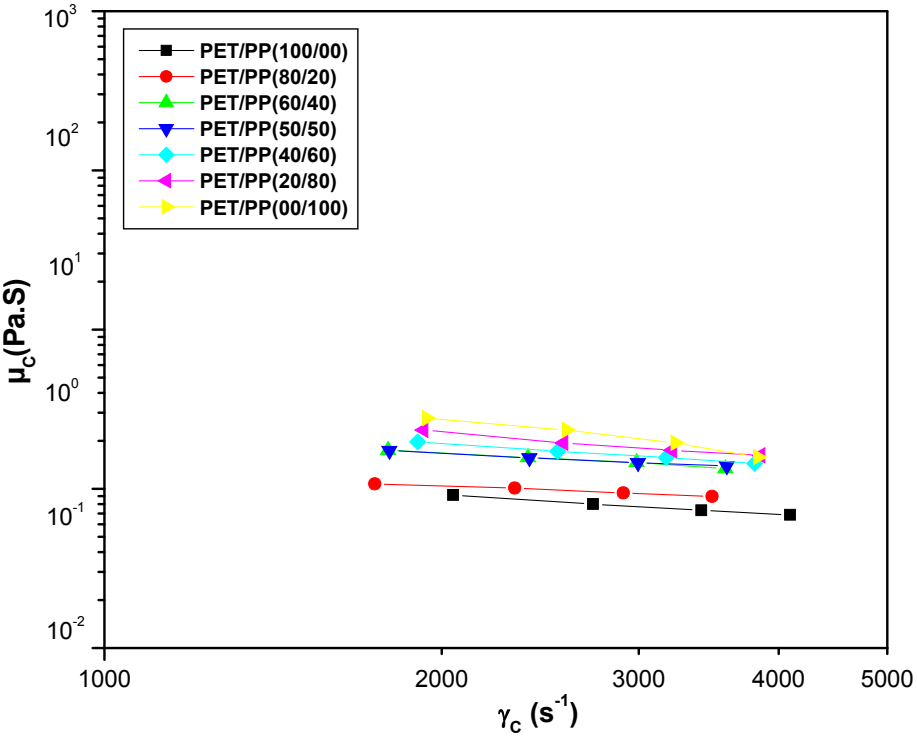

Figure VII-34: Variation of the viscosity with shear rate of the blends PET/iPP with 7% SEBS-g-MAH

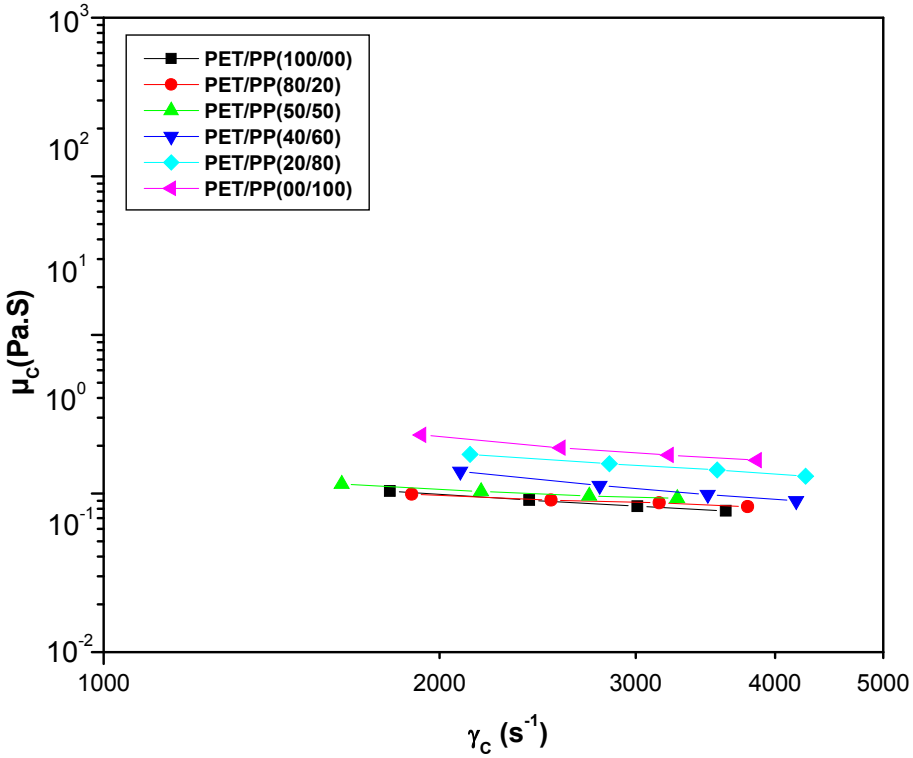

Figure VII-35: Variation of the viscosity with shear rate of the blends PET/iPP with 10% SEBS-g-MAH

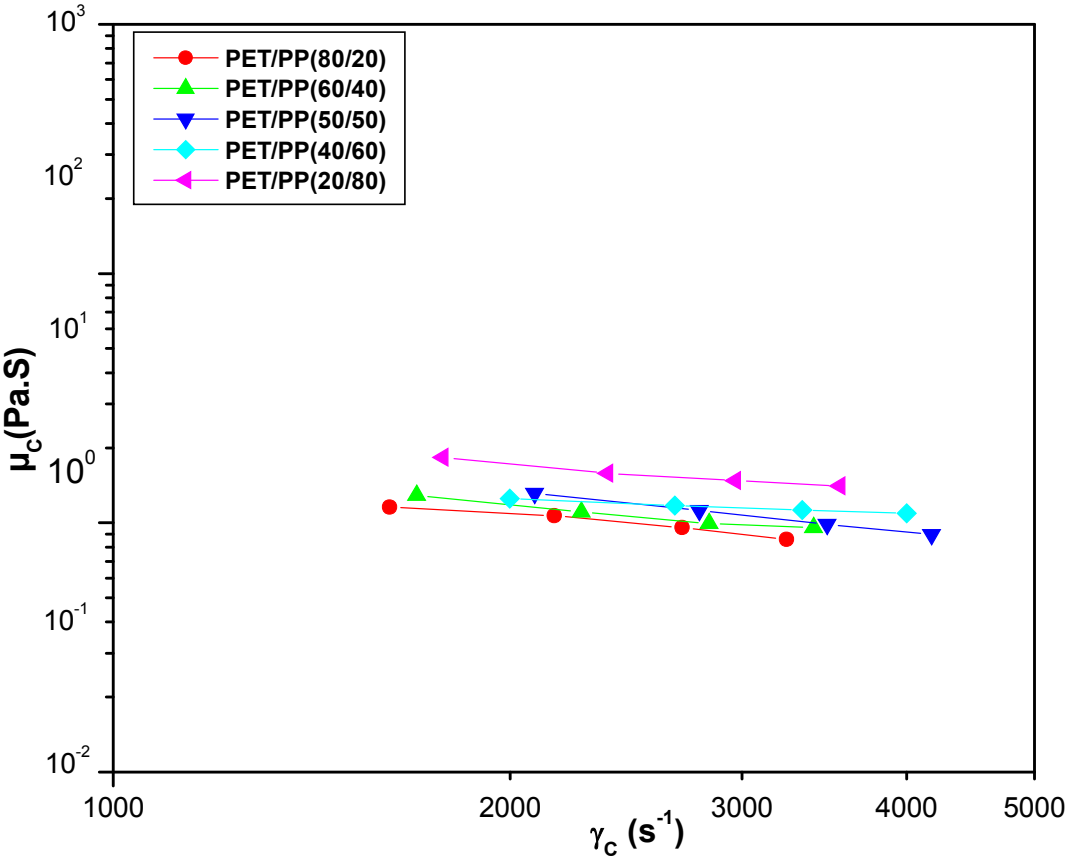

Figure VII-36: Variation of the viscosity with shear rate of the blends PET/iPP with 15% SEBS-g-MAH

Figure VII-37 shows the effect of varying the concentration of SEBS-g-MAH on the variation of corrected viscosities with shear rate for the blends of PET/iPP (50/50). It is found that the viscosity increases with increasing concentration of SEBS-g-MAH this is much more significant with high concentrations of PET phase . Whereas with high concentrations of iPP phase the viscosity decreases with increasing concentrations of SEBS-g-MAH.

With the addition of the clay to the blends containg 15% SEBS-g-MAH, the viscosity shows the same trend as seen with the blends without clay(see figure VII-38).

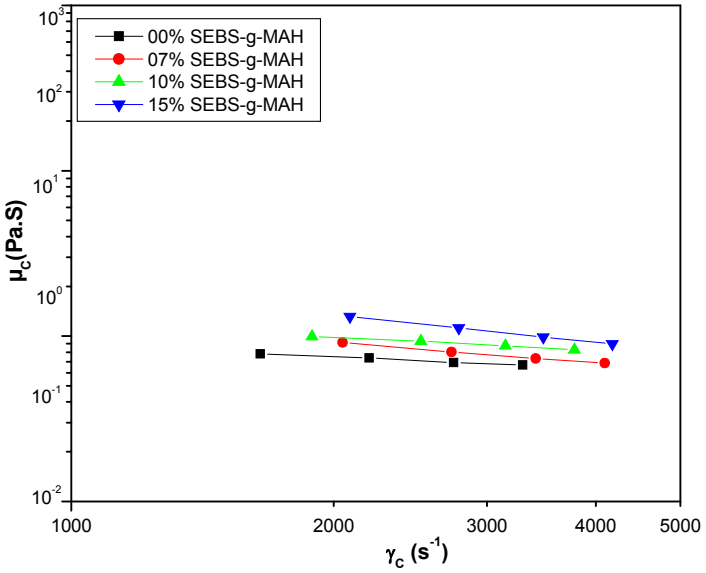

Figure VII-37 Variation of the viscosity with shear rate of the blends PET/iPP (50/50) without and with 7, 10 15% SEBS-g-MAH

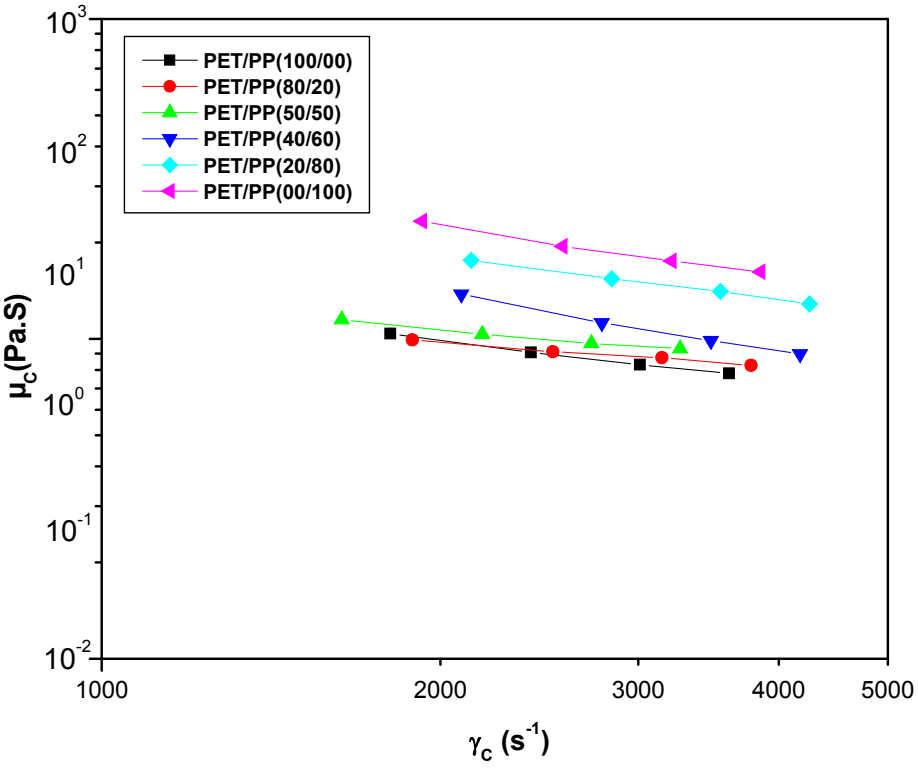

Figure VII-38: Variation of the viscosity with shear rate of the blends PET/iPP with 15% SEBS-g-MAH and with clay

VII-8. Conclusion

The characterization of the properties of mixtures PET/iPP showed a typical behavior of a completely immiscible blend. Indeed, it was noted that the values of Tm of both polymers for all the compositions have not changed significantly, the results obtained by TGA confirmed that the thermal decomposition onset temperature for the whole composition remain constant.

The DSC analysis showed no significant variations in both the melting and cristallisation peaks for the blends without compatibilizer. Indeed, we noted that increasing the rate of SEBS-g-MAH, the critalline peaks disappear reflecting the role of the compatibilizer on the change in morphology. However, the study of thermal properties revealed that the degree of crystallinity, the melting and crystallization and thermal stability were slightly affected by the addition of the SEBS-g-MAH and the clay

The WAXS patterns obtained for the blends of PET/iPP compatibilized with SEBS-g-MAH show the appearance of new peaks which are attributed to a certain amount of crystallized PET, in addition we have noticed the disappearance of the d-spacing of the clay indicating the formation of the nanocomposite dtructure.

The FT-IR study reveals that the spectra obtained for all the blends show only the peaks characteristic of the four compounds which are PET, iPP, SEBS-g-MAH and the Mmt- ODA

From the optical microscope observations it was observed a uneven dispersion of the size and shape of the dispersed phase (PET or iPP) where as the clay particles are in the form of stacks located vertically and horizontally within the matrix.

GENERAL CONCLUSIONS:

- From the preceding results, It was clear that PET was incompatible with iPP. However, the presence of SEBS-g-MAH allowed us to compatibilize these polymers.
- Whereas the initially amorphous PET was capable of crystallizing to a certain extent in the presence of iPP, probably as a consequence of the blending process , the crystallizability of iPP was strongly reduced by the PET component. Nevertheless, in the presence of the compatibilizer SEBS-g-MAH, the iPP chains became more flexible so that they could crystallize much more easily. However, the hardness of the blends strongly decreased as the compatibilizer content increased.
- In the pure PET/iPP blends, the increase in Hardness as a function of PET content, was simply due to the composition. However, the effect of mixing contributes largely to the increase in disorder in the crystal surface, providing hardness values much lower. The presence of the compatibilizer helps enlarge this vacuum effect in microhardness. Thus, mixtures without additive show values of H higher than their counterparts with compatibilizers.
- The clay seemed to have a nucleating effect on the iPP and also induced a slight hardness increase in the compatibilized blends.
- the study by FT-IR confirmed the absence of new peaks and only the bands of the four compounts are observed
- The SEM and optical microscope observations highlight the effect of addition of the SEBS-MAH on the reduction of the domaine size of the dispersed phase and therefore strong interactions are create and good adhesion is achieved
- Finally the rheological study reveals that the shear stress increases whereas a slight decrease of the viscosty is observed while increasing the shear rate for all blends,

[1] J.Scheirs, Polymer Recycling: Science, Technology and Applications; Ed.; Wiley: Chichester, England **(1998)**.

[2] R. J Erigh, Plastics Recycling: Products and Processes; Ed.; Hanser: New York **(1992)**.

[3] L. M. Robeson, Polymer Blends: A Comprehensive Review; Ed. Hanser: Munich **(2007)**.

[4] D. R. Paul, C. B. Bucknall, Polymer Blends; Vols. 1 and 2. Ed. Wiley: New York **(2000).**

[5] G. O. Shonaike, G. P. Simon, Polymer Blends and Alloys; Ed. Marcel Dekker: New York **(1999)**.

[6] L. A. Utracki, J. Can. Chem. Eng., Vol 80, pp 1008 **(2002)**.

[7] S. Sinha Rao, M. Okamoto, Prog. Polym. Sci., Vol.28, pp 1539 **(2003)**.

[8] C. O. Rohlmann, M. D. Failla; L. M Quinzani, Polymer, Vol, 47, pp 7795 **(2006)**.

[9] H. Palza, R. Vergara, M. Yazdani-Pedram, R. Quijada, J. Appl. Polym. Sci., Vol. 112, pp 1278 **(2009)**.

[10] E. P. Giannelis, Adv. Mater., Vol. 8, pp 29 **(1996)**.

[11] P. Bataille, S .Boisse, H P. Schreiber, Polym. Eng. Sci.,Vol. 27, pp 622 **(1987)**.

[12] M. Xanthos, M W. Young, J. Biesenberger, A. Polym. Eng. Sci., Vol. 30, pp 355 **(1990)**.

[13] K Heino, J Kirjava, P Hietaoja, J.Seppa,, J. Appl. Polym. Sci., Vol.65, pp 241 **(1996)**.

[14] S. S. Morye, D. D. Kale, J. Polym. Mater., Vol. 13, pp 217 **(1996)**.

[15] C. I. W. Calcagno, C. M. Mariani, Teixeira, R. S. Mauler, Composites Science and Technology, Vol. 68, pp 2193 **(2008)**.

[16] L. A. Utracki, "Commercial Polymer Blends", ed. Chapman and Hall, London **(1998)**.

[17] D. R. Paul, "Interfacial Agents, compatibilizers for polymer Blends" in D. R. Paul and S. Newman editors, "Polymer Blends", Vol. 2, Ed. Academic Press, New York **(1978)**.

[18] L. A. Utracki, "Polymer Alloys and Blends, Thermodynamics and Rheology'', Ed. Hanser Publishers, Munich **(1989)**.

[19] D. R. Paul, J. W. Barlow and H. Keskkula, " Polymer Blends", in H. F. Mark, N. M. Bikales, C. G. Overberger and G. Menges editors "Encyclopedia of Polymer Science and Engineering", Vol. 12, Ed. John Wiley and Sons, New York **(1988).**

[20] M. Xanthos, Polym. Eng. Sci., Vol. 28, pp 1392 **(1988)**.

[21] C. Koning, V. Van Duin, C. Pagnouille and R. Jerôme, Prog. Polym. Sci., Vol. 23, pp 707 **(1998)**.

[22] A. Ajji and L. A. Utracki, Polym. Eng. Sci., Vol. 36, pp 1574 **(1996)**.

[23] O. Olabisi, L. M. Robeson and M.T. Shaw, "Polymer-Polymer Miscibility", Ed. Academic Press, New York **(1979)**.

[24] Developments in clay science vol.1 in Handbook of clay science Edited by F. Bergaya, B.K.G., Theng and G. Lagaly, Elsevier **(2006)**.

[25] Q.H. Zeng, A.B. Yu, G.Q. Lu, D.R. Paul, J. of Nanoscience and Nanotechnology, Vol. 5, pp 1574 **(2005)**.

[26] M. Alexandre, P. Dubois, Polymer-layered silicate nanocomposites: preparation, properties and uses of a new class of materials. Mater. Sci. Eng., Vol. 28, pp 1 **(2000).**

|27] A. Okada, A. Usuki, Twenty years of polymer-clay nanocomposites. Macromol Mater. Eng. Vol. 291, pp 1449 **(2006).**

|28] E. Manias, A.Touny, L. Wu et al, Polypropylene/montmorillonite nanocomposites., Review of the synthetic routes and materials properties., Chem. Mater., Vol.13, pp 3516 **(2001)**

|29] J. H. Koo, Polymer nanocomposites: processing, characterization, and applications. McGraw-Hill, New York **(2006).**

|30] T. Sun and JM. Garces, High-performance polypropylene-clay nanocomposites by in situ polymerization with metallocene/clay catalysts. Adv. Mater., Vol, 14, pp128, **(2002).**

|31] J. S. Bergman, H. Chen, E. P. Giannelis et al, Synthesis and characterization of polyolefin silicate nanocomposites: a catalyst intercalation and in situ polymerization approach, J. Chem. Soc., Chem. Commun.,Vol. 21, pp 2179 **(1999).**

|32] J. Tudor, L. Willington, D. O'Hare and B. Royan, Intercalation of catalytically active metal complexes in phyllosilicates and their application as propene polymerization catalyst. Chem. Commun.,Vol.17, pp 2031 **(1996).**

|33] Y-H. Jin, H-J. Park, S-S. Im et al, Polyethylene/clay nanocomposite by in situ exfoliation of montmorillonite during Ziegler-Natta polymerization of ethylene. Macromol. Rapid Commun.**(2002).**

|34] Y. C. Ke, C. F. Long and Z. N. Qi, Crystallization properties and crystal nanoscale morphology of PET-clay nanocomposites., J. Appl. Polym. Sci.,Vol. 71, pp 1139 **(1999).**

|35] M. Okamoto, S. Morita and T. Kotaka, Dispersed structure and ionic conductivity of smectic clay/polymer nanocomposites. Polymer, Vol. 42, pp 2685 **(2001).**

|36] F. Hussain, M. Hojjati et al, Review article: polymer-matrix nanocomposites, processing, manufacturing, and application: an overview. J. Compos. Mater., Vol. 40, pp1511 **(2006).**

|37] H. C. Koh, J. S. Park, Preparation and gas permeation properties of biodegradable polymer/layered silicate nanocomposite membranes, Desalination, Vol. 233, pp 201 **(2008).**

|38] B. Pourabas and V. Raeesi, Preparation of ABS/montmorillonite nanocomposite using a solvent/non-solvent method. Polymer, Vol. 46, pp 5533 **(2005).**

[39] T. Tanaka, GC. Montanari and R. Mulhaupt, Polymer nanocomposites as dielectrics and electrical insulation-perspectives for processing technologies, material characterization and future applications, Vol. 11, pp 763 **(2004).**

[40] D. R. Paul, L. M. Robeson, Polymer nanotechnology: nanocomposites. Polymer, Vol. 49, pp 3187 (**2008).**

[41] L. A. Utracki, Polymeric nanocomposites: compounding and performance. J. Nanosci. Nanotechnol., Vol. 8, pp 1582 **(2008).**

[42] A. Frache, O. Monticelli, Preparation of nanocomposites based on PP and PA6 by direct injection molding, Polym. Eng. Sci., Vol. 48, pp 2373 **(2008).**

[43] S. Bouhelal, M. E. Cagiao, S. Khellaf, D. Benachour, F. J. Balta Calleja "Nanostructure and micromechanical properties of reversibly crosslinkined isotactic polypropylene/clay composites". J. Appl. Polym. Sci., Vol. 115, pp 2654 **(2010).**

[44] W. H. Awad, J. W. Gilman, M. Nyden, R. H. Harris, Thermochimica Acta, Vol. 3, pp 409 **(2004)**.

[45] W. Xie, Z. Gao, W.P. Pan, Chem. Mater., Vol. 13, pp 2979 (**2001)**.

[46] L. A. Utracki, M. R. Kamal, The Arabian Journal for Science and Engineering, Vol, 27(1C): pp43 **(2002).**

[47] J. H. Chang, S. J. Kim and S. Im., Polymer, Vol. 45, pp 5171 **(2004).**

[48] W. Xie, Z. Gao, K. Liu, W.P. Pan, R. Vaila, D. Hunter, A. Singh, Thermochim. Acta, Vol. 339, pp 367 **(2001).**

[49] S. Pavlidou , C. D. Papaspyridesb, A review on polymer-layered silicate nanocomposites. Prog. Polym. Sci., Vol. 33, pp1119 **(2008).**

[50] S. S. Ray and M. Bousima, Biodegradable polymers and their layered silicate nanocomposites: in greening the 21st century materials world. Prog. Mater. Sci.,Vol, 50, pp 962 **(2005).**

[51] MZ .Rong, MQ .Zhang, WH .Ruan, Surface modification of nanoscale fillers for improving properties of polymer nanocomposites: a review. Mater. Sci. Technol., Vol. 22, pp78 **(2006).**

[52] A. Di Gianni, E. Amerio, Preparation of polymer/clay mineral nanocomposites via dispersion of silanated montmorillonite in a UV curable epoxy matrix. Appl. Clay Sci., Vol. 42, pp 116 **(2008).**

[53] I. J. Chin, T. Thurn-Albrecht, H. C. Kim, On exfoliation of montmorillonite in epoxy, Polymer, Vol. 42, pp 5947 **(2001).**

[54] G.C. Montanari, F. Palmieri, Polarization processes of nanocomposite silicate-EVA and PP materials, Trans IEEJ, Vol.126, pp 1090 **(2006)**

[55] E. Vijaykumar Sinha, R.Mayank, E. Patel, V. Jigar, J. Patel, Polym. Environ, Vol.18, pp 825 **(2010)**.

[56] L.M.Warren, R.Burns,Plast. Technol. Vol, 6, pp 41 **(1988).**

[57] C. W. Neale, N. C. Hilyard, P. Barber, Conserv. Recyc.Vol, 6, pp 91 **(1983).**

[58] J. H. Schut, Plast.Technol, Vol. 80 **(1993)**.

[59] J. Snyder, Mod. Plast. Int., Vol. 73, October **(1994).**

[60] J. W .Jensen, J. L. Holman, J. B. Stephenson, Recycling and disposal of waste plastics. Ann. Arbor Science, chap7 **(1974)**.

[61] www.wasteonline.org.uk/resources/informationsheets/plastics.htm **(accessed April 2010)**

[62] Nguyen Phuc Thanh · Yasuhiro Matsui Takeshi Fujiwara, Environ Monit Assess, Published on line 20May **(2010)**

[63] www.polyester-technology.com/.../Polyester_Recycling_Industry_Wiki_1-2009.pdf **(accessed Oct 2010)**

[64] D. Tabor, the hardness of metals, Oxford C. Press, New York **(1951)**.

[65] H.O'Neill, Hardness Measurment of metals and alloys, Chapmann Hall, London, 1967**.**

[66] P. Eyerer and G. Lang Kungstoff, Vol. 62, pp 222, **(1972).**

[67] F. J. Balta Calleja, Advanced Polymer science, Vol. 66, pp 117 **(1985).**

[68] Y. Deslandes, E. Alva rosa, F. Brisse and T. Meneghini, J. Mat. Sci., Vol. 26, pp 2769 **(1991)**.

[69] D. M. Marsh, Proc. Phys. Soc., London A279, pp 420 **(1964)**.

[70] D.C. Bassett, Principle of polymer Morphology Cambridge university Press Cambridga, **(1981)**.

[71] R. Poppli and L. Mandelkern, J. Polym. Sci.; Polym. Phys., Vol. 25, pp 441 **(1987)**.

[72] B. Crist, C.J. Fisher and P.R. Howard, Macromolecules, Vol. 22, pp 1709 **(1989)**.

[73] F. J. Balta Calleja and H. G. Kilian, Colloid and Polymer Science, Vol.263, pp 697 **(1985)**.

[74] D. R. Rueda, A. Viksne, L. Malers and F.J. Balta calleja, J. Mater. Sci., Vol. 29, pp 1109 **(1994)**.

[75] R. Krache, D. Benachour, M.E Cagiao, F.J. Balta Calleja, R.K.Bayer, F.Tschope, Int. J. Polym. Mater., Vol.52, pp 939 **(2003).**

[76] G. Verfaillie, J. Devaux, R. Legras, Polymer, Vol.40, pp 2929 **(1999)**.

[77] C. P. Papadopoulou, N. K. Kalfoglou , Polymer, Vol. 41, pp 2543 **(2000).**

[78] M. A. Lopez-Manchado and M. Arroyo, Polymer, Vol. 42, pp 6557 **(2001).**

[79] S. Palova, H. P. Sérgio, Journal of Materials Processing Technology, Vol.143, pp517 **(2003)**.

[80] K. Friedrich, M. Evstatiev, S. Fakirov, O. Devastative , M. Ishii , M. Harrass, Composites Science and Technology, Vol. 65, pp 107 **(2005)**.

[81] C. Fuchs, D. Bhattacharyya, S.Fakirov, Composites Science and Technology, Vol. 66, pp 3161 **(2006)**.

[82] A. A Postolov, M. Evstatiev Z. Denchev K. Friedrich S. Fakiro, J. Mater. Sci., Vol. 42, pp 1245 **(2007).**

[83] C. I. W. Calcagno, C.M.Mariani, S.R.Teixeira, R.S.Mauler, Composites Science and Technology, Vol. 68, pp 2193 **(2008).**

[84] Youji Taoa and Kancheng Mai, European Polymer Journal, Vol, 43, pp3538, **(2007).**

[85] H. Khelaf, O. Bouras and V. Perrichon, Synthesis and characterization of Alpillared and cationic surfactant modified Al-pillared algerian bentonite, Microporous materials, Vol. 8, pp 41 **(1997).**

[86] O. Bouras, Synthèse et caractérisation des montmorillonites pontées à base de bentonites algériennes, thèse de magister, Institut de Chimie Industrielle, Université de Blida (Algérie) **(1992)** .

[87] http://en.wikipedia.org/wiki/Differential_scanning_calorimetry (accessed Oct. **2010)**

[88] B. F. Mathot, Vincent, Calorimetry and Thermal Analysis of Polymers, Hanser, **(1993)**.

[89] Rohan Labde, Preparation and Characterization of Polyethylene Terephthalate/Montmorillonite Nanocomposites by In-situ Polymerization Method, Ph.d., University of Toledo, May **(2010).**

[90] P. C. Painter, M. M. Coleman, and J. L. Koenig, The Theory of Vibrational Spectroscopy and Its Application to Polymer Materials. Ed, Wiley, New York **(1982)**.

[91] K. Nichidia and J. Coats, Infrared and Raman Analysis of Polymers in HANDBOOK OF PLASTICS, Marcel Dekker, Inc, New York **(2003).**

[92] ATHAS Databank. http://athas.prz.rzeszow.pl **(accessed Sept. 2009).**

[93] A. Flores, J. Aurrekoechea, R. Gensler, H.H. Kausch, and F.J. Balta Calleja, Colloid Polym. Sci., Vol.276, pp 786 **(1998).**

[94] A. Celli and E. D. Zanotto, Thermochimica Acta,, Vol.269, pp 191 **(1995).**

[95] G. Gallego Ferrer, M. S. Salmeron, E. S. Verdu, F.C. Romero, J. L. G. Ribelles, Polym. Int., Vol., 49, pp 853 **(2000).**

[96] S. Mbarek, M. Jaziri, Y.Chalamet, B. Elleuch, C. Carrot, Int. J. Mater. Form., Vol.2, pp15 **(2009).**

[97] Y. Xi, W. Martens, H. He and R. L. Frost, J. Therm. Analys. and Calorim., Vol. 81, pp 91 **(2005).**

[98] F. Gong, M. Feng, C. Zhao, S. Zhang, M. Yang, Polym. Degradation and Stability, Vol. 84, pp 289 (**2004).**

[99] M. S. Lakshmi, B. Narmadha, B. S. R. Reddy, Polym. Degradation and Stability, Vol, 93, pp201, **(2008).**

[100] Y. Wang, J. Gao, Y. Ma, U. Agarwal, Composites: Part B, Vol. 37, pp 399 **(2006).**

[101] A. Leszczynska, J. Njuguna, K. Pielichowski, JR. Banerjee. Thermochim Acta., Vol. 453, pp 75 (**2007).**

[102] B. Lotz, J. C. Wittmann And A. J. Lovinger, Polymer, Vol. 37, pp 4979 (**1996).**

[103] C. P. Papadopoulou, N. K. Kalfoglou, Polymer, Vol. 41, pp 2543 **(2000).**

[104] F.J. Balta-Calleja, S. Fakirov, Microhardness of Polymers; Solid State Science Series; Cambridge University Press: Cambridge, England,; Chapters 4 and 5 **(2000)**.

[105] F. J. Balta Calleja, A. Flores and GH. Michel, J. Appl. Poltm. Sci., Vol. 19, pp 3 **(2004).**

[106] A. Flores, F. Ania and F. J. Balta-Calleja, Polymer, Vol. 50, pp 729 **(2009)**

[107] A. Flores, M. Pieruccini, N. Stribeck, S.S. Funari, E. Bosch and FJ. Balta-Calleja, Polymer, Vol. 46, pp 9404 **(2005).**

[108] J. Kajaks, A. Flores, M.C. Garcia Gutierrez, D.R.Rueda and FJ. Balta-Calleja, Polymer, Vol. 41, pp 7769 **(2000).**

[109] C. Santa Cruz, N. Stribeck, H.G. Zachmann, F.J. Balta-Calleja, Macromolecules, Vol. 24, pp 5980 **(1991).**

[110] A. Flores, M. Pieruccini, U.No-chel, N. Stribeck, F. J. Balta-Calleja, Polymer, Vol. 49, pp 965 **(2008).**

[111] S. Henning, G. H. Michler, F. Ania, F. J. Balta-Calleja, Colloid Polym. Sci., Vol. 283, pp 486 (**2005).**

[112] S. Henning, R. Adhikari, G.H. Michler, F.J. Balta-Calleja and J. Karger-Kocsis, Macromol. Symp., Vol. 214, pp 157 **(2004).**

[113] J. C. Lepers; B.D. Favis; R.J.Tabar, J. Polym. Sci., Polym. Phys., Vol,35, pp271, **(1997)**.

[114] K. R. Ratinac, H. Y. Zhu, L. M. Stadtmueller and S. P. Ringer, Materials Forum, Vol. 26, pp 44 **(2002).**

[115] Xin Yi a, Ling Xu a, Yu-Ling Wang a, Gan-Ji Zhong a, Xu Ji b,*, Zhong-Ming Li a,*n, Eur; Polym. Jour., Vol. 46, pp 719 **(2010)**.

[116] A. B. Morgan, J. W. Gilman and C. L. Jackson, Macromolecules, Vol. 34, pp 2735 **(2001).**

Annexes

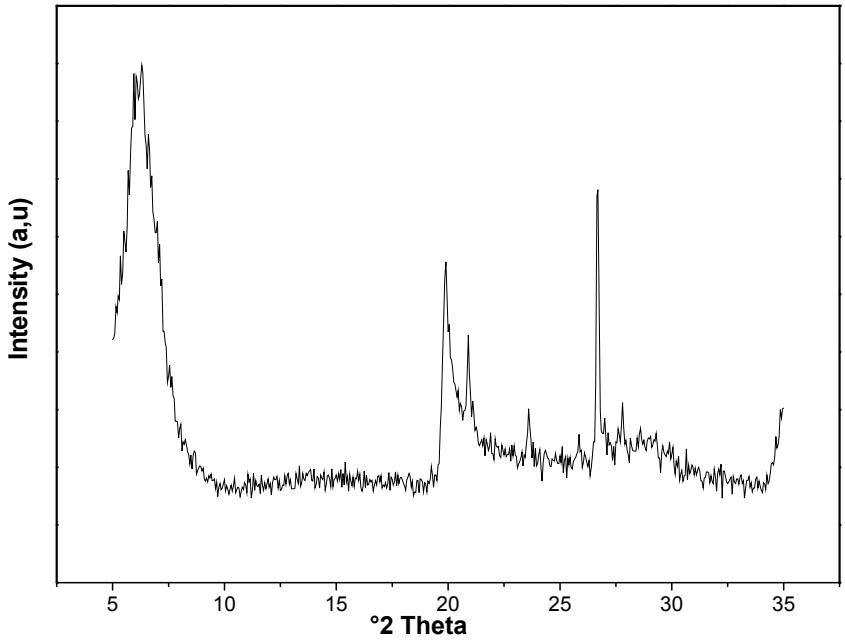

Figure VIII-1 : X-ray difractogram of raw clay (bentonite)

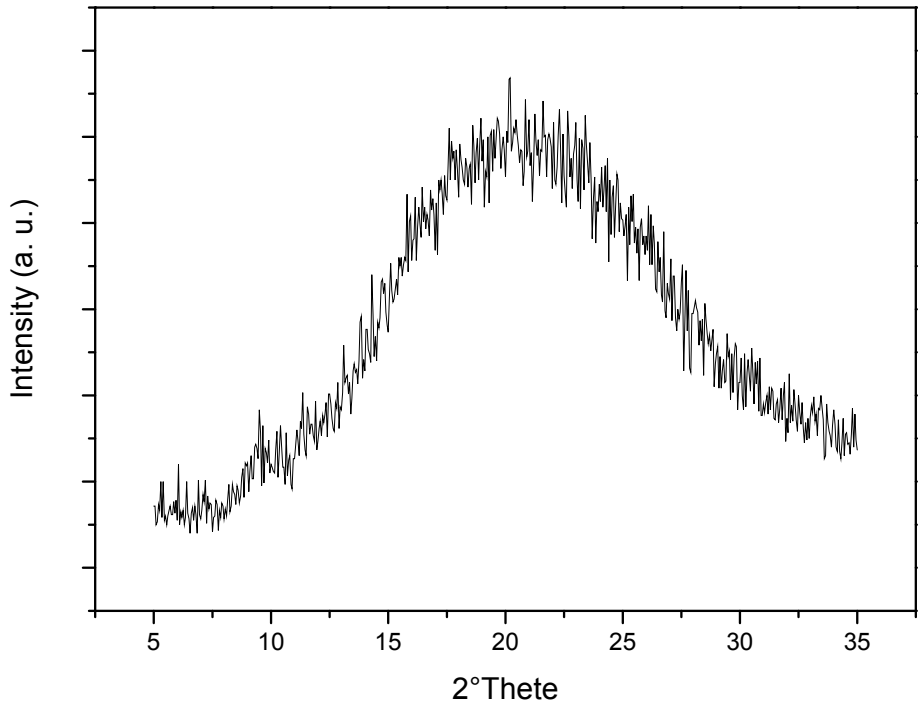

Figure VIII-2: X-ray difractogram of neat PET

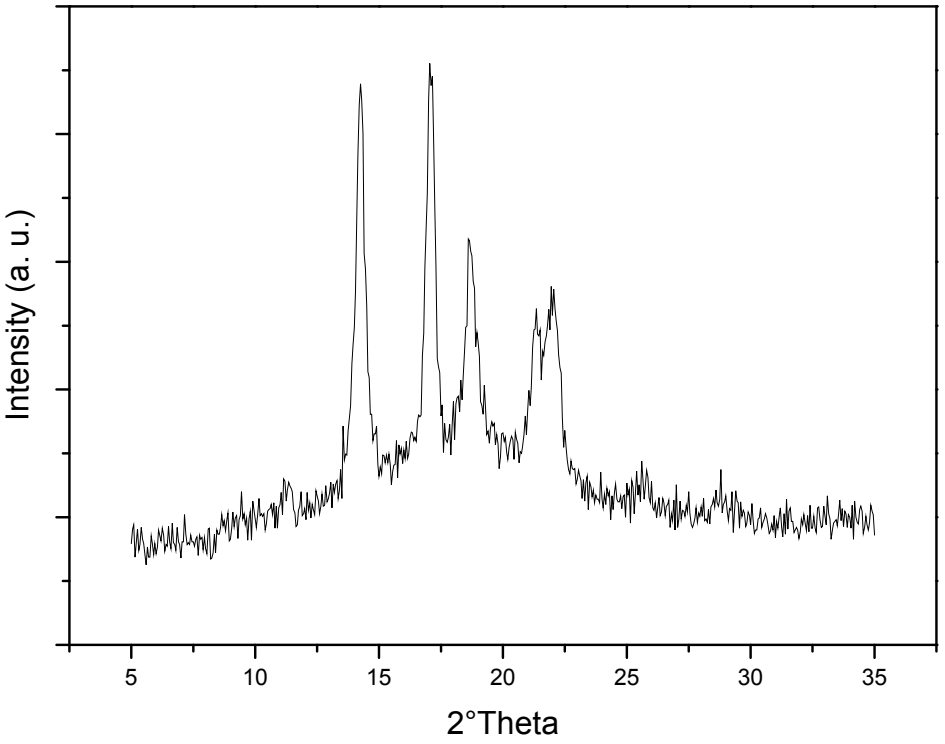

Figure VIII-3: X-ray difractogram of neat iPP

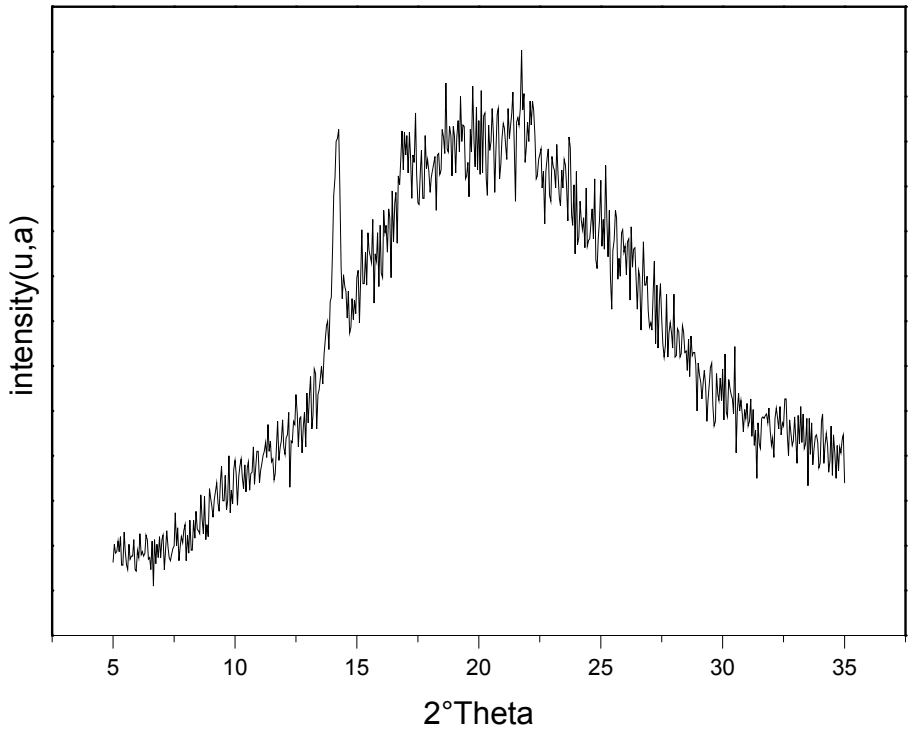

Figure VIII-4: X-ray difractogram of the blend PET/iPP (20/80)

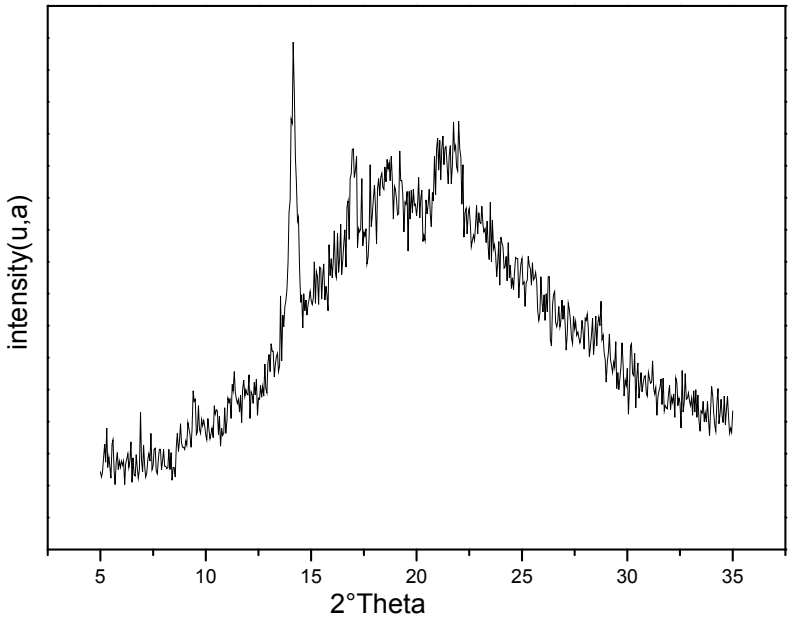

Figure VIII-5: X-ray difractogram of the blend PET/iPP (50/50)

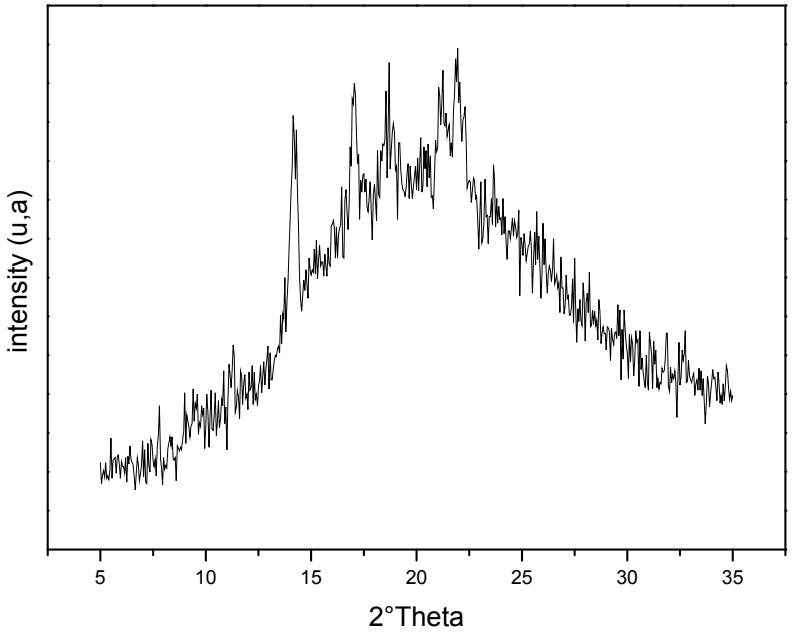

Figure VIII-6: X-ray difractogram of the blend PET/iPP (80/20)

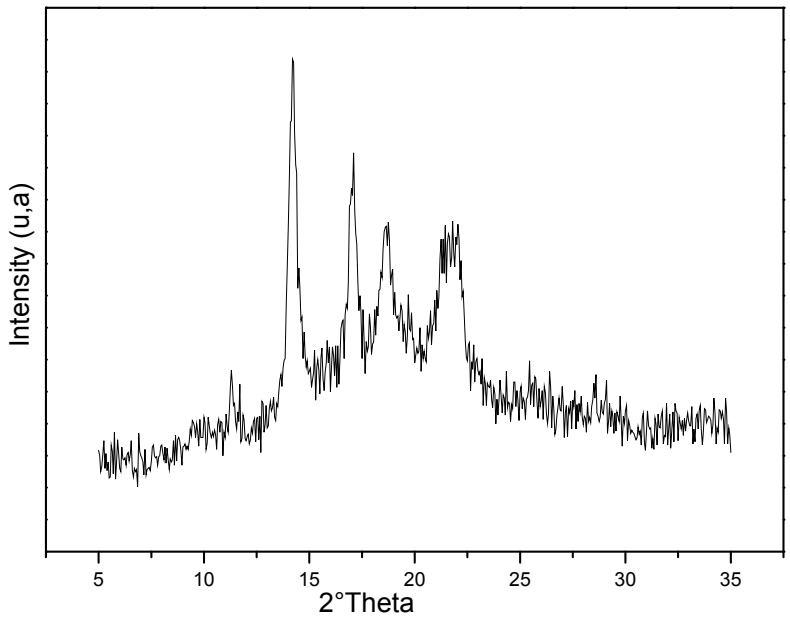

Figure VIII-7: X-ray difractogram of the blend PET/iPP/SEBS-MAH (80/20/7)

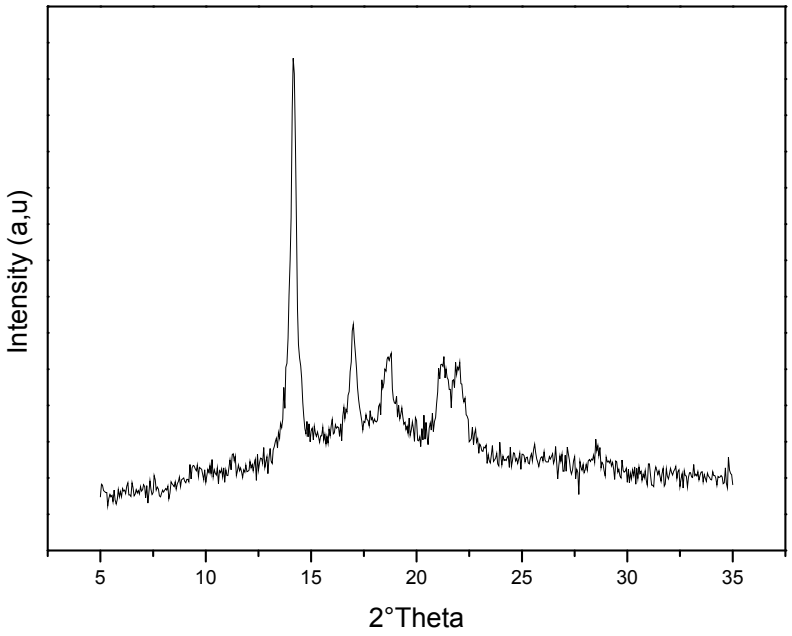

Figure VIII-8: X-ray difractogram of the blend PET/iPP/SEBS-MAH (80/20/10)

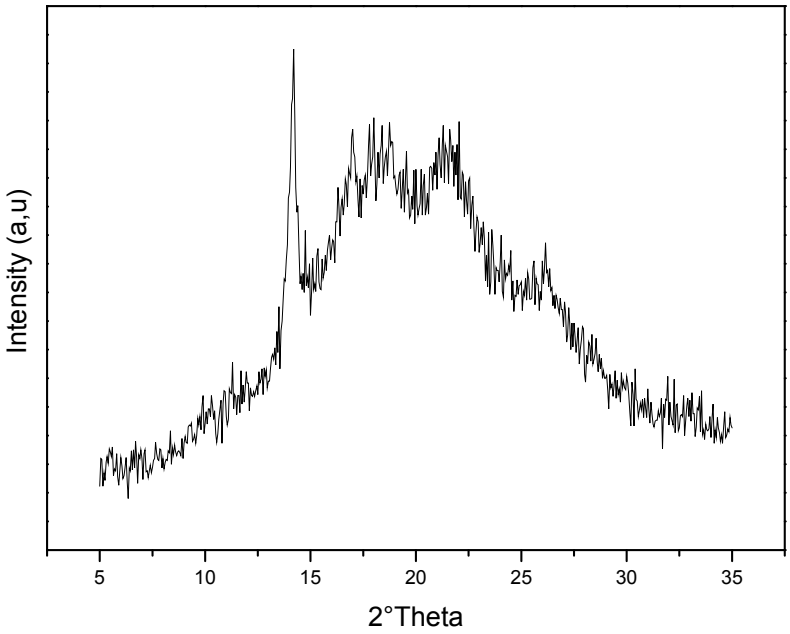

Figure VIII-9: X-ray difractogram of the blend PET/iPP/SEBS-MAH (80/20/15)

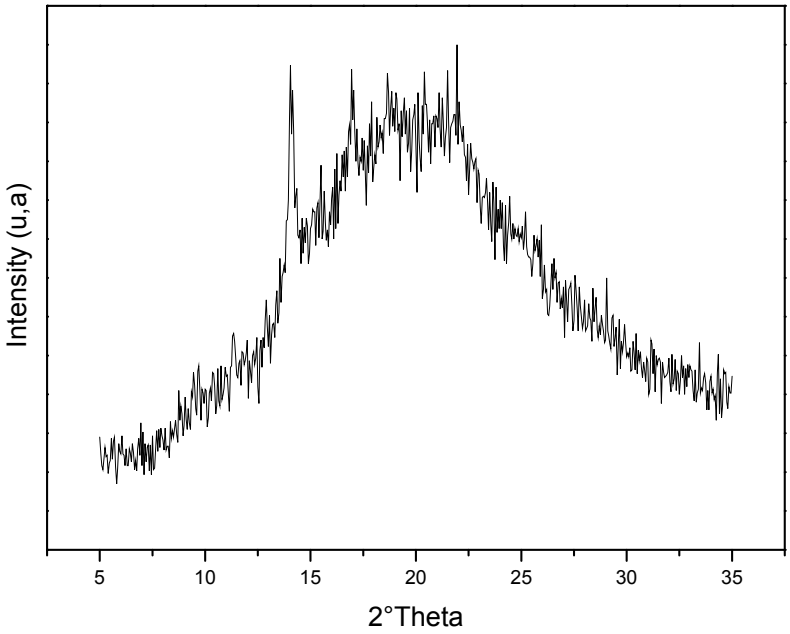

Figure VIII-10: X-ray difractogram of the blend PET/iPP/SEBS-MAH (60/40/7)

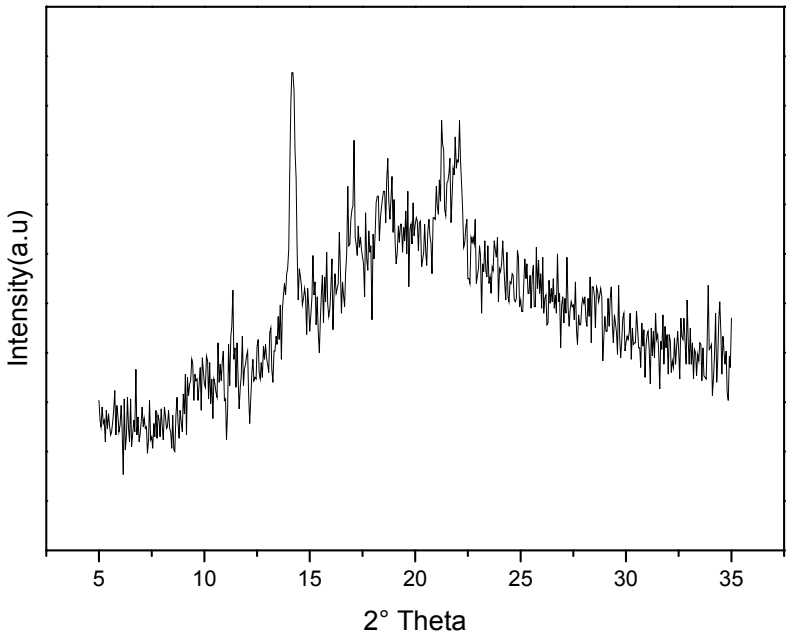

Figure VIII-11: X-ray difractogram of the blend PET/iPP/SEBS-MAH (60/40/10)

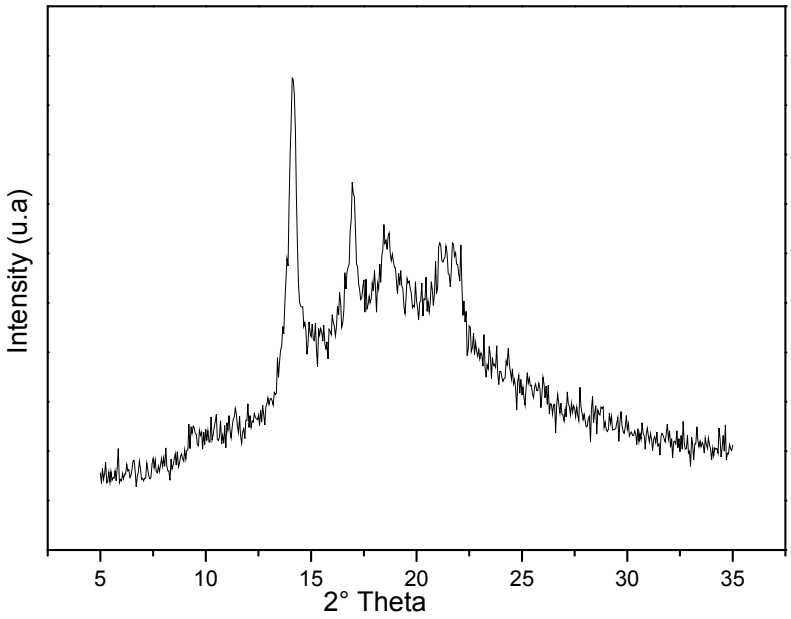

Figure VIII-12: X-ray difractogram of the blend PET/iPP/SEBS-MAH (60/40/15)

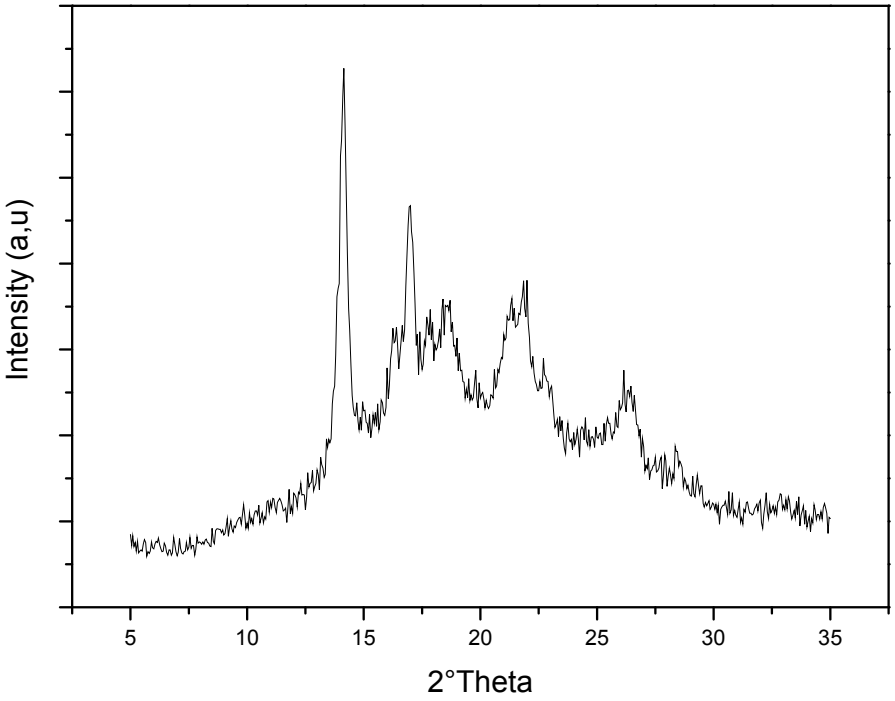

Figure VIII-13: X-ray difractogram of the blend PET/iPP/SEBS-MAH (50/50/7)

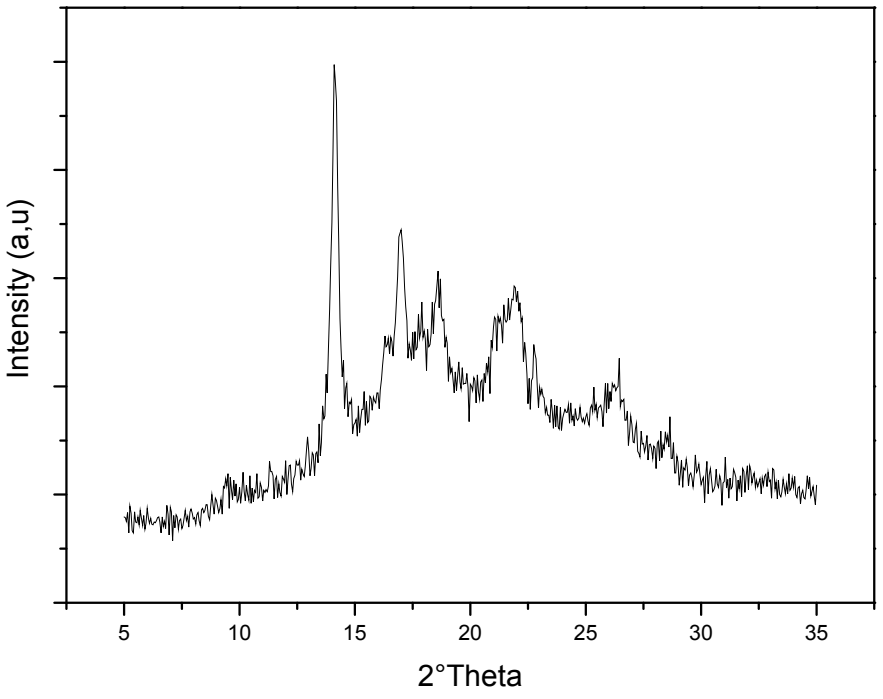

Figure VIII-14: X-ray difractogram of the blend PET/iPP/SEBS-MAH (50/50/10)

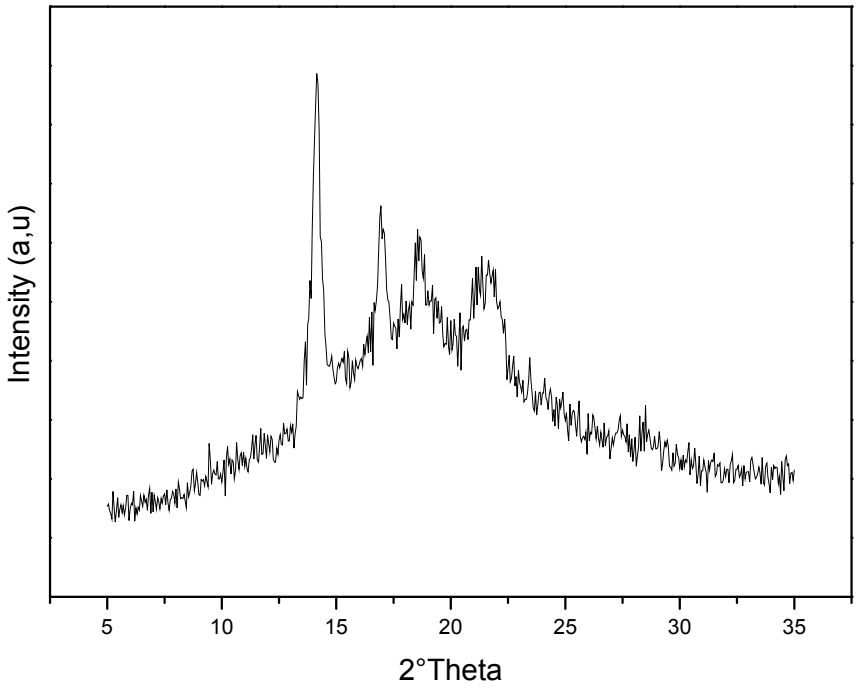

Figure VIII-15: X-ray difractogram of the blend PET/iPP/SEBS-MAH (50/50/15)

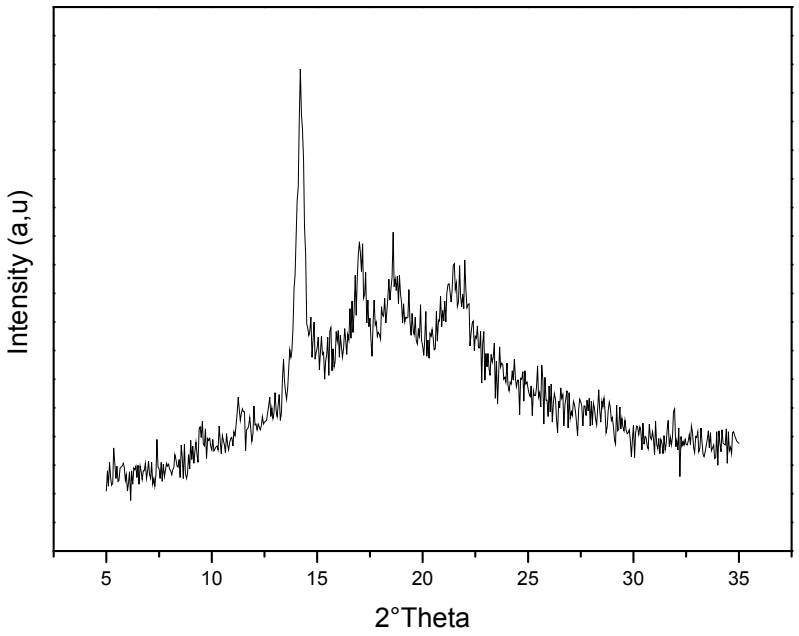

Figure VIII-16: X-ray difractogram of the blend PET/iPP/SEBS-MAH (40/60/7)

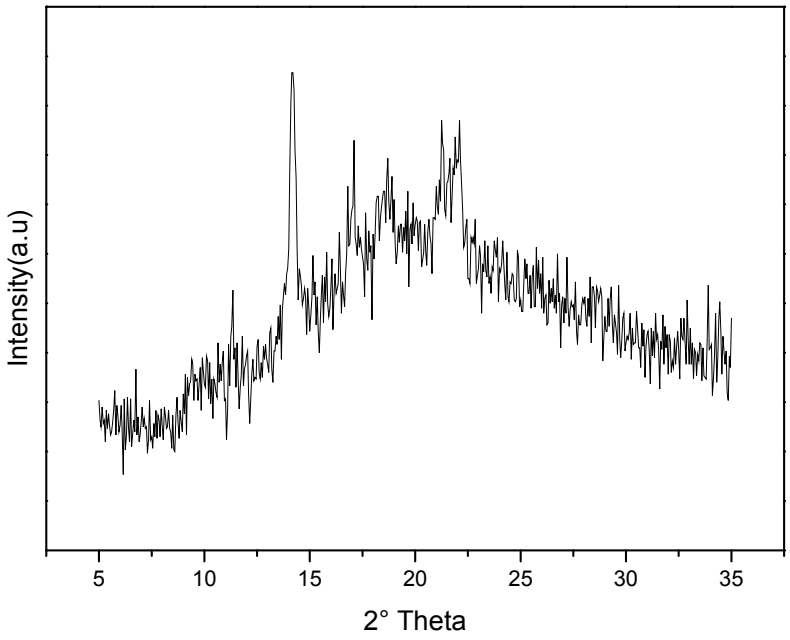

Figure VIII-17: X-ray difractogram of the blend PET/iPP/SEBS-MAH (40/60/10)

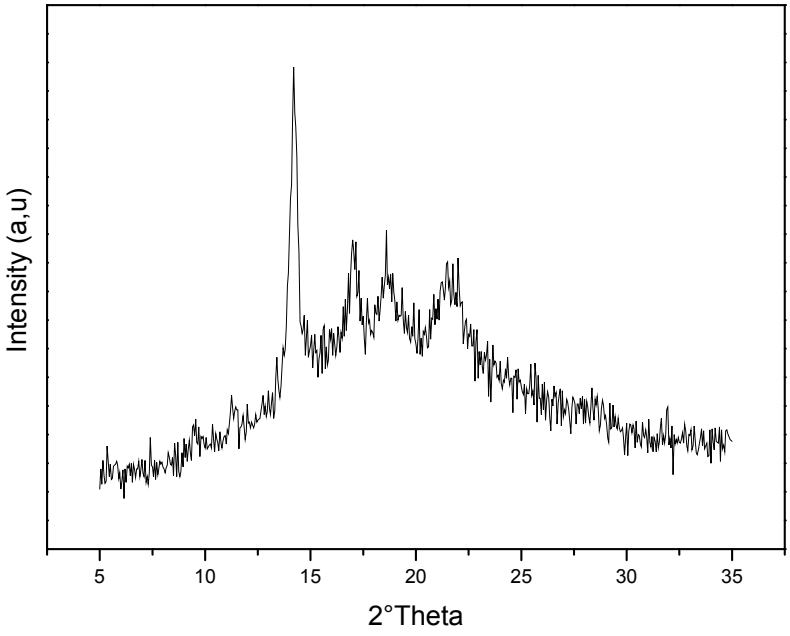

Figure VIII-18: X-ray difractogram of the blend PET/iPP/SEBS-MAH (40/60/15)

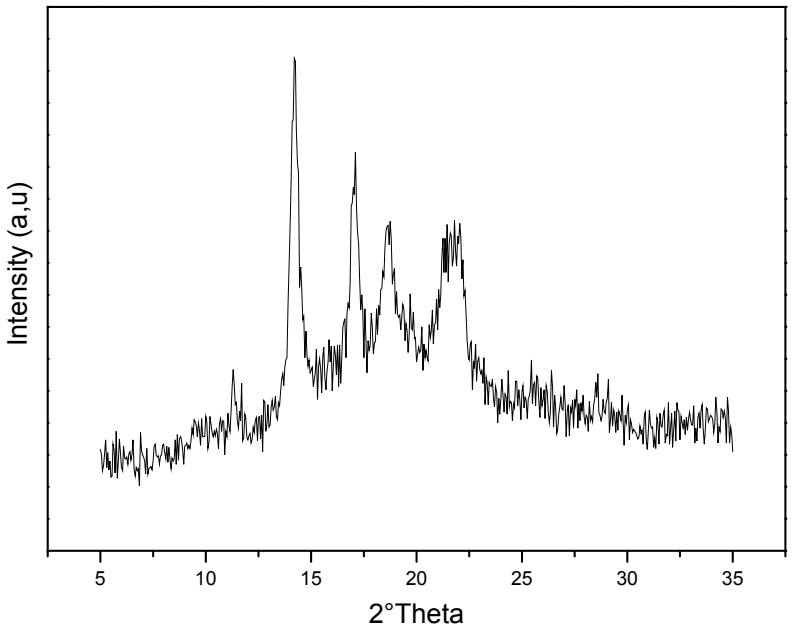

Figure VIII-19: X-ray difractogram of the blend PET/iPP/SEBS-MAH (20/80/7)

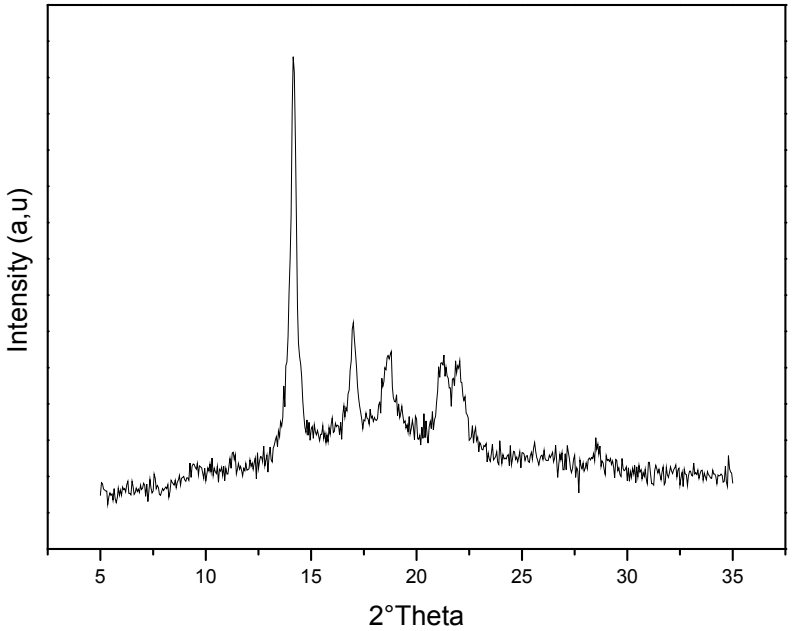

Figure VIII-20: X-ray difractogram of the blend PET/iPP/SEBS-MAH (20/80/10)

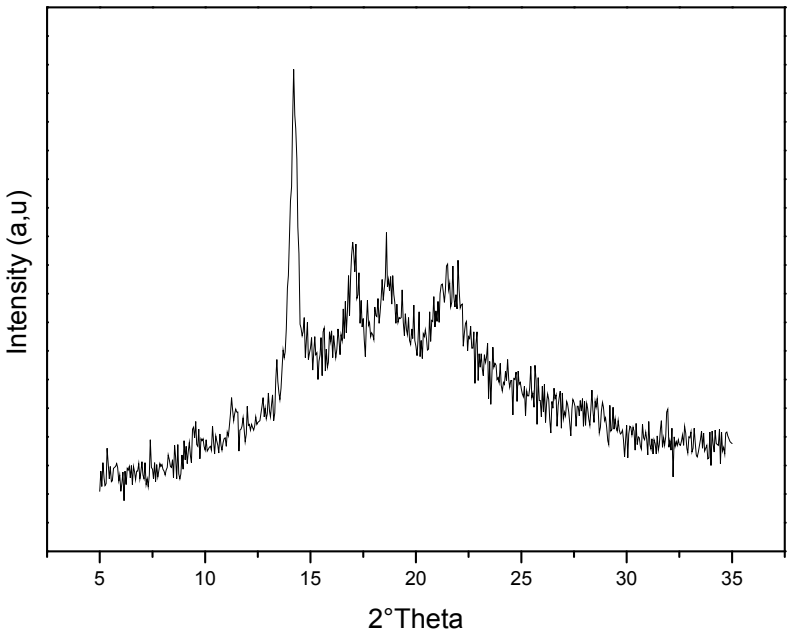

Figure VIII-21: X-ray difractogram of the blend PET/iPP/SEBS-MAH (20/80/15)

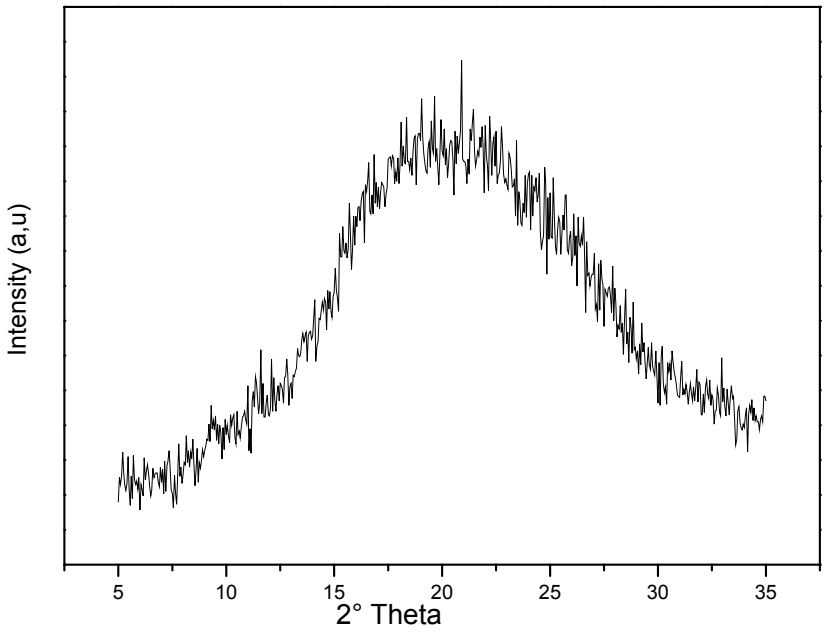

Figure VIII-22: X-ray difractogram of neat PET with 10% compatibilizer

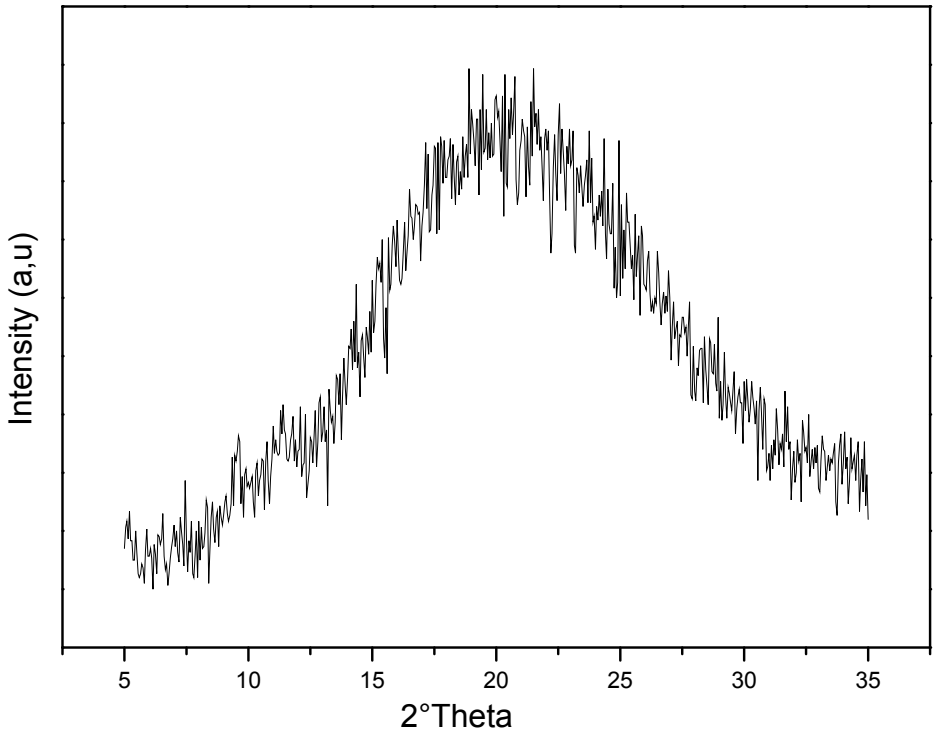

Figure VIII-23 : X-ray difractogram of PET with 15% compatibilizer

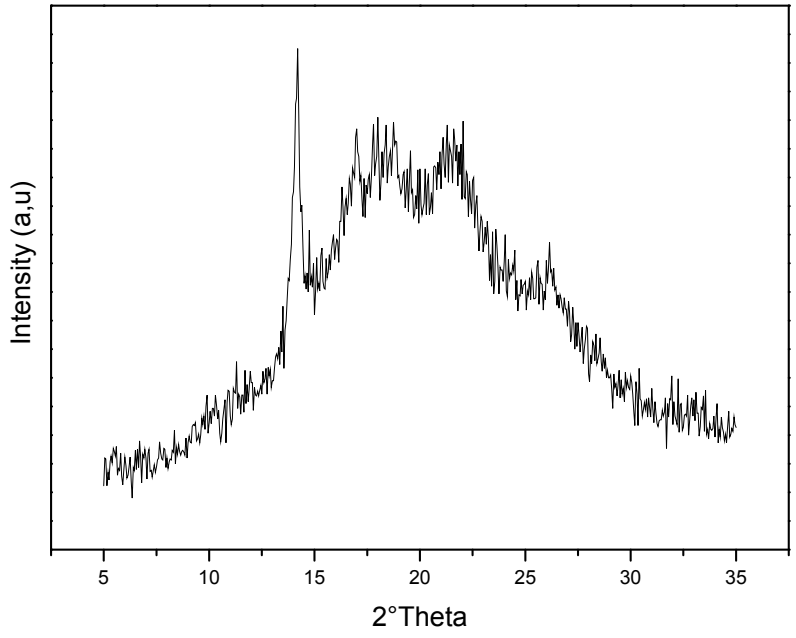

Figure VIII-24: X-ray difractogram of the blend (PET/iPP/SEBS-MAH(80/20/15)) with Clay

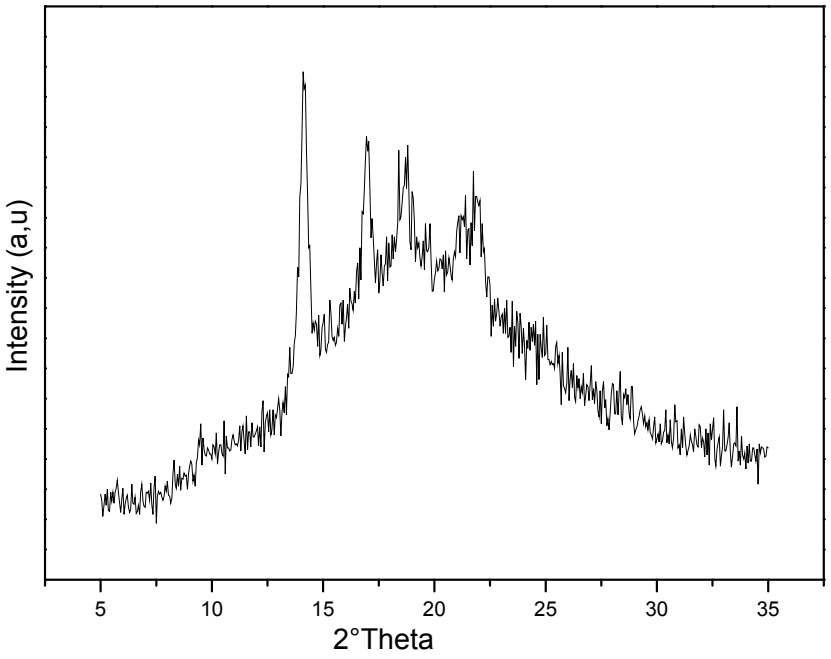

Figure VIII-25: X-ray difractogram of the blend (PET/iPP/SEBS-MAH(60/40/15)) with Clay

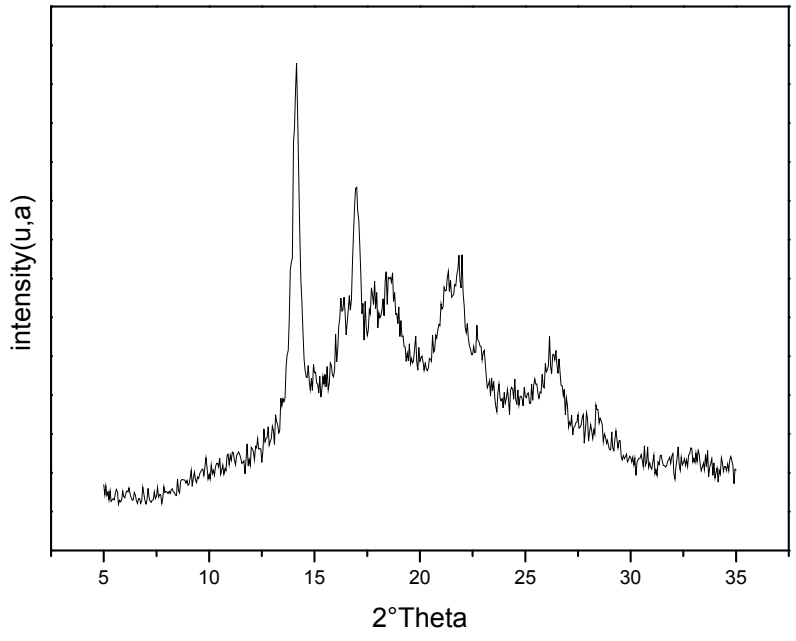

Figure VIII-26: X-ray difractogram of the blend (PET/iPP/SEBS-MAH(50/50/15)) with Clay

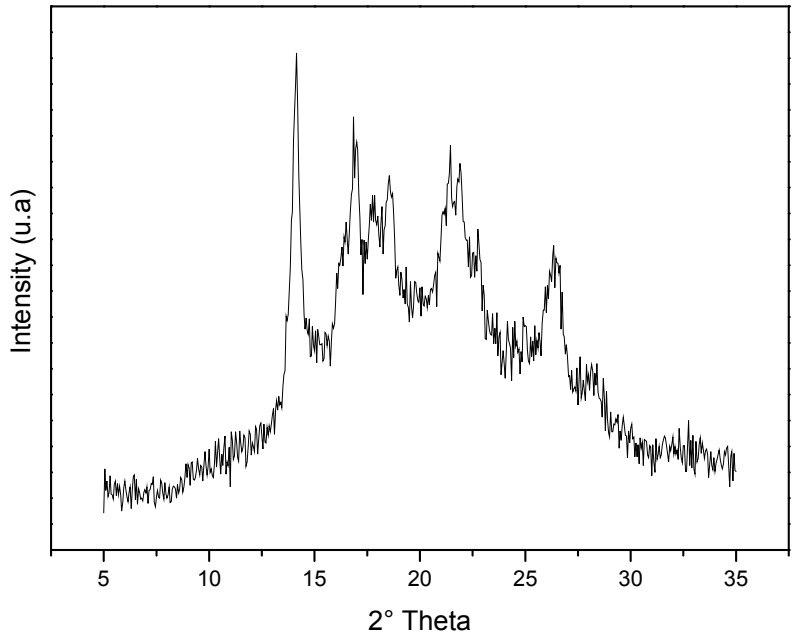

Figure VIII-27: X-ray difractogram of the blend (PET/iPP/SEBS-MAH(40/60/15)) with Clay

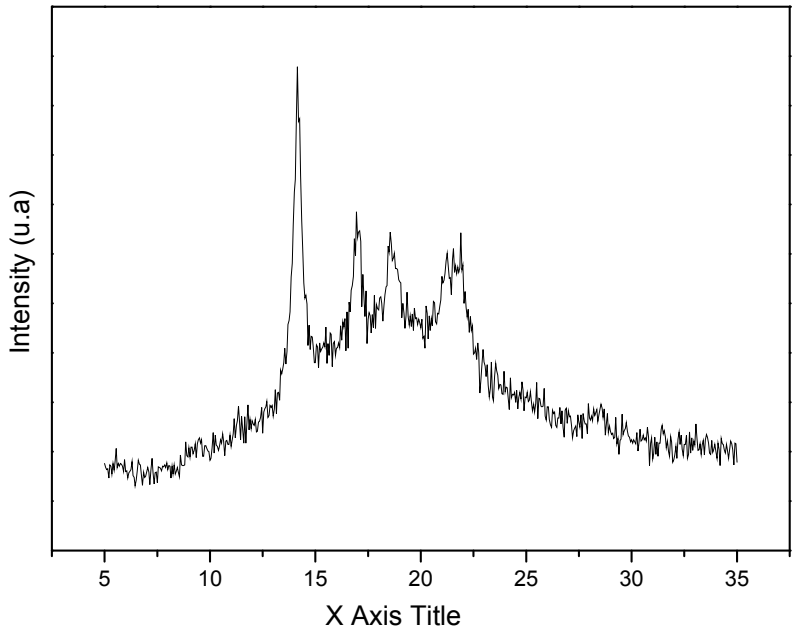

Figure VIII-28: X-ray difractogram of the blend (PET/iPP/SEBS-MAH(20/80/15)) with Clay

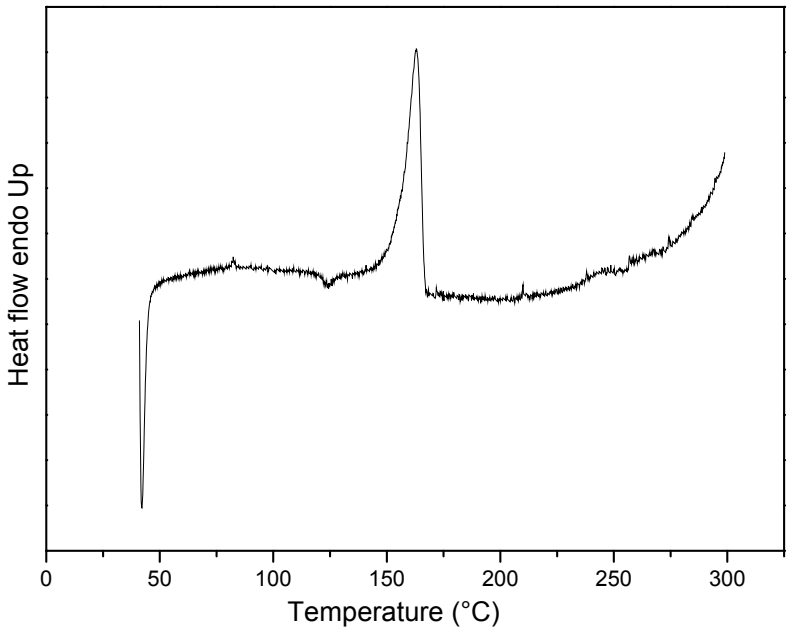

Figure VIII-29 : DSC thermographs of the blend PET/PP/SEBS-g-MAH (20/80/7)

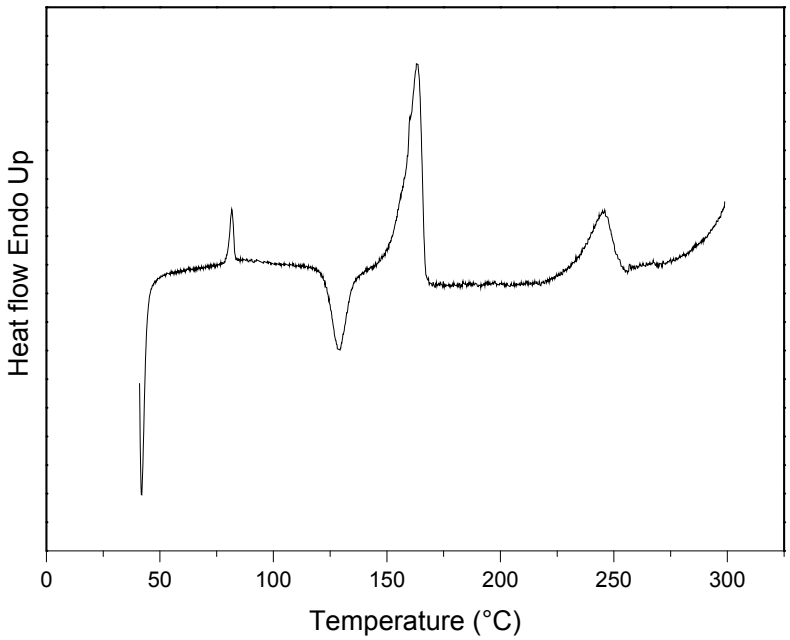

Figure VIII-30 : DSC thermographs of the blend PET/PP/SEBS-g-MAH (40/60/7)

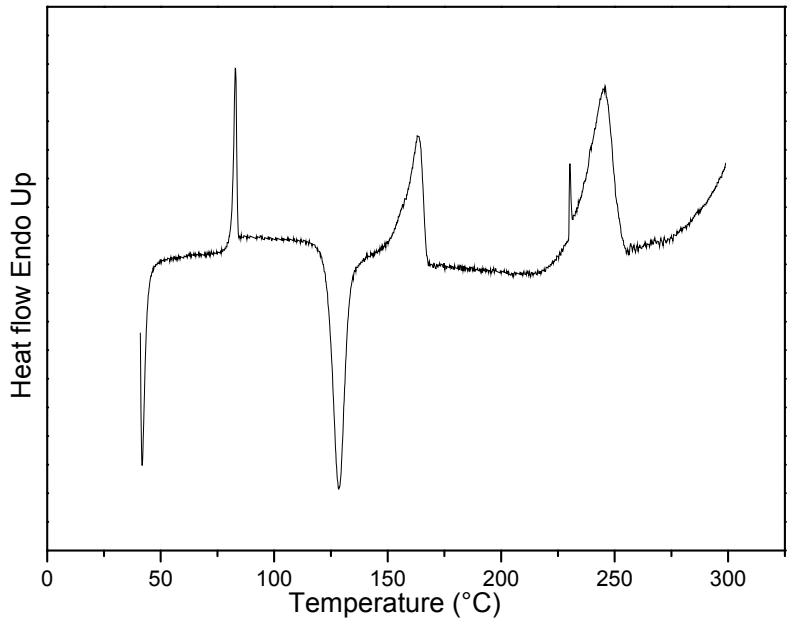

Figure VIII-31 : DSC thermographs of the blend PET/PP/SEBS-g-MAH (50/50/7)

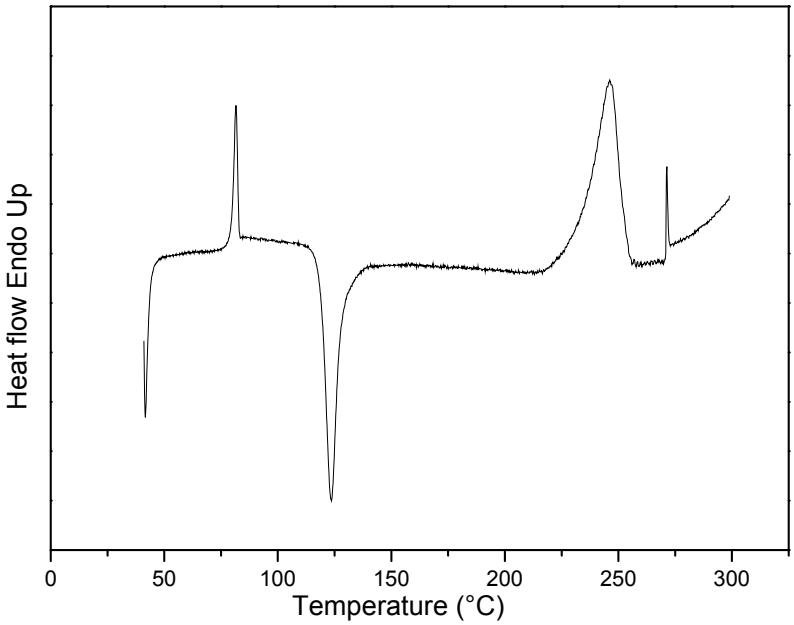

Figure VIII-32 : DSC thermographs of the blend PET/PP/SEBS-g-MAH (80/20/7)

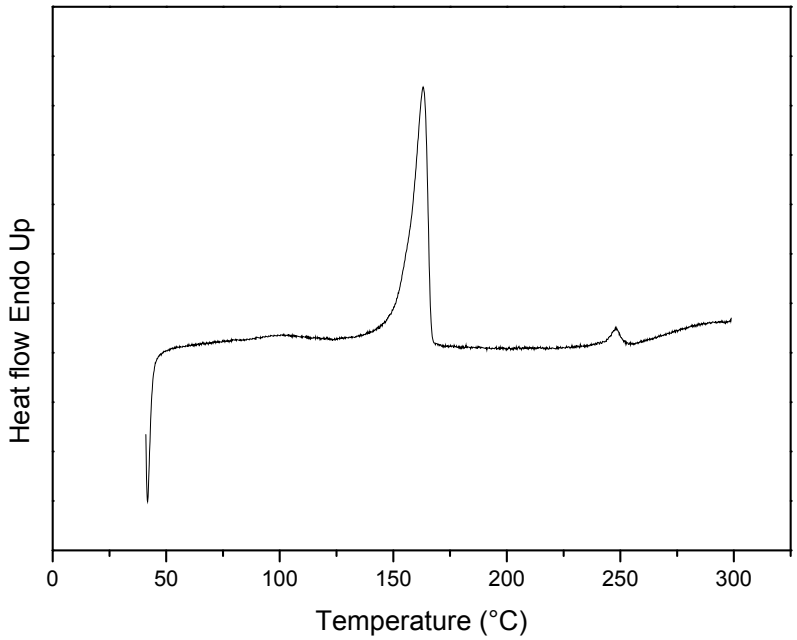

Figure VIII-33 : DSC thermographs of the blend PET/PP/SEBS-g-MAH (20/80/10**)**

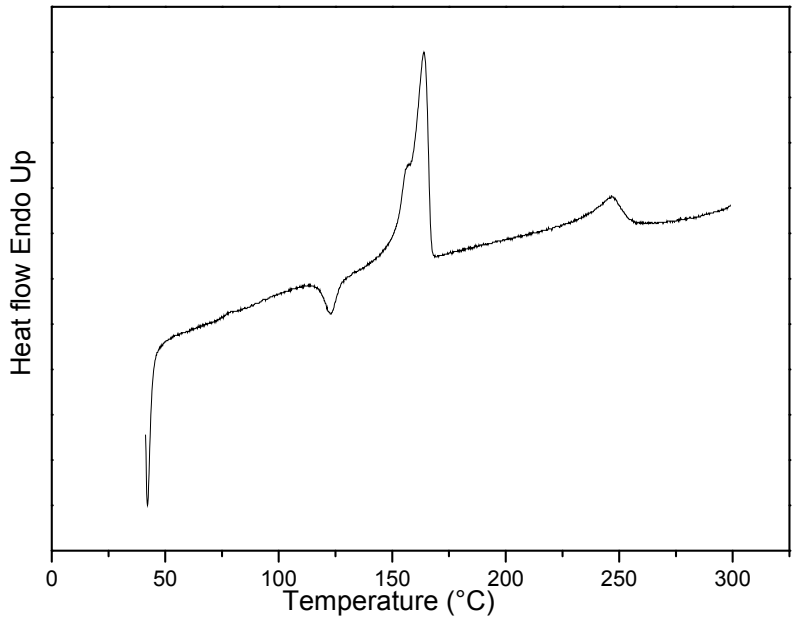

Figure VIII-34 : DSC thermographs of the blend PET/PP/SEBS-g-MAH (40/60/10)

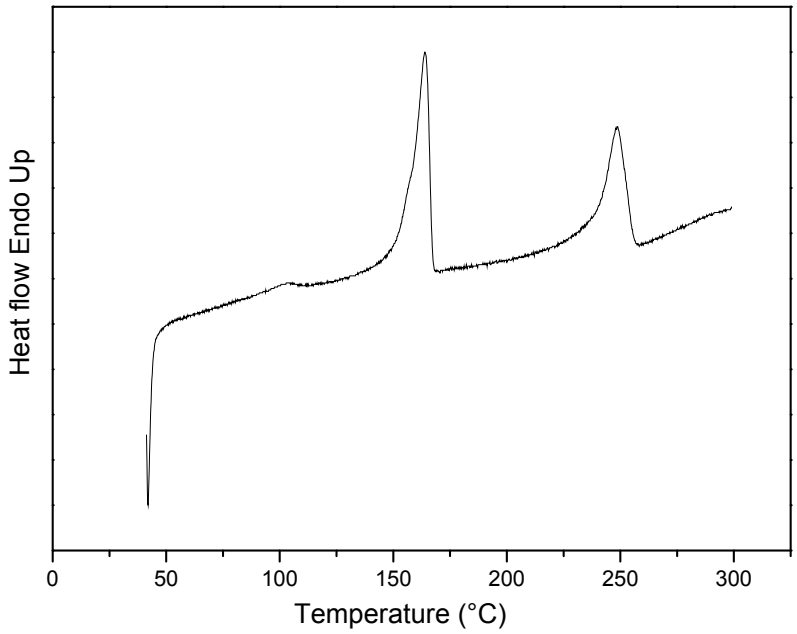

Figure VIII-35 : DSC thermographs of the blend PET/PP/SEBS-g-MAH (50/50/10)

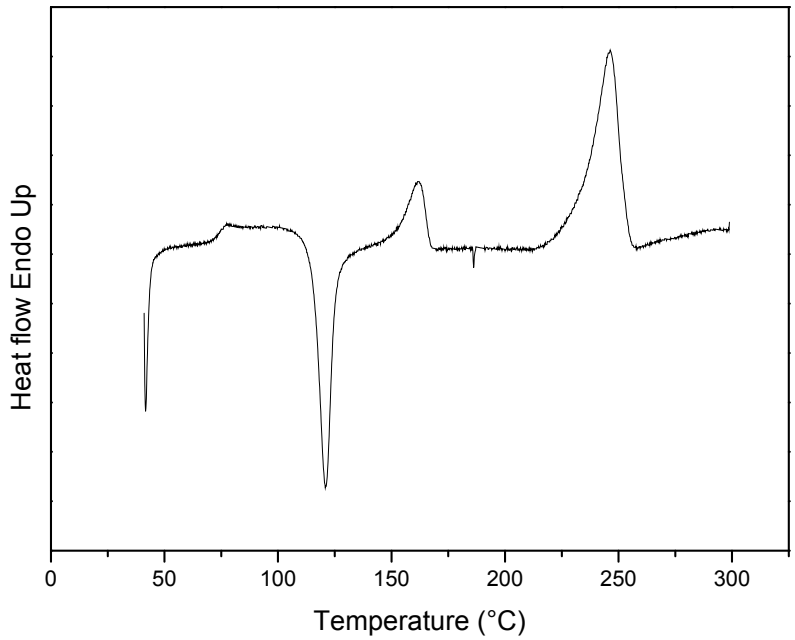

Figure VIII-36 : DSC thermographs of the blend PET/PP/SEBS-g-MAH (80/20/10)

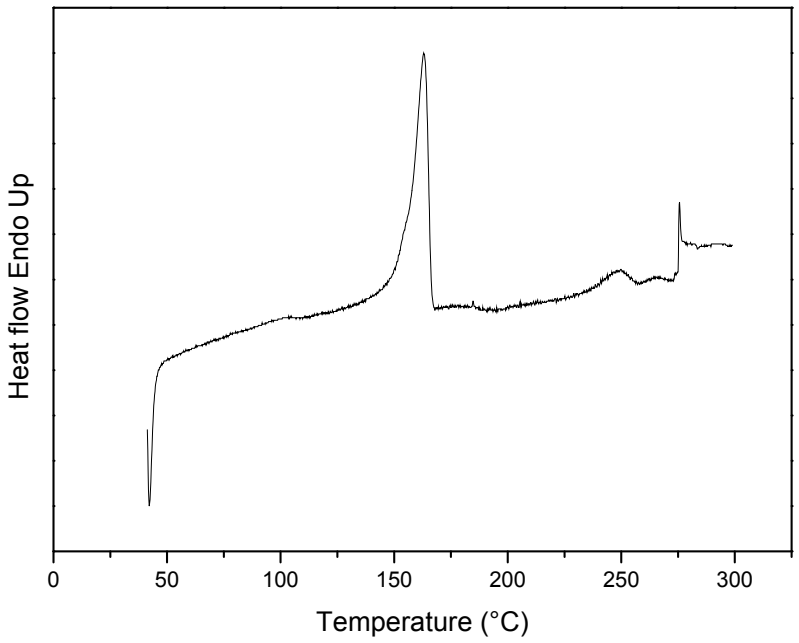

Figure VIII-37 : DSC thermographs of the blend PET/PP/SEBS-g-MAH (20/80/15)

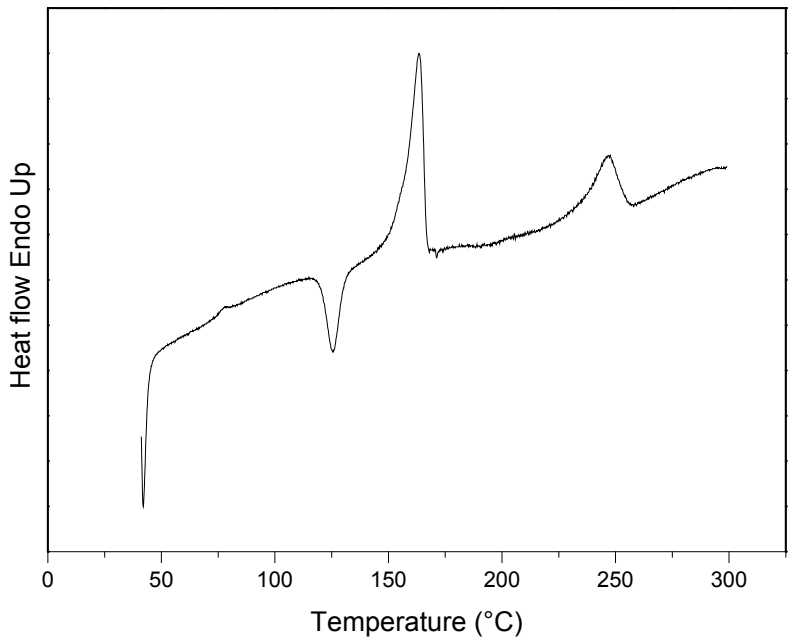

Figure VIII-38 : DSC thermographs of the blend PET/PP/SEBS-g-MAH (40/60/15)

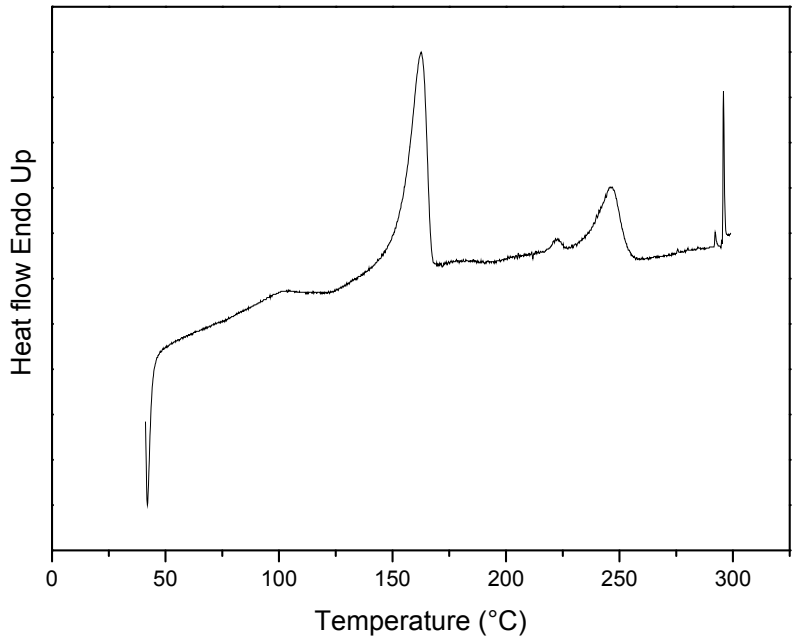

Figure VIII-39 : DSC thermographs of the blend PET/PP/SEBS-g-MAH (50/50/15)

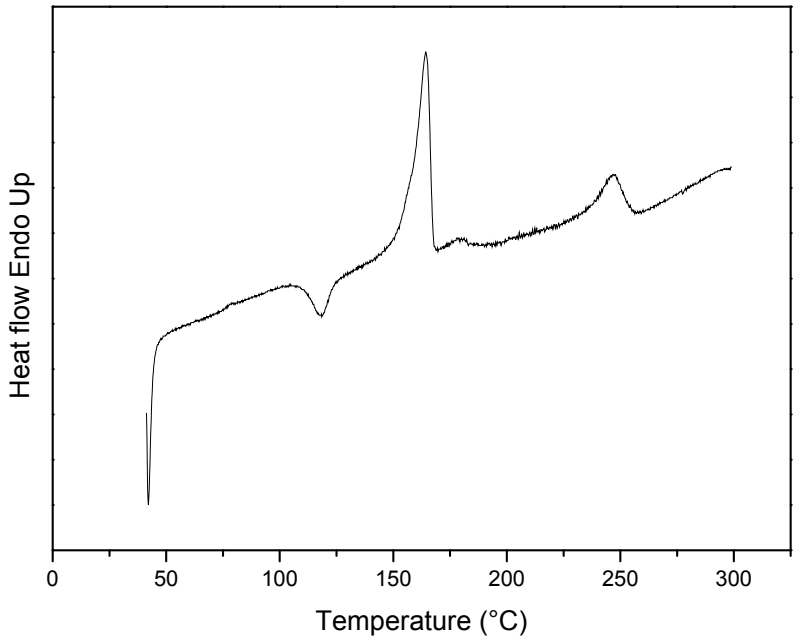

Figure VIII-40 : DSC thermographs of the blend PET/PP/SEBS-g-MAH (60/40/15)

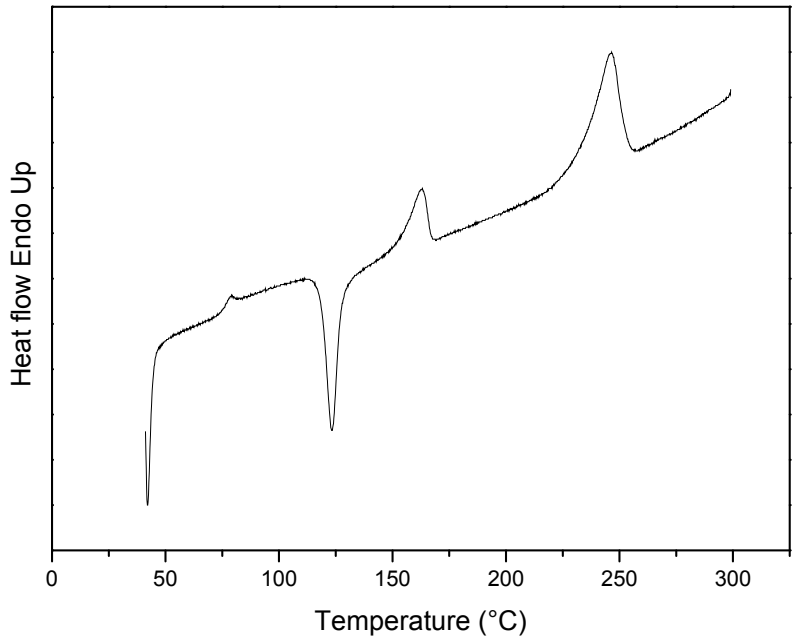

Figure VIII-41 : DSC thermographs of the blend PET/PP/SEBS-g-MAH (80/20/15)

Table N°8 : Results of the capillary rheometer

PET/PP/SEBS-MAH	γ_a (s^{-1})	τ(Pa)	μ_a (Pa.s)	γ_c(s^{-1})	μ_c (Pa.s)
100/0/0	1599,9	125	0,07813	1903,8	0,06566
	2133,2	162	0,07594	2538,5	0,06382
	2666,5	190	0,07125	3173,1	0,06288
	3199,8	230	0,07188	3807,7	0,0604
80/20/0	1599,9	187,5	0,11719	1647,5	0,078
	2133,2	218,75	0,10255	2197,1	0,07373
	2666,5	250	0,09376	2746,5	0,06918
	3199,8	290	0,09063	3295,8	0,06679
50/50/0	1599,9	187,5	0,11719	1615,8	0,11604
	2133,2	250	0,11719	2154,5	0,10153
	2666,5	312,5	0,11719	2693,1	0,09283
	3199,8	380	0,11876	3231,7	0,08974
20/80/0	1599,9	800	0,50003	1775,9	0,45048
	2133,2	980	0,45940	2368,2	0,41382
	2666,5	1150	0,43128	2959,8	0,38854
	3199,8	1300	0,40628	3551,8	0,36601
100/00/0	1599,9	875	0,54691	1623,8	0,53886
	2133,2	1062,5	0,49808	2165,1	0,49074
	2666,5	1250	0,46878	2706,5	0,46185
	3199,8	1390	0,43440	3247,8	0,42798
100/0/7	1599,9	312,5	0,19532	2047,8	0,09156
	2133,2	375	0,17579	2730,5	0,08011
	2666,5	437,5	0,16407	3413,1	0,07325
	3199,8	485	0,15157	4095,7	0,06867
80/20/7	1599,9	375	0,23439	1743,8	0,10752
	2133,2	437,5	0,20509	2325,1	0,1008
	2666,5	500	0,18751	2906,4	0,09418
	3199,8	550	0,17189	3487,8	0,0896
60/40/7	1599,9	312,5	0,19532	1791,8	0,17441
	2133,2	375	0,17579	2389,1	0,15696
	2666,5	437,5	0,16407	2986,4	0,1465
	3199,8	480	0,15001	3583,7	0,13394
50/50/7	1599,9	270	0,16876	1796,9	0,17391
	2133,2	312,5	0,14649	2395,8	0,15652
	2666,5	343,75	0,12891	2994,8	0,14609
	3199,8	375	0,11719	3593,8	0,13913

PET/PP/SEBS-MAH	γ_a (s^{-1})	τ(Pa)	μ_a (Pa.s)	γ_c(s^{-1})	μ_c (Pa.s)
40/60/7	1599,9	312,5	0,19532	1903,8	0,19697
	2133,2	375	0,17579	2538,5	0,17235
	2666,5	437,5	0,16407	3173,1	0,15757
	3199,8	500	0,15626	3807,7	0,14444
20/80/7	1599,9	250	0,15626	1927,1	0,23351
	2133,2	500	0,23439	2569,5	0,19459
	2666,5	760	0,28502	3211,9	0,17513
	3199,8	1062,5	0,33205	3854,3	0,16216
00/100/7	1599,9	450	0,28127	1940,6	0,27733
	2133,2	500	0,23439	2587,4	0,23424
	2666,5	562,5	0,21095	3234,3	0,19398
	3199,8	625	0,19532	3831,2	0,15833
100/00/10	1599,9	187,5	0,11719	1805,9	0,10383
	2133,2	218,375	0,10237	2407,9	0,09069
	2666,5	250	0,09376	3009,9	0,08306
	3199,8	281,5	0,08797	3611,8	0,07794
80/20/10	1599,9	187,5	0,11719	1889,5	0,09923
	2133,2	225	0,10548	2519,3	0,09108
	2666,5	250	0,09376	3149,2	0,08739
	3199,8	305	0,09532	3779	0,08263
50/50/10	1599,9	187,5	0,11719	1634,6	0,11471
	2133,2	234,75	0,11005	2179,5	0,10323
	2666,5	250	0,09376	2724,4	0,09676
	3199,8	312,25	0,09758	3269,3	0,09329
40/60/10	1599,9	288	0,18001	2088,7	0,13788
	2133,2	312,5	0,14649	2785	0,11221
	2666,5	343,75	0,12891	3481,2	0,09874
	3199,8	375	0,11719	4177,5	0,08977
20/80/10	1599,9	375	0,23439	2130	0,17606
	2133,2	437,5	0,20509	2840,1	0,15404
	2666,5	500	0,18751	3550,1	0,14084
	3199,8	548	0,17126	4260,1	0,12864

PET/PP/SEBS-MAH	γ_a (s^{-1})	τ(Pa)	μ_a (Pa.s)	γ_c(s^{-1})	μ_c (Pa.s)
00/100/10	1599,9	450	0,28127	1927,1	0,23351
	2133,2	500	0,23439	2569,5	0,19459
	2666,5	562,5	0,21095	3211,9	0,17513
	3199,8	625	0,19532	3854,3	0,16216
100/00/15	1599,9	200	0,12501	2411,9	0,08292
	2133,2	218,75	0,10255	3215,9	0,06802
	2666,5	234,375	0,08790	4019,9	0,0583
	3199,8	250	0,07813	4823,9	0,05183
80/20/15	1599,9	250	0,15626	1620,9	0,11568
	2133,2	312,5	0,14649	2161,2	0,10676
	2666,5	375	0,14063	2701,5	0,09568
	3199,8	437,5	0,13673	3241,9	0,08567
60/40/15	1599,9	218,75	0,13673	1699,9	0,12868
	2133,2	250	0,11719	2266,5	0,1103
	2666,5	281,25	0,10548	2833,1	0,09927
	3199,8	325	0,10157	3399,7	0,0956
50/50/15	1599,9	274	0,17126	2088,7	0,13118
	2133,2	312,5	0,14649	2785	0,11221
	2666,5	343,75	0,12891	3481,2	0,09874
	3199,8	375	0,11719	4177,5	0,08977
40/60/15	1599,9	187,5	0,11719	1999,8	0,12501
	2133,2	250	0,11719	2666,5	0,11719
	2666,5	312,5	0,11719	3333,1	0,11251
	3199,8	375	0,11719	3999,7	0,10938
20/80/15	1599,9	326	0,20376	1779,5	0,1832
	2133,2	375	0,17579	2372,7	0,15805
	2666,5	437,5	0,16407	2965,9	0,14751
	3199,8	500	0,15626	3559,1	0,14048
00/100/15	1599,9	690	0,43128	2239,8	0,30806
	2133,2	750	0,35158	2986,4	0,25114
	2666,5	812,5	0,30471	3733,1	0,21765
	3199,8	875	0,27345	4479,7	0,19533

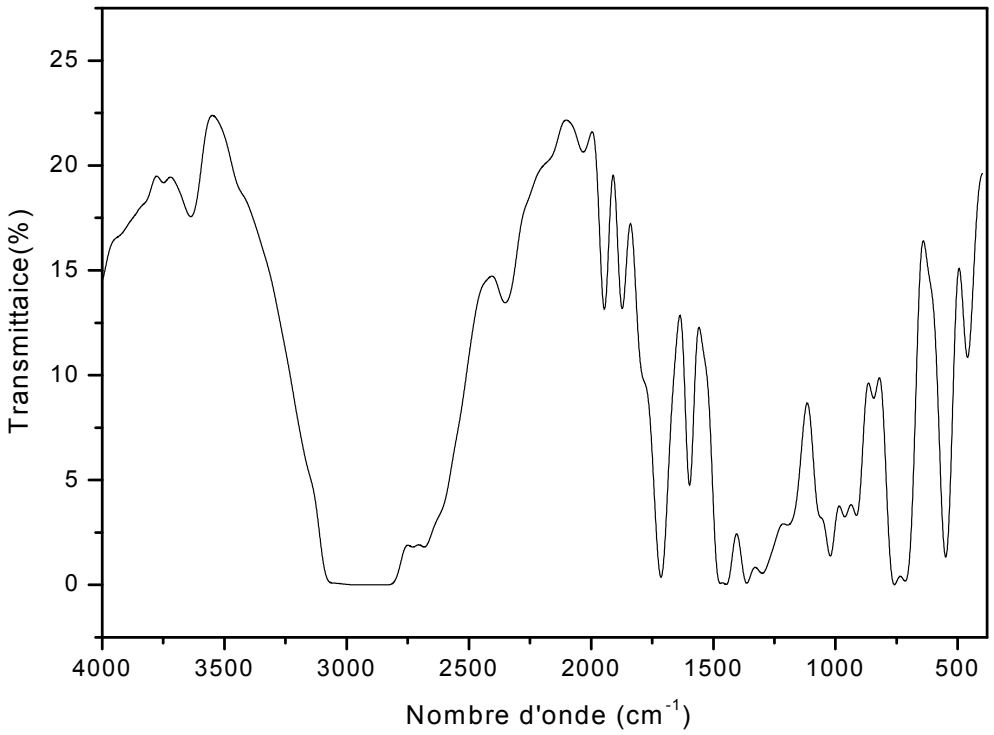

Figure VIII-42 : FT-IR spectrum of the SEBS-MAH

الخلاصة :

يركز هذا العمل على الدراسة الميكانيكية ، الريولوجية ,الهيكلية والحرارية للمزيج من البولي ايثيلين تيريفثالات الغير المتبلور المعاد تدويرها وisotactic البولي بروبلين ,مع التوافق SEBS-MAH بنسب مختلفة. و كدا الدراسة الفيزيائية للمركب مع التوافق و الصلصال و مناقشتها .،وقد أتاحت التحاليل اللتي أجريناها على (WAXS)، قياس الكالوري, فرق المسح والمسح الضوئي للمجهر الإلكتروني ، لوصف لنا على المستوى المجهري ، دور التوافق SEBS-g-MAH بشأن الهيكل وصلابة المخاليط التي درسنا .وبينت النتائج أن الدائرة لا يتفق مع التوافق .ومع ذلك ، فإن وجود SEBS-g-MAH سمح التوافق بين البوليمرات.

سمحت لنا أيضا الدراسة من استخلاص تأثيرالصلصال على مؤشر المنتجين ، وتسبب أيضا زيادة في صلابة الخلائط النقية والخلائط المتوافقة ب SEBS-g-MAH و الخلائط المتوافقة بالصلصال .

كلمات البحث : المزيج ؛ التوافق ؛ مسح قياس الكالوري ,WAXS, الصلابة, مسح المجهر اللألكترونى

Résumé

Ce travail porte essentiellement sur l'étude mécanique, rhéologique, structurale et thermique des mélanges de polyéthylène téréphtalate (PET) amorphe, recyclé et du polypropylène isotactique (iPP) avec un agent compatibisant à savoir le SEBS-g-MAH à des différentes proportions. L'étude physique des matériaux composites des mélanges compatibilisés renforcés par l'argile est aussi discutée. L'analyse, effectuée au moyen de la difraction des rayons X (WAXS), la calorimétrie à balayage différentielle et le microscope électronique à balayage, nous permet de décrire, au niveau microscopique, le rôle du compatibilisant sur la structure et la microdureté des mélanges que nous avons étudiés. Les résultats révèlent que le PET était incompatible avec iPP. Toutefois, la présence du compatibilisant à savoir le copolymère bloc styrène-éthylène-butylène-styrène greffé par l'anhydride maléique, a permis la compatibilisation de ces polymères. L'argile semble avoir un effet de nucléation sur l'iPP et a aussi provoqué une augmentation de la dureté dans les mélanges compatibilisés. D'autre part, la cristallinité de ces échantillons (mélanges purs, les mélanges avec compatibilisant, et les mélanges avec compatibilisant et argile) ne dépendait que de la composition des deux polymères.

Mots-clés: Mélanges; compatibilisation; Calorimétrie à balayage différentielle (DSC); WAXS ;Micro dureté ; microscope électronique à balayage

Abstract :

The mecanical, rheological, thermal and structural study of the blends of recycled amorphous polyethylene terephthalate (PET) with isotactic polypropylene (iPP) with a compatibilizer in different proportions is reported. The physical study of the composites of the compatibilized blends and clay is also discussed. The analysis, performed by means of wide-angleX-ray scattering, differential scanning calorimetry and scanning electron microscope techniques, permits us to describe, at microscale level, the role of the compatibilizer on the structure and microhardness of the polymer blends that we studied. The results reveal that PET was incompatible with iPP . However, the presence of the compatibilizer a styrene ethylene butylene styrene block copolymer grafted with maleic anhydride, allowed the compatibilization of these polymers. In the PET/iPP blends, the clay seemed to have a nucleating effect on the iPP and also induced a hardness increase in the compatibilized blends. On the other hand, the crystallinity of these samples (pure blends, blends with compatibilizer, and blends with compatibilizer plus clay) only depended on their composition.

Key words: blends;compatibilization; differential scanning calorimetry (DSC) ;hardness; WAXS; scanning electron microscope